Technical University of Denmark

DTU

Measurements on and modelling of offshore wind farms

Frandsen, Sten Tronæs; Chacón, L.; Crespo, A.; Enevoldsen, P.; Gómez-Elvira, R.; Hernández, J.; Højstrup, J.; Manuel, F.; Thomsen, K.

Link back to DTU Orbit

DTU Library
Technical Information Center of Denmark

Final Report on

Measurements on and Modelling of Offshore Wind Farms

S. Frandsen (editor), L. Chacón, A. Crespo, P. Enevoldsen,
R. Gómez-Elvira, J. Hernández, J. Højstrup, F. Manuel, K. Thomsen
and P. Sørensen

RISO-R--903(EN)

MASTER

MEASUREMENTS ON AND MODELLING OF OFFSHORE WIND FARMS

DISCLAIMER

Portions of this document may be illegible in electronic image products. Images are produced from the best available original document.

LIST OF SYMBOLS

SI units are used all through the report. Be aware, that some symbols are representing different variables.

All used symbols are also defined in the report in the context they are used.

A	-	Weibull scale parameter
a	-	constant
α	-	wake amplitude of flow and load parameters/constant in linear expression for equivalent width/angel of flow to row orientation
B	-	constant
b_e	-	equivalent wake width factor
β	-	wake width/constant in expression for equivalent width
c	-	ambient, non-wake level flow and load parameters
c_u	-	constant related to turbulence scale
C	-	constant
C_T	-	thrust coefficient of wind turbine
$[C]$	-	combined structural damping and Coriolis/gyroscopic matrix
D	-	rotor diameter/constant
Δ	-	relative damage
ew	-	equivalent load width
ϵ	-	turbulence dissipation rate
f	-	non-dimensional frequency
f_w	-	Weibull distribution
g	-	gravity
γ	-	constant related to flow coherence
Γ	-	gamma function
h	-	hub height/exponent of expression for s.
H	-	rotor filter function
I,I_o	-	turbulence intensity in ambient unobstructed flow
I_{wake}	-	maximum wake turbulence at hub height
k	-	Weibull shape parameter/constant in exponentially linear SN curve/kinetic energy
k_n	-	constant related to different wind farm configurations
$[K]$	-	stiffness matrix
κ	-	von Karmann constant
$ln()$	-	natural logarithm
L	-	scale of turbulence
L_o	-	ambient unobstructed scale of turbulence
m	-	exponent of exponential linear SN curve.
$[M]$	-	mass matrix
n	-	frequency
n_i	-	no. of load widths at load level s_i
n_{fat}	$=$	$n_{fat}(s)$ SN curve
n_t	-	reference frequency for equivalent load width
ω	-	frequency in rad/s
μ	-	(μ_o) mean values/viscosity of air
p	-	probability frequency distribution/power
p_o	-	mean power
P	-	power curve
r_e	-	correction factor for equivalent load width
R_x	-	increase factor of parameter x in wake
ρ	-	air density
s	-	equivalent load width
s_t	-	non-dimensional wind turbine separation
S_u	-	power spectrum of wind speed

σ_x - standard deviation of parameter x
$U, (U_o)$- mean wind speed
u, v, w wind speed components
u_* - friction velocity
Δu - speed deficit in wake
$\{x\}$ - translation and rotation matrix
x - non-dimensional parameter
z - height above ground
z_o - surface roughness
z_{ch} - "Charnock constant"

1 FOREWORD

The report is the final report of the project "Measurements on and modelling of offshore wind farms" and signifies the termination of contract JOU2-CT93-0350, pending on acceptance of the Commission of the European Communities, DG XII.

The original contract period was January 1 1994 to December 31 1995, the termination date later extended to April 1 1996.

The participating institutions/companies were Risø National Laboratory (Riso) as coordinator, Bonus Energy AS (Bonus), Universidad Politecnica de Madrid (UPM), Elkraft AS and Finish Meteorological Institute (FMI).

The following persons have contributed to the report:

From Riso: S. Frandsen (also editor), J. Højstrup, P. Sørensen and K. Thomsen.

From UPM: A. Crespo, L. Chacón, R. Gómez-Elvira, J. Hernández and F. Manuel.

From Bonus: P. Enevoldsen.

Contact person: Sten Frandsen
                        Test Station for Wind Turbines
                        Meteorology and Wind Energy Department
                        Risø National Laboratory
                        DK-4000 Roskilde

                        Phone: (+45) 4677 5072
                        Fax: (+45) 4237 2965
                        e-mail: vtk-stfr@risoe.dk

2 SUMMARY AND CONCLUSIONS

The primary project component was measurement on the Vindeby Offshore Wind Farm. Also included are analyses of fatigue loading on the turbines, sea climate, performance of the wind farm and modelling of flow characteristics inside the wind farm. These individual analyses were made to meet the overall objective, which was to devise an adequate design tool to take into account the increased dynamic loading in wind farms. We find that this goal was reached.

The experimental site, Vindeby Offshore Wind Farm. Measurements have been conducted for several years on the wind farm at Vindeby 2-3km off the coast of the island of Lolland in the South Baltic Sea. The Vindeby Wind Farm consists of 11 Bonus machines with installed capacities of 450kW, hub height 38m and rotor diameter 35m. The separations of the machines in the rows, see Figure 3.1, are 300m (8.6D), and the distance between the rows is equally 300m. Two machines, 4W and 5E are instrumented for structural measurements; tower base bending, yaw and tilt and edge and flapwise blade root bending moments are measured and statistics for ½hourly consecutive time periods are stored. The statistics include minimum, maximum, mean, standard deviation and the so-called equivalent load widths. The equivalent load width is popularly speaking the amplitude of a sinusoidal load with frequency equal - in this case - to rotational frequency of the wind turbine rotor that would consume the same fatigue life as the actual load sequence.

Wind climate measurements are made at three towers, one placed on the shore, and two, see Figure 3.1, close to the wind farm. The positions of the sea based tower are so that they match wind turbine positions in an imaginary larger wind farm with the same wind turbine separations. This gives the opportunity to also measure wakes as seen by the wind turbines. The analyses apply approx. 13,000 sets of valid ½hour statistics, meaning that the instrumented machines are in operation.

Flow modelling (section 4 and 5). The UPMPARK code developed within the project has been adapted to deal with offshore wind farms. A modified version of Charnock's equation to calculate the surface roughness of the sea has been incorporated in UPMPARK. The code gives the distribution of the different flow magnitudes: velocities, pressures, and - in this new version - also turbulence spectra. Analytical expressions providing values of the average velocity, turbulence intensity, turbulence scale and width of the wake, at different positions of each machine in a row, were obtained as functions of relevant turbine and array characteristics, by making the least square fit to the numerical results from UPMPARK. These expressions were validated by comparison with measurements of the Vindeby Wind Farm. While results of the model are promising, it has not been possible within the time frame of the project to integrate the model in the load analysis.

Also, a review has been made of the modelling methods for wind-turbine wakes and wind farms.

Sea climate (section 6). Regarding mean wind speeds, turbulence levels, turbulence scales and extreme wind statistics the following conclusions were made:
- Sea surface roughness lengths vary qualitatively as the Charnock relation, but attains somewhat higher values than predicted for near-coastal conditions.
- The flow accelerates more slowly over the sea than predicted by WASP.
- The apparent roughness length with flow coming from land (fetch about 2km) is for wind speeds > 5m/s on the average about 1-2 mm.
- The roughness length with flow from the sea is on the average 0.1-0.2 mm.
- The average turbulence intensity (30 min. avg. time) for the two sea masts is about 9% (increasing at high wind speeds) which is increased compared with the sea value because of the proximity of land. For the land mast the turbulence intensity is approx. 11%.
- The overall 'most common' length scale (corresponding to the spectral peak) is approx. 500m.
- Length scales with flow from land are smaller than for flow from the sea.
- Length scales in the multiple wake situation are diminished by a factor 2-5 (dependent on being exactly on wake-axis, or slightly off) compared with the free flow.
- The predicted 50 year value of 30 minute average wind speed at hub height (38m) is 37 m/s, and the predicted 2 second gust with the same recurrence period is 51m/s.

Fatigue loads (section 7 and 8). The concept of equivalent load width is extensively used to identify differences in fatigue loading under different load conditions. It was found that for the geometry of the Vindeby Wind Farm equivalent loads are approx. 15% lower offshore than onshore. Calculating an "effective" turbulence intensity, I_{eff}, to substitute detailed wake calculations it was found that offshore, I_{eff} is not expected to reach - under realistic circumstances - the 0.17-level presently prescribed in the EIC draft standard as a reference.

Figure 1.1 illustrates a proposal for future criteria for design of wind turbines for offshore as well as onshore. The figure shows equivalent load width derived from a comprehensive set of models for a wind turbine fully imbedded in a wind farm, for offshore and onshore conditions (full lines), and a very simple model for the effective turbulence intensity to be applied:

$$I_{eff} = \sqrt{k_n \frac{C_T}{s_t^2} + I_o^2}$$

where k_n is a constant for each of four wind turbine configurations, being equal to 0.4 for a wind turbine fully inside a wind farm, and less than 0.4 for three other cases: two neighboring machines, machines in one row and machines in two rows. C_T and s_t are thrust coefficient and wind turbine separation in rotor diame-

Farm-case, Offshore, and land I=0.12

Figure 1.1 *Comparison of integrated and simple models for farm-case, onshore and offshore; U = 8m/s.*

ters, respectively. The simplified curve fits of Figure 1.1 have been obtained simply by using the fatigue loading in the unobstructed flow and the above turbulence intensity as input parameters to the calculations. As seen the fits are excellent except for the smallest separations. Despite being based on data with rather large wind turbine separations, we find that the end result is reliable and may be used in future design codes, not being more uncertain than more comprehensive design studies.

Finally - to support the credibility of the above approach - it is suggested that some efforts are invested in the near future to a) verify assumptions in more details, b) verify the sub-models, and b) to verify and possibly calibrate the models for small wind turbine separations. Also, it should be carefully considered whether - as expected - machines other than the stall regulated concept display basically the same behavior.

Comparison of power production (section 9). The power performances of the wind turbines have been evaluated on basis of the Risø power measurements on the turbines 4W and 5E and control-system power measurements on all turbines. The aim was to determine the difference between the power curves of specimens of the same type of wind turbine. The Vindeby Wind Farm offers an excellent opportunity for that since in wide intervals of wind directions the flow is ideal because the wind turbines and one of the met masts presumably experience the same free flow. However, the amount of control system data was too small to be conclusive, especially because the dominating wind direction during the measurement period was outside the intervals with ideal flow. Thus, under presumed ideal conditions the variation in production was less than could be significantly deducted from measurements.
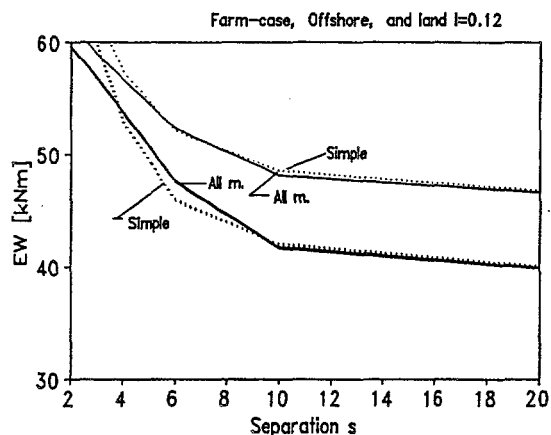
3   PROJECT OBJECTIVES AND SCENE OF MEASUREMENTS

Objectives and Deliverables

The main project **objectives** are

- To complement the existing base of wind farm data by gathering information on wind speed deficit, turbulence and structural loads at the Vindeby offshore wind farm and one wind turbine on the Finnish island Sottunga.

- To investigate the structure of single and multiple wakes under the ideal homogeneous, low-ambient turbulence conditions found offshore, and thus be able to model wake behavior more correctly.

- To be able to characterize turbulence and shear in the flow as a function of upstream turbine separation to be utilized in the design phase for calculation of loads on wind turbines to be located offshore.

- In addition, the hypothesis that in terms of structural loads special wind farm effects are only observed when ambient turbulence is very low may be tested.

In order to achieve the project objectives it is anticipated that measurements of the wind farm flow and wind turbine load characteristics should be performed for approximately two years.

In terms of manpower and cost the data collection and data analysis at Vindeby will dominate the present project. The tasks of gathering data from the Vindeby Wind Farm, pre-processing and extended data processing are undertaken by Risø with the support of ELKRAFT. The data collection at Sottunga is undertaken by FMI. Flow modelling is carried out by UPM, Risø and FMI with UPM in the leading role. The task of outlining load cases will to some extent be shared by all parties. The anticipated tasks have been divided into 4 sub-tasks: A) data collection and pre-processing of data, B) extended data analysis, C) flow modelling and load cases, and special analysis regarding D) power performance. These sub-tasks contain the following activities:

A. **Preparation of measurements** and collection of data at the two experimental sites.

B. **Data Analysis.** Apart from the described on-line computation of statistical quantities, more detailed analysis of the data will take place. The extended data analysis serves dual purposes: to evaluate flow and load characteristic of the specific wind farm and to verify and calibrate flow/load models to be used for design of (future) wind farms.

C. **Wake and Wind Farm Flow Modelling.** In order to generalize results of the measurements it is important that models of wake turbulence is tested/calibrated as part of the project. It is expected that measurements from other wind farms will be included in this study.

D. **Performance Analysis.** As for power performance and power quality especially the offshore site at Vindeby offers some special possibilities due to homogeneity of the site and the expected low turbulence levels.

Scene of Measurements, Vindeby Offshore Wind Farm

Measurements at the offshore Vindeby Wind Farm - consisting of 11 450kW BONUS machines (3-bladed, stall regulated, rotor diameter 35m and hub height 38m above average sea level) located 1.5 to 3 km off the coast of the island Lolland - will provide the main input to the data analysis of the project. This wind farm was commissioned and set into operation in September 1991.

The 11 machines are arranged in two rows, with 6 in one row and 5 in the other, Figure 1. The orientation of the rows is 140° azimuth so as to minimize wake effects, with the predominant wind direction being west-south-west. The distance between the turbines in each row is 300m (8.5 rotor diameters) and the distance between the rows is likewise 300m. The water depth varies between 3 and 5m.

Two machines, 4W and 5E, are instrumented for structural measurements: flap- and edgewise bending moments on one blade, bending moment in tower base, active and reactive power (voltage and current), yaw position and status. Three approx. 45m meteorological towers have been erected: one is located on land to provide information on the change of wind characteristic when the wind is coming from land, one is placed to the west of the wind turbines (serving basically as a reference mast, but in certain wind directions it will measure double-wake conditions), and one is placed at an imaginary wind turbine position in the western row to provide data on multiple wake situations. All meteorological towers being equipped with cup anemometers at least 5 levels, wind direction and temperature sensors. Also, two 3-D sonic anemometers are employed. At the base of one of the sea-bottom-based towers wave heights will be measured.

Sensor signals from the offshore meteorological towers are fed through multi-core cables to one of the instrumented wind turbines from where they are relayed - together with sensor signals from the wind turbines -

Figure 3.1 *Layout of the Vindeby Wind Farm.*

through an optical fibre cable to the central data storage and processing computer, which is placed in a cabin at the base of the onshore meteorological tower. Structural and meteorological data are sampled continuously at 25 Hz and stored as 30 minute records. Statistics such as mean, standard deviation, maximum and minimum of all signal and for the structural measurements also damage "equivalent stress" are computed on-line and stored. And finally, each 30 minute record is categorized (binned) according to wind speed and wind direction and stored until an adequate number of time series has been accumulated in each bin.

Meteorological data have been sampled from all three meteorological towers since November 1993, and data from the two instrumented wind turbines since April 1994.

Approx. 13,000 half-hour data series have been recorded, of which all have been statistically analyzed (including rain-flow analysis) and a limited number has been stored in its entirety.

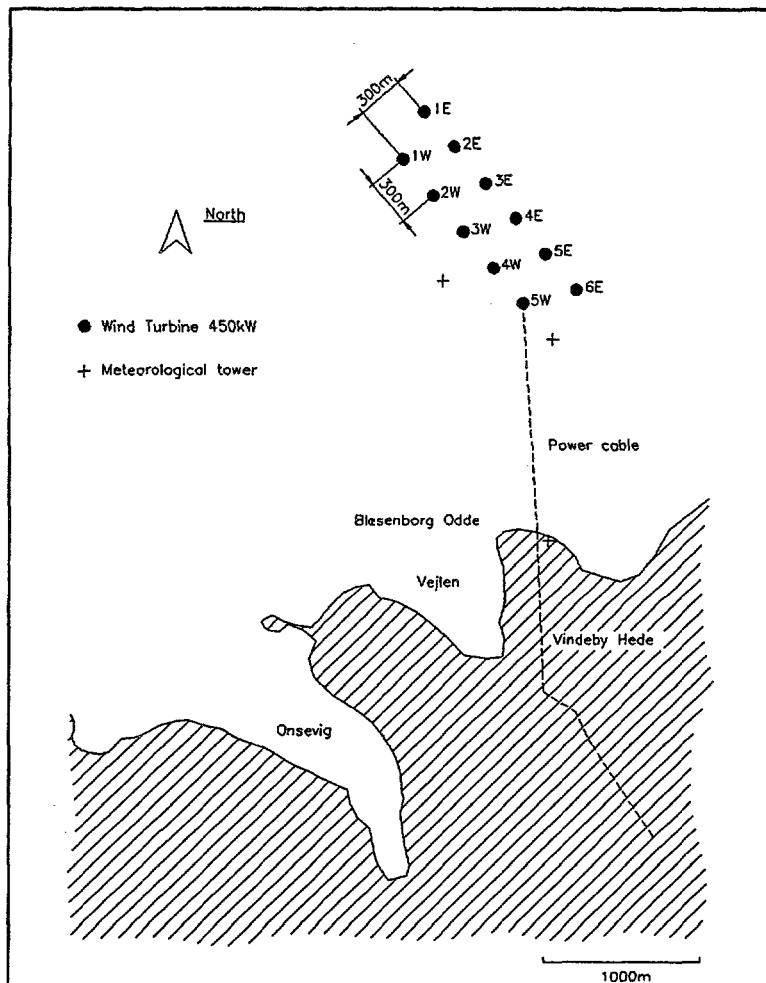The measurement system is described in detail in Barthelmie et al (1994).

4   REVIEW OF MODELLING METHODS WAKES AND WIND FARMS

The following short review of work in the field of wind turbine wake deficit and turbulence is included to broaden the scope of the present analysis of loads in wind farms offshore, and to prepared for possible further analysis of wind farm loads.

An early approach to the problem considered the turbines acting as distributed roughness elements over a wind farm containing a large number of machines (see review by Bossanyi et al., 1980). More recent work on this approach has been made by Frandsen (1992) and Emeis and Frandsen (1993). This topic on turbines acting as *distributed roughness elements* is treated in more detail in section 4.1.

However, the most common approach to the problem, initially presented in the classical paper of Lissaman (1979), implies taking into account individually each turbine wake of the wind farm and its interaction and superposition with neighboring ones, and thus calculate the detailed flow field, not its average distribution. Section 4.2 is dedicated to the individual wake behavior and section 4.3 to their superposition and the multiple wake case as it occurs in wind farms.

Frandsen (1992) compared the results of both approaches in a particular example; although further work in combining them will be desirable, this has to our knowledge not been done.

Section 4.2 starts with a description of the wake behavior, and continues with the kinematic-type models (Faxen, 1978; Lissaman, 1979; Milborrow, 1980; Vermeulen, 1980 1981, 1982; Katic et al., 1986; Voutsinas et al. 1990a), also known as explicit models, which have been used extensively because their simplicity and low computational cost. These models assume self-similar velocity defect profiles obtained from experimental and theoretical work on co-flowing jets. The wake growth rate is calculated as caused by the ambient turbulence, the turbulence created by the shear in the wake, and that created by the turbine itself; the magnitude of the maximum velocity deficit at each section is obtained from global momentum conservation. The ground effect is simulated by imaging techniques. These methods can give reasonable results if the adjustable coefficients are the appropriate ones.

The field models (Sforza et al. 1981; Taylor, 1980; Liu, 1983; Crespo et al. 1985, 1988, 1988a, 1989, 1990, 1991; Ainslie, 1986, 1987; Hernández and Crespo, 1991; Smith and Taylor, 1991; Taylor, 1993, Ansorge et al., 1994), also known as implicit models, calculate the fluid magnitudes at every point of the flow field. The field models require a substantially larger computer capability than the kinematic models. Today, their application is well within the possibilities of modern computers, for reasonable computing times. This is truth not only for single wakes, but also for multiple wakes combined in a wind farm, if appropriate simplifying assumptions are made, as will be explained later. The *field models* give an acceptable representation of the flow field, and a good insight of the processes governing the wake development.

Both the kinematic and field models use as starting or boundary conditions those at the end of the expansion region or at the beginning of the near-wake region. If a uniform velocity deficit is assumed, it can be estimated from the overall thrust on the machine, other possibilities are contemplated in section 4.2.

Kinematic and field models do not take directly into account the bodily movement of the wake with the large atmospheric eddies that is known as meandering, and is also examined in section 4.2. The problem of a single wake in uniform terrain is also dealt with in section 4.2. Section 4.3 is dedicated to the modelization of wind farms, taking into account the effects of both multiple wakes and terrain irregularities.

An presumed important issue regarding wind farm modelling is the interaction of several wakes, and how the velocity deficits and turbulence created by each machine accumulate at locations where several wakes meet. Different types of assumptions are made regarding the superposition rules. The most straightforward approach consists in adding the velocity deficits and turbulence kinetic energy; this and other alternative methods will be reviewed. The main problem is that any approach based on single-wake calculations would fail, because the ambient basic flow in which the wake diffuses is to some extent also affected by the wakes of the upstream machines, and it will also be an evolving one. A more correct approach would be to solve the flow equations

for the whole wind farm. At a first sight this looks, from a practical point of view, unfeasible for wind farms with a large number of wind machines; however, if some simplifying assumptions are made, namely the parabolic approximation, it can be shown that the field model for a single wake can be extended to the multiple-wake case, and be practically solved with reasonable CPU times, giving an acceptable agreement with experimental measurements. This issue is examined in more detail in section 4.3.

In section 4.3 is also contemplated the problem of how to take into account terrain effects, in wind farms of moderately irregular topography.

In many cases it is of interest for the designer to have analytical expressions that give an order of magnitude estimate of the values of the most important parameters and their tendencies, that can be used as an alternative to the numerical models. Regressions or correlations of this type were obtained by different authors to describe the single wake behavior, such as those of Crespo and Hernández (1986) Luken et al. (1986) and Högstrom et al. (1988) for the velocity deficit and the width of the wake; and by Vermeulen and Builtjes(1982a), Högstrom et al. (1988), Quarton (1989), and Crespo and Hernández (1993a) for the turbulence intensity. Taylor (1993) performs a parametrization of the calculated wake parameters as function of several non-dimensional input magnitudes, however, he makes a representation of the results in graphic form and does not make regressions. The case of wind clusters is covered in a review paper by Luken (1989) that proposes a correlation for the equilibrium value of the turbulence intensity reached in a row of turbines, using the experimental results of Builtjes and Vermeulen (1982). This point is discussed in more detail in section 5 of this report, where correlations are presented giving values of the average velocity, turbulence intensity, turbulence scale and width of the wake, at different positions of each machine in a row as functions of their operating characteristics. These correlations are obtained by making the best fit with numerical results from UPMPARK, and are validated by comparison with measurements of Vindeby wind farm.

In section 3.4 we present what we think is the state of the art regarding wind turbine wakes and wind farm modelization.

4.1 Turbines acting as distributed roughness elements

The models of Templin (1974), Newman (1977), Crafoord (1979) and Moore (1979), described by Bossanyi (1980), apply to infinite clusters; they assume a logarithmic wind profile for the unperturbed wind, that includes the ground roughness as a parameter. The presence of the turbines increases the roughness. From the modified wind profile the wind velocity incident over the machine can be obtained, and from it the power. Whereas the previous models assume a single logarithmic profile Emeis and Frandsen (1993) consider that below hub height there is a logarithmic profile with the real ground roughness, and above hub height another profile with a roughness related to the drag of the machine; both profiles match at hub height. Frandsen (1992) applies a logarithmic profile also above hub height and assumes the validity of a simplified form of the geostrophic drag law, from Rossby number similarity theory.

Bossanyi (1980) explains how the previous models can be extended for the case of finite clusters. Schmidt (1977) uses results obtained by Taylor (1969) for a step change in roughness to calculate the friction velocity at each row of turbines. Crafoord (1979), Moore (1979) and Musgrove (1980) consider a mixing layer of air above the ground and perform either a momentum or energy balance in this layer. It is assumed that sufficient mixing occurs so that, by the time the next row of turbines is encountered, the velocity deficit is averaged out across the whole mixing layer. The difference between the momentum (or energy) fluxes of two consecutive rows is due to the drag (or power extraction) of the turbine, the amount lost to the ground, and the amount entrained from greater heights through mixing processes. The difference between the last two quantities is termed the replenishment rate by Bossanyi (1980). He discusses several hypothesis about the way to estimate the parameters, in particular the mixing layer thickness and the replenishment rate, and compares the results.

4.2 Individual wakes

Description of the wake behavior.

As the flow approaches the wind turbine its velocity decreases and the pressure increases, and as it crosses the

rotor there is a sudden decrease in pressure. In the region immediately downstream of the rotor there are non-uniform deficits of pressure and axial velocity, associated to the axial thrust, as well as an azimuthal component of velocity, associated to the torque over the machine. Vortex sheets, associated to the variation of circulation along the blades, are shed from their trailing edge, and roll up in a short downstream distance forming tip vortices that describe helical trajectories. When the inclination angle of the helix is small enough, the tip vortex can be interpreted as a cylindrical shear layer, that separates the slow moving fluid in the wake from that in the outside. The velocity deficit can be considered as induced by the vortices. The difference in pressure between the fluid behind the rotor and that in the outside is supported by the centrifugal force due to the curvature of the streamlines. As we move downstream the cylindrical shear layer expands, the pressure increases, and the velocity inside the wake decreases until ambient pressure is reached. According to the simple actuator-disk theory, the velocity deficit at the disk itself is half of that in the expanded wake; this theory assumes that the flow is ideal and that the shear layer is infinitely thin. Although, because of turbulent diffusion, the thickness of the shear layer increases with downstream distance, if the length of this expansion region is sufficiently small it may not be a bad approximation to consider that the thickness of the shear layer is small compared to its diameter. The length of this expansion region is of the order of one turbine diameter.

As we proceed further downstream, turbulence diffusion becomes the dominant mechanism. Turbulence production is more important in the shear layer, because there the velocity gradients are larger. A well defined annular peak of turbulence intensity is observed, both experimentally (Alfredson et al., 1980; Green, 1986; Papaconstinou and Bergeles 1988; Högstrom et al., 1988; Højstrup, 1990; Ainslie et al., 1990; Smith and Taylor, 1991) and numerically (Hernández and Crespo, 1990, Crespo and Hernández, 1993a, Taylor, 1993), in this cylindrical shear layer. However, there are also significant velocity gradients both in the region inside the wake, as the velocity deficits created by the turbine are not uniform, and in the atmospheric flow, where the wind velocity changes with distance to the ground. Probably most of the turbulence that makes the wake to diffuse is at this stage created by the shear of the wake, mainly in the shear layer. However, the shear in the external atmospheric flow also plays an important role, at least in the redistribution of this turbulence production. As it will be shown later, the turbulence of the ambient flow is responsible for a nonuniform distribution of turbulence in the shear layer where the maximum peak is observed in the upper part (Crespo and Hernández, 1993a, 1996). Turbulent diffusion makes the shear layer thicker, and at a certain distance downstream, of the order of two to five diameters, it has penetrated up to the wake axis. This marks the end of the near wake region.

After the near wake region, there is a transition region leading to the far wake region where the wake is completely developed, and, in the absence of ambient shear flow, it could be assumed that the perturbation profiles of both velocity deficit and turbulence intensity are axis-symmetric and have self similar distributions in the cross-sections of the wake. The only overall properties of the turbine that appear as parameters in these profiles are the thrust of the turbine and the total turbulent kinetic energy produced by the rotor itself. This property of self-similarity of the velocity profiles is the basis of the kinematic models of wind turbine wakes. However, the presence of the ground and the shear of the ambient flow invalidate the assumption of axial symmetry and - to some extent - the hypothesis of self-similarity. It has been observed both numerically and experimentally that in the far wake the maximum turbulence intensity (Crespo et al. 1990; Højstrup, 1990) is located above the turbine axis, and the point of maximum velocity deficit is usually below the turbine axis (Crespo et al. 1985, 1988 and 1988a; Luken et al. 1986). The maximum of turbulence intensity is about a turbine radius above the axis, and this is probably related to what happens in the near wake. For large enough downstream distances the perturbation due to the machine is expected to be diffused and become very small, and the velocity gradients will only be due to the ambient shear flow; consequently, the ambient turbulence there is larger than that due to the wake itself.

Kinematic models for single wakes

It has already been indicated that the kinematic models use self-similar velocity defect profiles obtained from experimental and theoretical work on co-flowing jets. The wake description does not consider the expansion region and gives different types of profiles for the near wake, transition and far wake regions. For the far wake these profiles are self-similar and in the near wake there is usually a central core of constant velocity and diminishing radius; when this radius becomes zero, the near wake ends. Voutsinas et al. (1990a) and Lissaman (1979) use the velocity profiles proposed by Abramovich (1963). Vermeulen (1980) uses a Gaussian type of

profile quite similar to that of Abramovich (1963). Katic et al. (1986) simplify the problem further and assume a top-hat profile everywhere.

The initial velocity deficit is usually obtained from the thrust coefficient of the machine. Voutsinas et al. (1990) relate it to the power given by the machine, the advantage being that the power curve is usually more available than the thrust curve.

In all the cases the reference value of the velocity deficit at each section is obtained from global momentum conservation, except Voutsinas et al. (1990), claiming that they obtain it from mass conservation, based on the fact that the agreement with the results of Taylor (1990) are better; however, it is not clear what do they mean by this, in particular how do they take into account the mass entrainment through the lateral surface of their control volume (chapter 9 of Schlichting, 1972)). As a matter of fact, when applying the classical equation of momentum conservation (see for example Vermeulen, 1980), it is implicitly assumed that also mass is conserved.

Lissaman (1979) calculates the wake growth rate as caused by the sum of the ambient turbulence and the turbulence created by the shear in the wake. Vermeulen (1980) added another term taking into account the turbulence created by the turbine itself; however, in a later work, Voutsinas et. al (1990a), based on the experimental results of Taylor (1990), consider that this effect is negligible. Katic et al. (1986) assume that the wake radius increases linearly with downstream distance; the proportionality constant is adjusted by comparison with experiments.

The ground effect is simulated by imaging techniques. Lissaman (1979) includes a symmetrical turbine and adds the velocity defects of both the real and image ones, so that drag conservation is satisfied. He points out that the vertical dividing plane between two adjacent identical rotors abreast can be treated exactly like the ground plane of a single rotor. However, in the case there is ground, the total drag is not really conserved because of friction; the three-dimensional models show that there is a slight total deficit decrease as the downstream distance increases. According to the image procedure, the velocity defect will be doubled at the ground, whereas in reality any perturbation should be damped to zero. Crespo et al. (1985, 1986) and Kambezidis et al. (1990) use an anti-symmetric wake so that velocity defects are subtracted and give zero perturbation at the ground; then, if it is considered that in reality the ambient velocity is not uniform, as the kinematic models assume, but that it goes to zero at the ground, the perturbed velocity calculated will also be zero at the ground. However, although this alternative procedure eliminates the previously mentioned inconsistency occurring near the ground, it is not clear that it will give a more valid result in the rest of the flow field, where the ground effect is not so dominant. Another procedure followed by Voutsinas et al. (1990) consists in superimposing the squares of velocity defects, and taking into account the variability of the incident velocity to estimate the location of the image turbine; however, it does not look as though the procedure can handle the previously indicated difficulty. We think that the ground effect is an intrinsic difficulty of all the kinematic models that assume axial symmetry, and consequently there is no satisfactory way in which they can handle it; the ground effect can only be treated appropriately with the 3D models.

In spite of all the previous difficulties, the kinematic models give in many cases results in quite a good agreement with the experimental evidence if appropriate values of the parameters appearing in them are chosen (Faxen, 1978; Alfredson et al., 1980).

Field models for single wakes

Sforza et al. (1979, 1981) described the wake using only the linearized momentum equation in the main flow direction, with constant convective velocity and a constant eddy diffusivity; besides, they made the parabolic approximation. For bi-dimensional configurations they obtained analytical solutions giving reasonable wake shapes; in the 3D case they integrated numerically the equation using an alternating direction implicit (ADI) method. They made small-scale experiments and compared them with their numerical results. Considering the simplicity of the model the comparison was reasonable.

A numerical model based on the solution of the flow equations for wakes in neutrally-stratified atmospheric boundary layers was given by Taylor (1980). He considers an eddy viscosity gradient closure scheme. The wake

effect is supposed to be small enough for the equations to be linearized around a basic flow. A boundary layer approximation is used. The model is two dimensional and presents results integrated across turbine rows. Coriolis forces are retained and the pressure gradients are given by the geostrophic wind. This assumption is not justified because the length scale of the wake is not large enough to make the Coriolis forces play a dominant role; as a matter of fact we think that they can be neglected, and the pressure field will be the one resulting from the momentum conservation in the wake. If the parabolic approximation is made, pressure variations across the wake could be neglected in the momentum equation for the main flow direction, but not for the momentum components in the transverse direction, particularly when there is neither axial nor bi-dimensional symmetry. Taylor (1980) compares his results with those of other models, both kinematic and turbines acting like distributed roughness, and with experiments of Builtjes (1978), and obtains reasonable agreement, but he realizes that for the backrows the linear superposition of the effects of several rows of turbines may lead to low or even negative power outputs.

Liu et al. (1983) proposed another model which is three-dimensional and includes atmospheric stability effects; however, they neglect the diffusion due to the turbulence originated in the wind turbine and that caused by the shear in the wake, and consider the turbulent viscosity and the diffusion coefficients to be those of the unperturbed flow. As Taylor (1980), they also retain Coriolis forces and assume that the pressure gradients are given by the geostrophic wind.

Ainslie (1986, 1988) developed a parabolic model which assumes axis-symmetric wake flow. Pressure variations are uncoupled in the analysis and only the continuity and the main momentum equations have to be solved. Consequently, the model is not able to deal neither with ground effects nor with variations of ambient flow conditions with height. The turbulent shear stresses are described using an eddy viscosity closure scheme in which the eddy viscosity is represented by a simple analytic form based on Prandtl's free shear layer model, but also including a contribution due to the ambient turbulence. This eddy viscosity is an average value over a cross-section and variations of turbulent properties across the wake cannot be estimated from the model. At small downstream distances the eddy viscosity is modified by an empirical filter function to account for the lack of equilibrium between the mean velocity field and the developing turbulence field. Several constants appear in the problem that are adjusted by comparison with some particular experiments, but it is not clear how generally valid these are in other cases. The model is fairly simple and gives reasonable results when compared with wind tunnel experiments; for large scale experiments the results are corrected taking into account meandering effects as it will be indicated at the end of this section.

Crespo et al. (1985) developed the UPMWAKE model in which the wind turbine is supposed to be immersed in a nonuniform basic flow corresponding to the surface layer of the atmospheric boundary layer; further development of the model is presented by Crespo and Hernández (1989). The properties of the nonuniform incident flow over the wind turbine are modelled taking into account the atmospheric stability, given by the Monin-Obukhov length, and the surface roughness. This basic flow, described by analytical expressions obtained from theoretical considerations and experimental results given by Panofsky (1984) is supposed to be perturbed by the wind turbine. The equations describing the flow are the conservation equations of mass, momentum, energy, turbulent kinetic energy, and dissipation rate of the turbulent kinetic energy. The modelization of the turbulent transport terms is based on the k-ε method for the closure of the turbulent flow equations. This set of equations has been solved numerically using the SIMPLE algorithm proposed by Patankar and Spalding (1972). Finite-difference methods have been used in the discretization of the equations. The parabolic approximation has been made, and the numerical solution of the parabolic equations has been carried out by using an alternating direction implicit (ADI) method. The developed wake model is three-dimensional and pressure variations in the cross-section have to be retained in order to calculate transverse velocities.

A simplified version of UPMWAKE, where all convection was assumed due to the ambient unperturbed flow was also presented by Crespo et al. (1985). The idea was very attractive, because it was still possible to retain the three-dimensional character of the problem, and reduce the system of partial differential equations from seven to three. However, this approximation is not justified, except very far downstream where the wake perturbation is small, and although in some cases the results obtained were in quite a good agreement with the full model and with experiments, in other cases the results, particularly in the near wake, were wrong; for these cases, the convergence of the seven equation model, for iterations in the transverse plane, was very slow. Most of UPMWAKE calculations that have been published correspond to the seven equations code.

Crespo et al. (1986, 1988, 1989 and 1990) have compared UPMWAKE results with experiments from wind tunnel experiments by Luken et al. (1986) and from field experiments with full-scale machines by Taylor et al. (1985). The wake problem has also been solved numerically by using the PHOENICS code (Hernández and Crespo, 1990), and the corresponding results agree well with those of UPMWAKE. The code can predict effects such as the downwards displacement of the wake centerline, the upwards displacement of the point of maximum added turbulent kinetic energy, and the different vertical and horizontal growths of the wake width. However, some discrepancies with the experiments of Taylor (1985) were found in the initial wake region, where the predicted velocity deficits were smaller than the measured ones. More recently, Crespo and Hernández (1993a, 1996), based on the results of the code, have developed correlations to calculate the turbulence intensity both in the near and far wake, and compared it with a great number of experiments (many of them compiled by Quarton, 1989), both of wind tunnel (Vermeulen, 1978, 1980; Milborrow and Ross, 1983; Green and Alexander, 1985; Talmon, 1985; Ross and Ainslie, 1981, 1982 and Alfredson et al., 1980) and field experiments (Högstrom et al., 1988; Baker and Walker, 1985 and Cleijne, 1992). The agreement is acceptable, and shows that UPMWAKE may be a useful tool to estimate the turbulence characteristics. In those papers Crespo and Hernández (1993a, 1996) also propose a simple method to obtain the turbulence spectra in the wake from the values of k and ϵ, obtained from UPMWAKE, and they compared their results with the experiments from Højstrup (1990), obtaining a good agreement in some cases; the results of this procedure to calculate the spectra are compared in another chapter of this report with measurements in Vindeby wind farm. Some of the results obtained for the turbulent length scale needed to estimate the spectrum seem to be smaller than those measured and presented in another chapter of this report. Possible reasons for this discrepancy are that, on one hand, UPMPARK does not take into account the small scale (large frequency) turbulence originated by the boundary layers of the blades of the wind turbines, and, on the other hand, that the wind turbine is capable of responding to low frequency fluctuations of wind speed, and extract energy from the wind in the low frequency (large scale) range (Højstrup, 1990). Scheppers (1995) has also used UPMWAKE to combine it with a dynamic load code and noted that the agreement with experiments is good but it could be better if a displacement of the origin to account for the development of the expansion region is considered. The physical reason for this displacement is not clear; because although the expansion region is located downstream of the rotor, there is a shear layer right after the rotor where the diffusion process should start.

Smith and Taylor (1991), and in more detail Taylor (1993), present a non-symmetric two-equation model that is in many ways similar to the three equation model of Crespo et al. (1985). They neglect transverse velocities so that they just solve the momentum equation in the axial direction. To model the turbulent viscosity they use a k-L method, where the turbulent length scale L is related to the width of the wake, obtained by fitting a Gaussian profile to the calculated profile. The value of the dissipation rate of the turbulence kinetic energy, ϵ, is obtained from an algebraic combination of k and L, and consequently a partial differential equation for ϵ is not needed. We suppose that the same type of problems previously mentioned for the three-equation version of UPMWAKE should also appear in this case. However, the results they obtain when comparing with their wind-tunnel experiments are very good, but on the other hand, when comparing with full-scale Nibe experiments they obtain that the model over-predicts; they attribute this discrepancy to meandering and obtained a better agreement when they corrected for this effect using the method proposed by Ainslie (1988) that will be discussed later. The starting conditions are imposed at the end of the near wake where a gaussian velocity deficit profile is imposed. This correction is even larger than that suggested by Scheppers (1996) to UPMWAKE, that was only to account for the length of the expansion region. In this case, besides the previous objection, there is a contradiction of Taylor's results with this assumption, because he shows a quite nice annular peak of turbulence intensity, that compares quite well with experiments, but that should be precisely in the near wake.

In the initial region of the wake were observed some important discrepancies between the results of UPMWAKE and the Nibe experiments (Taylor, 1985). Crespo et al. (1990, 1991) instead of the boundary layer approximation used in UPMWAKE, propose an elliptic model to deal simultaneously with the axial pressure gradients and diffusion effects, retaining both the axial and transverse diffusion terms. This way they obtained a model simultaneously describing the evolution of the expansion region and the diffusion processes. No fundamental differences with the elliptic model were found, and the displacement of the origin apparently was not necessary. Other elliptic models have also been proposed by Voutsinas and Huberson (1993) and Ansorge et al. (1994). The improvement in the agreement with experiments when comparing the elliptic and parabolic codes is not too important and does not justify the additional computational effort, that is considerable.

Another reason for the discrepancies between models and experiments in the near wake may be the uncertainty in the initial velocity defect, which is assumed to be either uniform or of a prescribed shape (gaussian in Taylor, 1993), and is obtained from the thrust coefficient. Zervos et al. (1988) relate the initial wake development to the aerodynamics of the rotor, using a vortex-particle method governed by the vorticity transport equations and the Biot-Savart law; they do not need initial data to start the calculation of the wake, but the validity of the solution is limited to the short initial expansion region, where diffusion effects can be neglected. In general, non-uniform values of axial azimuthal velocity components at the end of the expansion region could be obtained using a classical blade element model, a strip model (Wilson et al, 1976) or even vortex particle and lifting line methods, such as those proposed by Zervos et al. (1988) or Voutsinas and Huberson (1993). The blade element and strip methods include the effect of drag on each blade section, and this can be used to estimate the dissipated power and the turbulent kinetic energy produced, whereas vortex particle methods which do not include aerodynamic losses do not have this possibility. Attempts have been made by Cleijne et al (1993), Voutsinas and Huberson (1993), and Crespo et al. (1993c) to put together field and vortex particle models so that the field model uses as boundary conditions the results obtained from the vortex particle method; although some improvement relative to experiments is noted in some cases, they do not justify the complications and additional computing cost.

All the previous models solve the Reynolds averaged turbulence flow equations, and use a closure scheme, based on zero, one or two equation models to calculate the turbulence transport terms. In all cases use has been made of an eddy viscosity, which implicitly assumes an isotropic turbulence field, that obviously is not correct. The use of the Reynolds stress equations to calculate this type of wakes has been made only occasionally. Ansorge et al. (1994) have used a Reynolds-stress turbulence model based on the commercial code PHOENICS, and obtained promising results, although the computational effort may still be too large from an engineering point of view.

In general, the field models give an acceptable representation of the flow field, and a good insight of the processes governing the wake development, better than the kinematic models.

Meandering of the wake

The agreement of field models with wind tunnel experiments is in general better than with field experiments; one reason for the disagreement is the meandering of the wake. The individual wakes calculated by both kinematic and field models do not take directly into account eddies that are large compared to the size of the wake and move it bodily, a phenomenon known in studies of atmospheric dispersion as meandering. Usually, in wind tunnel tests this effect is not included either. The maximum velocity deficit will be smaller than the one predicted by the theoretical models or wind tunnel tests, and, on the other hand, additional velocity fluctuations will appear that can be interpreted as an additional contribution to the turbulent kinetic energy. Baker and Walker (1985), Ainslie (1986) and Taylor (1993) took into account meandering by assuming that the large eddies have a size that increases linearly with downstream distance, x, and is proportional to the standard deviation of the wind direction, σ_θ. Högstrom et al. (1988) argue that this is wrong because σ_θ is caused by eddies of all sizes, including those that are smaller than the wake diameter, and take for their analysis a value of the large eddy size given by $0.053x$, based on the results of some oil-fog experiments.

4.3 Wind farm models

Interaction of several wakes

In a wind farm there are many interacting wake, and a wind turbine may be affected by the wakes of several machines located upstream. Usually, wind farm codes rely on the results of single wake calculations, and use some superposition assumption to take into account the combined effect of different wakes. The linear superposition of the perturbations created by wakes of different machines in a wind farm model was first used by Lissaman (1979); this assumption fails for large perturbations as it overestimates velocity deficits and it could lead to the absurd result of negative velocities when many wakes superimpose. Katic et al. (1986) assumed instead linear superposition of the squares of the velocity defects; then, the cumulative effect when there are many wakes will be smaller than for linear superposition, and, in some cases, this assumption gives better agreement with experiments than the linear one. Voutsinas et al. (1990, 1993) formulated an explicit energy

equation by setting the total energy loss at each point of the flow field equal to the sum of the individual energy losses of each machine, in this way they obtain the velocity field and in turn they calculate the incident velocity on each machine by making an average over the disk. When evaluating the individual energy losses of each wake they consider the difference between the wake velocity and the inflow velocity in the machine that creates the wake, whereas Katic et al. (1986) consider the difference between ambient and wake velocity; for small velocity defects both methods should give similar results.

Smith and Taylor (1991) found, for a particular experimental configuration of two machines in a row, that the wake of the downstream machine recovers more rapidly than the one upstream, so that at the same relative position the velocity defect is smaller in the downstream machine; this result contradicts the qualitative behavior predicted by the two previous superposition assumptions, and may be explained because the turbulence levels and shear stress profiles generated by the upstream machine will enhance diffusion of momentum, and lead to a faster recovery in the downstream machine. By making a number of gross assumptions concerning the momentum transfer within the downstream wake that is imbedded in the upstream wake, Smith & Taylor (1991) are able to formulate a semi-empirical superposition law that works quite well, but it is cumbersome and can only be applied for the interaction of the wakes of two turbines in a row. For small velocity defects the method reduces to the linear superposition assumption; but it is not clear in which limit is the quadratic superposition assumption recovered; Voutsinas et al. (1990, 1993) claim that their explicit energy equation gives results similar to those of this method without giving a physical reason for it.

When there are many turbines in a line it is observed experimentally Van Leuven (1992) that the first turbine produces full power, there is a significant decrease of power at the second turbine, and, after the third one there is practically no further loss. Based on this observations, and on the results of the calculations of Crespo et al. (1990), Van Leuven (1992), assumed in his wind farm model that on each turbine only acts the wake of the closest one upstream, and obtained good agreement when comparing with the measurements of the Zeebrugge Wind Farm. This is also supported by the findings of section 8 of this report.

Regarding the increase in turbulence intensity for many turbines in a line, Builtjes and Vermeulen (1982) carried out an experimental investigation in wind tunnel with wind-turbine simulators. They found that the turbulence intensity reaches an equilibrium value after three to four rows of turbines, and that in the second row of turbines the turbulence intensity is a maximum, higher than the equilibrium value. According to the previous paragraph, the saturation of turbulence intensity is reached after that of the velocity deficit, and the procedure used by Van Leuven (1992) will predict the turbulence saturation, but will shift its location upstream. Luken (1989) proposed a simple correlation to calculate the equilibrium value of turbulence intensity as function of turbine spacing, which will be discussed and compared with those obtained in another chapter of this report, based on the UPMPARK model an measurements in Vindeby.

Crespo et al. (1990) applied their elliptic model to study the interaction of two wakes of two turbines for two configurations: abreast and in a line. Agreement with experiments was found to be good, and, when comparing with other superposition assumptions, it was found that the linear superposition worked well for the case of two machines abreast, in which velocity defects in the interference region are small; on the other hand, for the two turbines in a row the linear superposition, as expected, overestimates the velocity defect. The previously mentioned method (Van Leuven, 1992) of considering that over each turbine only acts the wake of the closest one upstream gives also good agreement when comparing with the results of the elliptic model.

However, looking at the results of the elliptic model of Crespo et al. (1990), it can be observed that the really elliptic effects, such as axial pressure variations, occur only very close to the turbine, so that the parabolic approximation may not be a bad approximation to study wake interaction over most of the region were this interaction occurs. On the other hand, to extend the fully-elliptic code to a wind farm with many machines, besides consuming a lot of calculation time, will surpass the capacity of most computers, and will not be a practical tool to model wind farms. Based on this idea Chacon (1994) and Crespo et al. (1993, 1994) have developed a code named UPMPARK, that is an extension of the parabolic UPMWAKE code for a single wake to the case of a wind farm with many machines. No assumptions are required regarding the type of superposition nor the type of wake to be used, as all the wakes and their interactions are effectively calculated by the code. A brief description of UPMPARK follows and a more complete one is given in section 5 of this report.

The conservation equations solved are the same ones of the single wake code, UPMWAKE, as specified in Crespo and Hernández (1989), and turbulence is closed using a k-ε model. The wakes of the machines diffuse in an ambient flow that represents the surface layer of the atmospheric boundary layer, in which instability effects are retained through the Monin-Obukhov length. For uniform terrain, this ambient basic flow is the same over all the wind farm; however, the code could also handle moderate terrain irregularities, using a superposition assumption for the effects of terrain and the wakes (Crespo et al., 1993b), that will also be reviewed below. At infinity, in regions not perturbed by the wind turbines, and in the upstream section, boundary conditions that correspond to the ambient flow being unperturbed are imposed. Every turbine that is found at each cross-section of the farm, as we progress in the marching procedure associated to the parabolic model, acts as a source (or sink) of the three components of velocity, k, and ε. The number of grid points should be large enough to contain the whole cross-section of the wind farm, and to consider that the lateral sides are at infinity. As the code is parabolic, there is no limit to the downstream distance, except for the fact that if the wakes diffuse very much, the number of grid points may not be large enough to be able to apply the boundary conditions at infinity. The case of wind turbines in a row is particularly suited for this code.

UPMPARK has been validated by comparison with measurements of the following wind farms: Nibe, Zeebrugge, Sexbierum and Vindeby.

Orographic effects.

Usually in wind farm models the terrain is assumed flat and the unperturbed wind velocity uniform. These assumptions are not correct in many cases of interest; as it is well known, terrain irregularities can be used to enhance or concentrate wind power. For terrains that are moderately complex a simple procedure to handle this problem is to add linearly the velocity perturbations due to the terrain and the wakes; that procedure was applied to the Ampurdán wind farm (Crespo et al., 1986, 1988a), and apparently the results were satisfactory. A similar procedure has been used by Van Leuven (1992) to take into account the interaction of an obstacle and turbine wakes in the Zeebrugge wind farm. Nevertheless, in all the previous cases there were simultaneously interactions of terrain and several wakes, creating some uncertainty about the validity of the results; as it is well known, the linear superposition of several wind turbine wakes overestimates the velocity defect, as indicated in the previous section. Crespo et al. (1993b) studied the Monteahumada wind farm, in which the velocity irregularities of the terrain and the velocity defect created by a single wake interact and are both of a similar order of magnitude; this configuration is thus appropriate to examine the validity of the assumption of linear superposition of wake and terrain effects. Although the data were scarce and not easy to interpret, the work shows that for a moderately irregular terrain, the linear superposition of wake and terrain effects gives good results, whereas for the interaction of two wakes with perturbations of a similar order of magnitude, this assumption is not valid.

Voutsinas et al. (1990) give a procedure to take into account non-uniformity in wind velocity and the curvature of the streamlines in wind farms with small terrain irregularities, that is similar to the linear superposition; some sample calculations are made, but no experiments are presented to validate the method. Taylor and Smith (1991) made measurements in wind tunnel that show that the changes in the wake characteristics due to topography may be important. Hemon et al. (1991) study theoretically the modification of aerodynamic and near-wake characteristics due to the terrain. Second-order corrections to the linear superposition of terrain and wake effects are given by Van Oort et al. (1989), that have been calculated using PHOENICS; it has been found that near the ground the terrain irregularity creates additional turbulent diffusion that diminishes the wake effect; on the other hand, above the apex of a hill the streamlines concentrate, thus enhancing wake defects.

Crespo et al. (1993), Günther et al. (1993) and Ansorge et al. (1994) have also used the commercial code PHOENICS to model the interaction of wakes with obstacles and terrain irregularities.

4.4 State of the art and summary

There are many different models to simulate the behavior of wind-turbine wakes and wind farms. Most of them are based on a deterministic simulation that takes into account each individual wind-turbine; those wind farm models that consider the turbines as distributed roughness elements are not much used now, although they may be of interest in a future to predict global changes in wind characteristics originated by the large wind-farms

that are foreseen.

Many of the models proposed by the different authors show an acceptable agreement with the experiments with which they are compared. The problem usually is that the assumptions and coefficients that have been chosen are such that the agreement with some particular experiments is good, but its validity has not been checked in more general situations. The models with less simplifying assumptions are better suited to deal with different configurations and to reproduce more details of the wake development. For example, an axis-symmetric model will never be able to reproduce the peak in turbulence intensity in the upper part of the shear layer in the near wake. In general, the most complicated and sophisticated models have more possibilities to reproduce more details and characteristics of the flow field, although in many cases the physical reasons for the hypothesis used, particularly in those aspects related to turbulence modelling, are not always clear.

The classical wind farm model relies on an individual wake model, usually a kinematic model, and some sort of superposition assumption. In general, the superposition assumptions are not justified physically, and can even lead to absurd or contradictory results; the corrections and alternatives to handle the physically unrealistic situations are either not justified or difficult to implement.

There has been a general opinion that the field models are too complicated and that it is impossible to extend them to a wind farm with many turbines. We don't think that this is the case any more. The UPMPARK model that retains all the characteristics of one of the most complete, non-symmetric, k-ϵ wake models, UPMWAKE, can be successfully ran in a workstation in reasonable short times for large wind farms such as Sexbierum or Taendpibe, or even in a PC for wind farms with a smaller number of machines. The most important simplifying assumption used by UPMPARK is the parabolization of the mathematical problem in the direction of the main wind direction.

Formerly, more emphasis was put in the calculation of velocity deficits and wind farm efficiency regarding energy production. Nowadays, the calculations are more oriented to other issues, such as the estimation of the structural and fatigue behavior, or the fluctuations in electrical energy production of machines affected by upstream wakes. To estimate these magnitudes it is necessary to know the turbulence characteristics of the flow (turbulence intensity, correlations and spectrum), and wind shear, that obviously can not be supplied by simple kinematic models.

An important issue is the non-isotropy of the turbulence of the ambient atmospheric flow, and the tendency to isotropy in the wakes. This problem can not be dealt with the k-ϵ or eddy-viscosity wake models. The use of Reynolds Stress models leads to a tremendous increase in the mathematical difficulties, that we do not think that can be treated in codes of general engineering use. Alternative ways should be explored.

Probably, one of the most difficult issues that has not been treated satisfactorily is the choice of the appropriate input parameters defining the ambient unperturbed flow, particularly for complicated terrains. Usually, the comparison with wind tunnel experiments is reasonable and precise, but when comparing with field experiments there are many difficulties; effects like meandering have never been satisfactorily modeled. Results from experimental and modelling studies for terrain with changing roughness, and the appearance of internal boundary layers, such as for wind farms located near the coast or offshore, should be incorporated into the description of the ambient flow. For a terrain that is moderately irregular, UPMPARK assumes a superposition of the perturbations due to the wakes and those of the terrain, estimated either from measurements or from codes such as WASP. However, for complicated topography this approach may not work. The detailed solution of a code that takes into account simultaneously terrain and wind-turbine wakes will be too difficult, and with a lot of uncertainties regarding the appropriate boundary conditions. Some work has been done, and more is needed, to estimate the local effects of interference of single wakes and terrain irregularities, the problem is that it is difficult to envisage general solutions, and we will always be solving particular problems, that at most could gives an idea of the tendencies of the results. A possible alternative for cases in which turbine spacing occurs in distances small compared to the characteristic length of variation of terrain irregularities, could be to treat the problem as the flow over an irregular terrain of changing roughness, as indicated in section 5.

Finally, the case of offshore machines should be mentioned, to which this report is dedicated, and, in which, besides the effect of surface roughness that is dependent on atmospheric conditions, there are many other

problems regarding the additional loads due to the waves and water currents that should also be modelled.

5 APPLICATION OF UPMPARK TO OFFSHORE WIND FARMS

5.1 Model Description

The equations solved are the same ones of the single wake code, UPMWAKE, as specified in Crespo and Hernández (1989), namely: the conservation equations of mass, three components of momentum, energy, turbulent kinetic energy, k, and its dissipation rate, ϵ.

The wakes of the machines diffuse in an ambient flow corresponding to the surface layer of the atmospheric boundary layer, which is described by three parameters: the surface roughness of the ground, the friction velocity, and the Monin-Obukhov length. The friction velocity may be substituted by the wind velocity at a reference height. The inverse of the Monin-Obukhov length increases with atmospheric stability, and is zero for neutral atmospheres. This ambient basic flow is the same over the whole wind farm for the cases solved below; however, the code could also handle moderate orographic irregularities, using a superposition assumption for the effects of terrain and the wakes, as explained by Crespo et al. (1993b).

The computational domain is a rectangular box limited by the ground and an upper horizontal surface, two vertical surfaces parallel to the wind, and two vertical surfaces normal to the wind that correspond to the upstream and downstream boundaries. The two lateral surfaces parallel to the wind and the upper horizontal surface are supposed to be far enough from the machines, so that the boundary conditions correspond to the unperturbed ambient flow. The same condition is applied in the part of the upstream section where there are no turbines, and in the ground. As the model is parabolic no conditions are needed in the downstream section.

The main difference with the single-wake code is that now source terms should be introduced simultaneously in all the turbines that are found at each cross-section of the farm, as we progress in the marching procedure associated to the parabolic model. The number of grid points should be much larger now, as the computational grid should contain the whole cross-section of the park, and should allow to put boundary conditions in the lateral and upper surfaces as though they were at infinity. The source terms essentially represent a jump in the three components of velocity, potential temperature, k and ϵ; however, in the cases presented below we have only considered that there is a jump in the velocity component normal to the rotor plane. As the model is parabolic, it can not take into account the local pressure changes associated to the expansion in the near wake; then, the turbine is simulated by a circle whose radius is that of the expanded wake, calculated from the physical radius and the thrust coefficient, using the classical ideal actuator-disk theory. Then, the diameter of the machines may change, not only because there are different machines, but also because of changes of the thrust coefficient. The circle of the rotor is represented by an octagon. The size of the grid cells in transverse directions, that is uniform over the whole domain, is selected properly, so that all the turbines can be represented in an approximate way by using an appropriate number of grid cells forming an octagon.

The computing difficulties increase as the frontal part of the park becomes large compared to the size of the turbines. With a PC we are able to handle a rectangle whose width is a maximum of about 15 turbine diameters. For the more unfavorable situation in Vindeby, SW winds as shown in Figure 3.1, the farm has a width of about 50 turbine diameters, and the code has to be implemented in a workstation. As the code is parabolic, there is no limit in the downstream distance, except for the fact that, if the wakes spread very much, the number of grid points may not be large enough to apply the boundary conditions at infinity. The case of wind turbines in a row is particularly easy to handle with UPMPARK.

Surface roughness in the sea.

To simulate the ambient atmospheric conditions UPMPARK has three parameters: turbulent friction velocity, surface roughness and Monin-Obukhov length. Although there is no general rule for their choice, the normal procedure is that, in each situation, the ambient flow is as closely reproduced as it is possible. However, in some cases the available measurements are scarce and there is an uncertainty in the choice of the above parameters, so that it is convenient to have additional procedures that, based on the physical interpretation of these parameters, give more information about their value. For land, these may be the tables relating the surface roughness to the terrain characteristics or the graphs relating the Monin-Obukhov length to the climatological

and terrain characteristics, through the Turner or Pasquill classes (see for example Panofsky, 1984). However, for the water surface the roughness is not in general an independent datum, and it has to be estimated from the wind characteristics as described in section 6, where the approach of Charnock is reproduced.

It is found, section 6, that the Charnock approach underestimates the sea surface roughness and thus σ_u. Here, we offer an empirical fit to measured data. The nondimensional surface roughness is assumed to be a function of x:

$$\frac{z_o}{z_{ch}} = f(x) \qquad (5.1)$$

where

$$x = \frac{\rho\, u_*^3}{g\, \mu}, \qquad (5.2)$$

and z_{ch} is

$$z_{ch} = \frac{A u_*^2}{g} \qquad (5.3)$$

Figure 5.1 *Non-dimensional roughness, $z_o/z_{och} = z_o g/(A u_*^2)$, as function of $\rho u_*^3/(g\mu)$.*

A is given in section 6. An average value of 0.015 is chosen here. Several experimental results taken from Højstrup et al. (1994), corresponding to measurements in Vindeby and Nibe wind farms, have been put in this nondimensional form and are represented in Figure 5.1. The points fall approximately on a curve that - for large enough values of the second parameter - give a constant value of the first parameter, recovering for z_0 the functional dependence predicted by Charnock, although affected by a larger factor than the one originally predicted by Charnock. The results of Figure 5.1 can be fitted by the following an analytical expression, corresponding to the function appearing in equation (5.1):

$$f(x) = \frac{87881}{x^2} - \frac{57.30}{x^{-\frac{1}{2}}} + 4.48 \qquad (5.4)$$

For large enough values of the nondimensional turbulent friction velocity, Charnock's equation is recovered, except for a factor. The modified coefficient A of (5.3) should be 0.067. Although Charnock's equation may be the appropriate one in many applications of wind energy, nevertheless the modification proposed here is still of interest in some practical cases.

If the analysis is made with surface tension instead of viscosity, the nondimensional parameter, x, of equation (5.1) and the function f of (5.1) will be different, although the end result is expected to be the same, because in both cases z_o/z_{ch} is expressed as a function of u_* made non-dimensional with physical properties of air, that are not expected to change dramatically from one case to another. A similar result was obtained by Wu (1994).

Graphic output of upmpark.

The graphic output of UPMPARK allows to visualize the behavior of the different flow magnitudes in the wakes, and to obtain a physical interpretation of the multiple-wake interaction process. As an example, in Figures 5.2 to 5.5 are presented contour lines of turbulent kinetic energy, k, and velocity deficits in different cross sections of the Vindeby wind farm. The flow conditions for the calculations are: a wind speed of 10 m/s and a surface roughness $z_o = 10^{-3}$ m; the corresponding friction velocity is 0,4 m/s, that approximately satisfies equation (5.2), (5.3) with the modified value of $A = 0.067$. Figures 5.2 and 5.3 show the contour lines for the
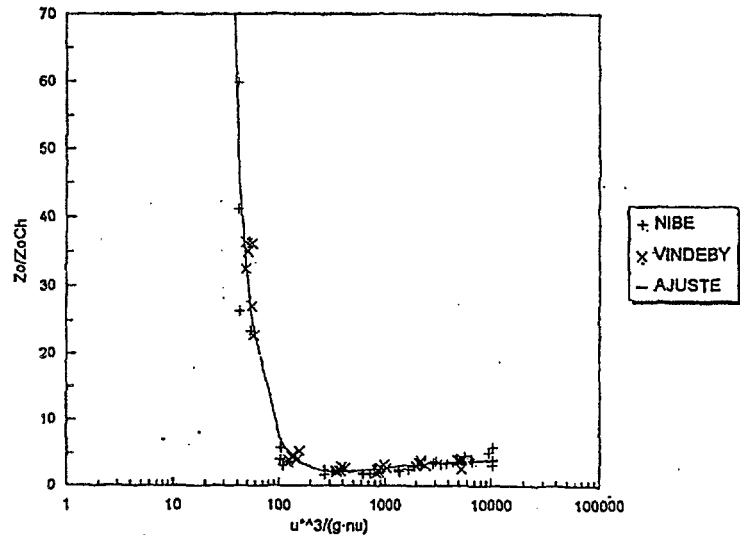
turbulent kinetic energy, k, and the velocity deficit, respectively, in a vertical plane containing the centers of turbines 1E to 6E for NW winds. In Figure 5.2 can be observed how k increases as we move to downstream wakes, and that in the wake of the first machine the values of k in the upper part of the wake are larger than in the lower part, whereas, in downstream wakes they become more uniformly distributed. On the other hand, in Figure 5.3 it can be seen that the velocity deficit saturates and reaches a steady state after the second or third turbine. Also in Figure 5.3 it is observed that the wakes have a certain tendency to move downwards. Figures 5.4 and 5.5 show the contour lines for the turbulent kinetic energy, k, and the velocity deficit, respectively, in a horizontal plane containing the centers of all turbines; the rows do not interfere, and the flow is symmetric with respect to vertical planes passing by the center.

5.2 Analytical approximations obtained from UMPARK

In many cases it is of interest for the designer to have analytical expressions that give an order of magnitude estimate of the values of the most important parameters and their tendencies, that can be used as an alternative to the 3D code. The magnitudes estimated in this way are only approximate and the designer should recur to the 3D code or to experimental results when he needs more accurate values. These expressions given below provide values of the average velocity, turbulence intensity, turbulence scale and width of the wake, at different positions of each machine in a row, as functions of their operating characteristics. They are obtained by making the least square fit with numerical results from UPMPARK, and are validated by comparison with measurements of Vindeby wind farm.

Correlations of a similar nature were obtained by Crespo and Hernández (1986) Luken et al. (1986) and Högstrom et al. (1988) for the velocity deficit and the width of the wake; and by Vermeulen and Builtjes (1982a), Högstrom et al. (1988), Quarton (1989), and Crespo and Hernández (1993a) for the turbulence intensity. All these correlations are for single wakes, although Luken (1989) proposes a correlation for the equilibrium value of the turbulence intensity reached in a row of turbines, using the experimental results of Builtjes and Vermeulen (1982). Taylor (1993) performs a parametrization of the calculated wake parameters as function of several non-dimensional input magnitudes, however, he makes a representation of the results in graphic form and does not make regressions.

In this work we present correlations for magnitudes affected by the wakes of several machines upstream.

Alteration factors for a series of six turbines in a row, aligned with the wind.

UPMPARK has been applied to calculate the values of the speed deficit factor, R_u, turbulence increase factor, R_I, and scale of turbulence decrease factor, R_L, at positions immediately upstream of the center of the second, third and sixth turbines, in a row aligned with the incident wind. All the turbines are supposed to be equal. The sixth turbine is supposed to be representative of a situation in which there are infinite turbines ahead and equilibrium is reached.

The speed deficit factor is

$$R_u = \frac{\Delta u}{U_o},\qquad (5.5)$$

where Δu is the velocity deficit at the rotor center of the wind turbine, and U_o is the unperturbed ambient wind velocity.

The turbulence increase factor is

$$R_I = \frac{I}{I_o}, \tag{5.6}$$

where I is the turbulence intensity incident immediately upstream of the center of the wind turbine, and I_o the unperturbed value at the turbine height. It can also be given by the following expression:

$$R_I = \sqrt{\frac{k}{k_o}} \tag{5.7}$$

where k and k_o are the turbulent kinetic energy at the turbine center and in the unperturbed flow at the turbine height, respectively. It has been assumed that in both the ambient and perturbed values of the turbulence intensity, the unperturbed wind velocity has been used to nondimensionalize the standard deviation of the wind velocity, σ_u, that it is equal to a constant multiplied by $k^{1/2}$.

The scale of turbulence factor is

$$R_L = \frac{L}{L_o}, \tag{5.8}$$

where L is a turbulent length scale at the center of the wind turbine, and L_o the unperturbed value at the turbine height, that is equivalent to the turbine height, or this value multiplied by a constant factor that will cancel in equation (5.8). It can also be given by the following expression:

$$R_L = \frac{R_I^3}{R_\epsilon}, \text{ where } R_\epsilon = (\epsilon/\epsilon_o), \tag{5.9}$$

where ϵ and ϵ_o are the dissipation rates of the turbulent kinetic energy at the turbine center and in the unperturbed flow at the turbine height, respectively.

These three magnitudes will be expressed as functions of three input parameters in the non-dimensional form:

$$R_u = R_u (s_t, C_T, I_o), \quad R_I = R_I (s_t, C_T, I_0) \quad \text{and} \quad R_L = R_L (s_t, C_T, I_o) \tag{5.10}$$

where s_t is the distance between turbines nondimesionalized with the turbine diameter, $s = x/D$, and C_T is the thrust coefficient of the first machine. UPMPARK calculates the thrust coefficient in the downstream machines from the characteristic thrust curves, $C_T(\lambda)$ (see also section 8), of the Bonus 450 turbines of Vindeby, where $\lambda = \omega D/(2U)$, and U is the value of the incident velocity; the tip speed, $\omega D/2$, is also considered as fixed. These assumptions obviously limit the validity of the present analysis, although the behavior of the Vindeby turbines can be considered as representative of typical turbines, and the variation of C_T for the different machines should not be too large.

The ambient turbulence intensity is related to the surface roughness through the equation

$$I_o \approx \frac{1}{\ln(h/z_o)}, \tag{5.11}$$

where h is the turbine height. It is assumed that the atmosphere has neutral stability, and that the standard deviation of the wind velocity in the incident wind direction is $\sigma_u = 2.4u_*$ (Crespo and Hernández, 1993a). This analysis is restricted then to neutral stability cases, and to turbines having a ratio of height to diameter approximately equal to one as in the Vindeby wind turbines. As the ratio z_o/D (or z_o/h) is changed independently, and use is not made of equations (5.1) to (5.4), the results that we will obtain can be applied

both to inland and offshore wind farms.

In order to obtain expressions (5.10), 60 runs have been made with UPMPARK, corresponding to the following values of the input parameters,

$$s_i = 4, 8, 16, 32$$

$$C_T = 0.75\text{-}0.8, 0.5, 0.2$$

$$I_o = 0.05, 0.08, 0.10, 0.15, 0.20$$

The maximum value of C_T, between 0.75 and 0.8, has been chosen to obtain values of C_T smaller than 1 in the downstream machines. The expressions (5.10) are represented in the form:

$$R_u = A \, s^a \, C_T^b \, I_o^c \tag{5.12}$$

$$R_I = 1 + B \, s^d \, C_T^e \, I_o^f \tag{5.13}$$

$$R_L = \frac{R_I^3}{R_\epsilon}, \quad where \quad R_\epsilon = 1 + C \, s^g \, C_T^h \, I_o^{\ j} \tag{5.14}$$

The scale of turbulence factor can be either smaller or larger than one, so that the perturbed turbulence length can either be larger or smaller than the unperturbed one, this indeterminacy appears mainly in turbine 2, but for the third and sixth machines this factor is usually larger than one. Then, it is not possible to use a simple correlation like that for R_u or R_I and it has been necessary to use an auxiliary expression for the increase factor of the dissipation of turbulent kinetic energy, R_ϵ (5.14); both the turbulent kinetic energy and the dissipation rate increase in the wake, but none of them dominates always over the other in the ratio R_I^3/R_ϵ.

The coefficients and exponents of equations (5.12) to (5.14) are given in tables 1 to 3 for the second, third and sixth turbines. In Figures 4.6 to 4.14 the values are compared obtained from these expressions with those obtained using UPMPARK and the experimental ones from the Vindeby wind farm, when they are available. In each figure is also given the corresponding expressions (5.12) to (5.14).

In Figure 4.6 and 4.7, referring to the speed deficit factor and the turbulence increase factor of the second turbine, respectively, the agreement of the correlation with UPMPARK results is good, although there is some disagreement with experiments, that are too widely spread. A reason for this may be that the number of experiments is scarce, and the input parameters of equation (5.9) can not be very precisely determined from the measurements. In particular, for N and E winds (see Figure 3.1) we have some problems in estimating the unperturbed flow conditions, mainly the turbulence intensity (the mean velocity can be estimated from the power of machine 5E); we have tried to use the land mast measurements, but it is too far, and we are not sure whether its measurements correspond to unperturbed flow in the open sea.

The second turbine is in a single wake and can be compared with other single wake results; the decay of R_u with downstream distance is like $s_i^{-0.77}$, that is slightly slower than the value predicted by Högstrom et al. (1988), $s_i^{-1.06}$, and is closer to the one predicted by Crespo and Hernández, $s_i^{-0.8}$. For the turbulence intensity a direct comparison with the correlations of Crespo and Hernández (1993a, 1996), and Quarton (1989) is not straightforward, because in those cases they operate with the added turbulence intensity instead of R_I. When the appropriate change of variables is made it is found that Crespo and Hernández (1993a, 1996) give a value of decay with distance of R_I-1 like $s_i^{-0.64}$, quite close to the one calculated here, Quarton (1989) like $s_i^{-1.14}$, and Högstrom (1988) like $s_i^{-0.5}$. later in this report, section 8, it is found that - taking the large uncertainties of the measurements into account - to a good approximation $I_{add} \sim s_i^{-1}$. The closer data analysis, section 8, of the data

also reveals that it is difficult - if at all possible - to detect differences in turbulence of single and multiple wake cases.

In Figures 5.9 and 5.10, referring to the speed deficit factor and the turbulence increase factor of the third turbine, respectively, the agreement of the correlation with both UPMPARK and experimental results is acceptable. However, in Figure 5.9 there is some spread of experimental results, and in Figur 5.10 the experimental results seem to be consistently lower that the calculated ones.

In Figure 5.12, showing the speed deficit factor of the sixth turbine, the agreement of the correlation with UPMPARK results is acceptable except for a few points that correspond to large thrusts and small separation, s_r. However, the discrepancy with experiments is more important; the correlation usually gives smaller values of the speed deficit factor than the experiments. In Figure 5.13, providing the turbulence increase factor of the sixth turbine, the agreement of the correlation with both UPMPARK and experimental results is acceptable, although again the experimental results give smaller values of the turbulence increase factor, and there are three points, that, as in the previous figures, correspond to the largest perturbation, for which there is some discrepancy of the correlation with UPMPARK calculations.

In Figures 5.8, 5.11 and 5.14, referring to the scale turbulence factor of the second, third and sixth turbines, respectively, the comparison with UPMPARK results is acceptable except for three points that correspond to the lowest ambient turbulence intensity, I_o=0.05, and highest thrust coefficient, C_T=0.75-0.8. In Figure 5.8, for the second turbine, it is seen that there are a few points with a scale turbulence factor smaller than one. Usually, the points with a scale turbulence factor smaller than one correspond to large values of the thrust coefficient, C_T. However, in Figure 5.11 and 5.14, that refer to the third and sixth turbines, respectively, most of the cases correspond to scale turbulence factors larger than one. When this chapter was first written no experiments were available to compare with this scale factor. Later, we have been informed that, for the experiments carried out within this project, that are presented in another chapter of this report, this scale factor is always smaller than one; as we don't know the details yet, it is difficult to evaluate this discrepancy. It may be that the experiments are carried out for a range of parameters that, in Figures 5.8, 5.11 and 5.14, correspond to values of this factor smaller than one. Another possible reasons for this discrepancy are that, on one hand, UPMPARK does not take into account the small scale (large frequency) turbulence originated by the boundary layers of the blades of the wind turbines, and, on the other hand, that the wind turbine is capable of responding to low frequency fluctuations of wind speed, and extract energy from the wind in the low frequency (large scale) range (Højstrup, 1990). These two factors are most relevant in the wake center where these measurements are taken, and the above correlations apply; however, the comparisons carried out by Crespo and Hernández (1993a, 1996) for the spectra, that gave quite a good agreement with experiments, corresponded to points located in the upper and lower part of the layer where turbulence production is dominated by shear. It should also be pointed out that in the next section, in Figures 4.31 to 4.33, a comparison is made of the measured spectra in the free flow and in the wake with the corresponding calculated values, the agreement seems to be quite good, and either the length scale influence is not too important or there is not so much discrepancy between the calculated and measured lengths.

Alteration factors for a series of six turbines in a row disaligned with the wind.

Now we consider the case in which the incident wind forms an angle α with the row. The following alteration factors and geometric characteristics have been calculated using UPMPARK:

The maximum speed deficit factor:

$$R_{u,max} = \frac{\Delta u_{max}}{U_o}, \tag{5.15}$$

where Δu_{max} is the maximum velocity deficit in a plane normal to the wind direction and passing through the grid point immediately upstream of the corresponding wind turbine center.

The speed deficit factor at the turbine center:

$$R_{uc} = \frac{\Delta u_c}{U_o}, \tag{5.16}$$

where Δu_c is the velocity defect in the grid point immediately upstream of the corresponding wind turbine center.

Non-dimensional half-width of wake, r_w/D,

$$R_w = \frac{r_w}{D}, \tag{5.17}$$

where r_w is the average of the lengths of the four lines contained in the above mentioned plane (normal to the wind direction and passing through the grid point immediately upstream of the corresponding wind turbine center), and going, vertically upwards and downwards and horizontally left and right, from the point of maximum velocity defect to the points where the velocity defect is half of this maximum. The height of the point of maximum velocity defect is approximately the turbine height, although slightly below, as discussed by Crespo et al. (1985); then, this parameter, together with the two previous ones, can give us an estimation of the distribution of the velocity defect in each cross-section.

The maximum turbulence increase factor is

$$R_{Imax} = \frac{I_{max}}{I_o} = \sqrt{\frac{k_{max}}{k_o}} \tag{5.18}$$

where I_{max} and k_{max} are respectively the maximum turbulence intensity, and turbulent kinetic energy in a plane normal to the wind direction and passing through the grid point immediately upstream of the corresponding wind turbine center. The point where R_{Imax} is reached is usually above the one where R_{umax} occurs.

The turbulence increase factor at the turbine center is

$$R_{Ic} = \frac{I_c}{I_o} = \sqrt{\frac{k_c}{k_o}}, \tag{5.19}$$

where I_c is the maximum turbulence intensity in the point immediately upstream of the corresponding wind turbine center.

These five quantities will be expressed as functions of three input parameters in the non-dimensional form:

$$R_{umax} = R_{umax}(s,\alpha,I_o), \quad R_{uc} = R_{uc}(s,\alpha,I_o), \quad R_w = R_w(s,\alpha,I_o), \quad R_{Imax} = R_{Imax}(s,\alpha,I_o),$$
$$\text{and } R_{Ic} = R_{Ic}(s,\alpha I_o), \tag{5.20}$$

The thrust coefficient C_T has been fixed to a value of 0.75 for the first upstream turbine; as discussed previously, this is the value that avoids exceeding the value of one in the downstream machines.

In order to obtain expressions (5.20), 72 runs have been made with UPMPARK, corresponding to the following values of the input parameters,

$s_t = 4, 8, 16, 32$

$\alpha = 0°, 1°, 2°, 4°, 8°, 16°$

$I_o = 0.05, 0.10, 0.15$

The expressions (5.20) are represented in the form:

$$R_{umax} = A \ s^a \ (\cos\alpha)^b \ I_o^c \tag{5.21}$$

$$R_{uc} = A' \ s^{a'} \ (\cos\alpha)^{b'} \ (\cos\alpha)^{b'} \ I_o^{c'} \tag{5.22}$$

$$R_{Imax} = E + B \ s^d \ (\cos\alpha)^e \ I_o^f \tag{5.23}$$

$$R_{Ic} = 1 + B' \ s^{d'} \ (\cos\alpha)^{e'} \ I_o^f \tag{5.24}$$

$$R_w = D + C \ s^g \ (\cos\alpha)^h \ I_o^j \tag{5.25}$$

The coefficients and exponents of equations (5.21) to (5.25) are given in Tables 5.4 to 5.8 for the second, third and sixth turbines. In Figures 5.15 to 5.29 the values obtained from these expressions with those obtained using UPMPARK, and the experimental ones from the Vindeby wind farm when they are available, are compared. In each figure is also given the corresponding expressions (5.21) to (5.25).

In Figures 5.15 to 5.19, that refer to the alteration factors for the second turbine, can be observed that there is an acceptable agreement of the correlation with UPMPARK calculations, except for a few isolated cases, that correspond to largest values of these alteration factors. Similar comments can be made for figures 5.20 to 5.24 for the third turbine and Figures 5.25 to 5.28 for the sixth turbine; however, in Figure 5.29 for the width of the wake upstream of the sixth turbine the data dispersion of the values calculated with UPMPARK with respect to the correlation is so large that it is not clear that this correlation will be representative of the calculations.

In Figures 5.26 and 5.28, that correspond respectively to the velocity deficit factor and turbulence increase factor at the center of the sixth turbine, are also presented results from experiments; as it should be expected, their behavior is similar to that of the corresponding cases with wind aligned with the row of turbines, Figures 5.12 and 5.13, respectively.

4.3 SPECTRA IN THE WAKE OF WIND TURBINES

The procedure to calculate the spectra is the same one used by Crespo and Hernández (1993a). The unperturbed atmospheric flow is supposed to have a typical spectrum for the u component (in the direction of the incident wind), that can be expressed in the following form (Panofski and Dutton, 1984)

$$n \, S_u = \frac{19 \, f \, k_o}{(1 + 33 \, f)^{5/3}} \qquad (5.26)$$

where f is a nondimensional frequency:

$$f = \frac{n \, z}{U_o} \qquad (5.27)$$

and z is the height. It is assumed that the spectrum in the wake has the same form given by equation (5.26):

$$n \, S_u = \frac{19 \, f' \, k}{(1 + 33 \, f')^{5/3}} \qquad (5.28)$$

where

$$f' = \frac{n \, z'}{U_o}, \quad and \quad z' = z \, R_L. \qquad (5.29)$$

R_L is the scale of turbulence factor defined in (5.14). The value of k_o is substituted by k, and the height, z, is substituted by the new length scale.

In Figures 5.30 to 5.32 is presented a comparison of the measured and calculated spectra in both masts, SMS (Sea mast South) and SMW (Sea mast West) for NW winds, at different heights: 7 m, 38 m and 48 m. As can be observed in Figure 3.1, mast SMS is simultaneously in the wake of five machines (1W to 5W), and mast SMW is in the free flow. The corresponding free wind velocity at 20 m is supposed to be 9.5 m/s, and the value of k_o has been chosen so that in each case the unperturbed spectra, equation (5.27), fits best to that measured in SMW. It turns out that, for neutral atmosphere, this procedure does not give the same surface roughness for the three heights, that, besides, are too small: $z_o = 1.6 \times 10^{-5}$ m for 7 m, and $z_o = 7 \times 10^{-8}$ m for 38 m and 48 m. The corresponding values of the ambient turbulence intensity are also extremely small: $I_o = 0.068$ for $z = 7$ m, and $I_o = 0.05$ for $z = 38$ and 48 m. It may be that the real value of the free speed velocity is actually smaller than the assumed one. On the other hand, once the parameters defining the basic flow are chosen so that the correct Kaimal spectra of the basic flow is obtained, the calculated spectra in the multiple wake situation is in very good agreement with the measurements, in spite of the previously discussed disagreement regarding the measured and calculated values of the turbulent length scale.
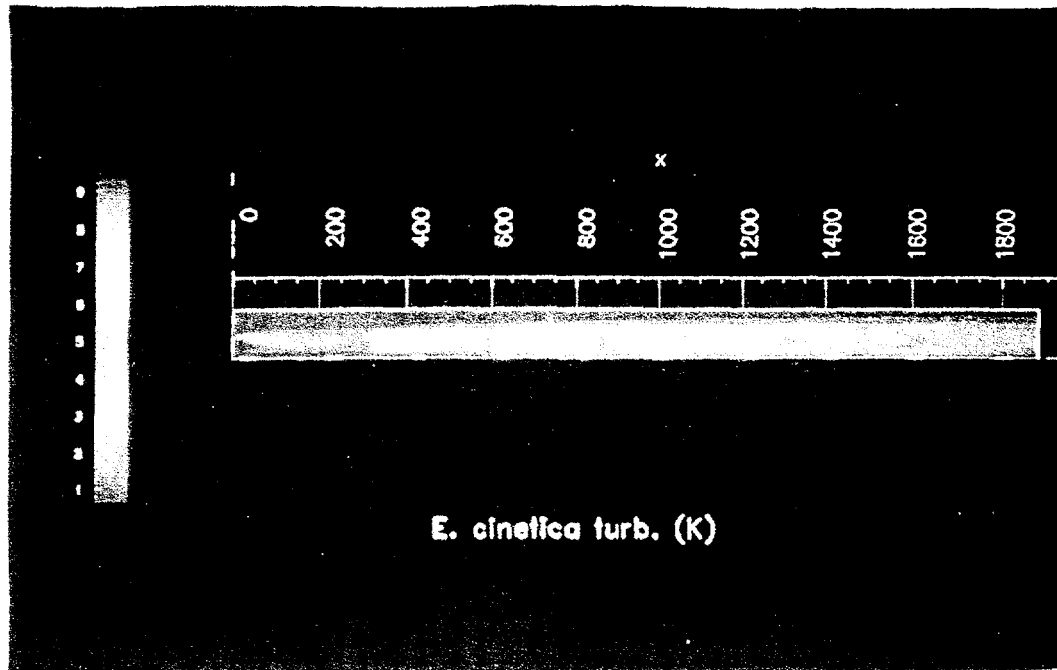
Figure 5.2 *Contour lines for the turbulent kinetic energy, k, in a vertical plane containing the centers of turbines 1E to 6E for NW winds.*
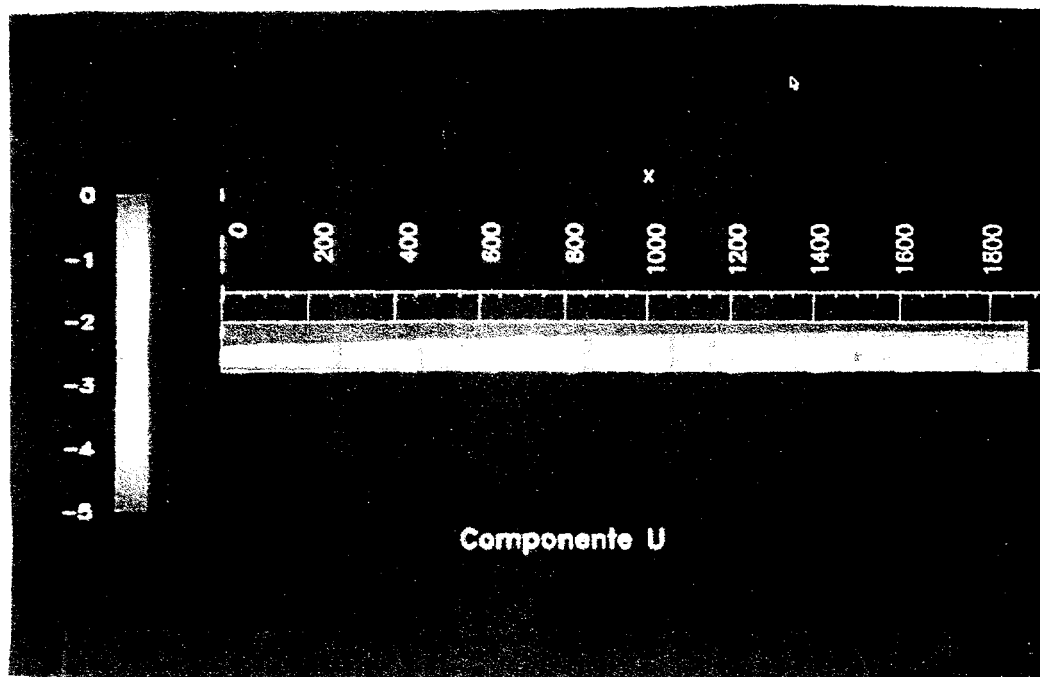
Figure 5.3 *Contour lines for the velocity deficit in a vertical plane containing the centers of turbines 1E to 6E for NW winds.*
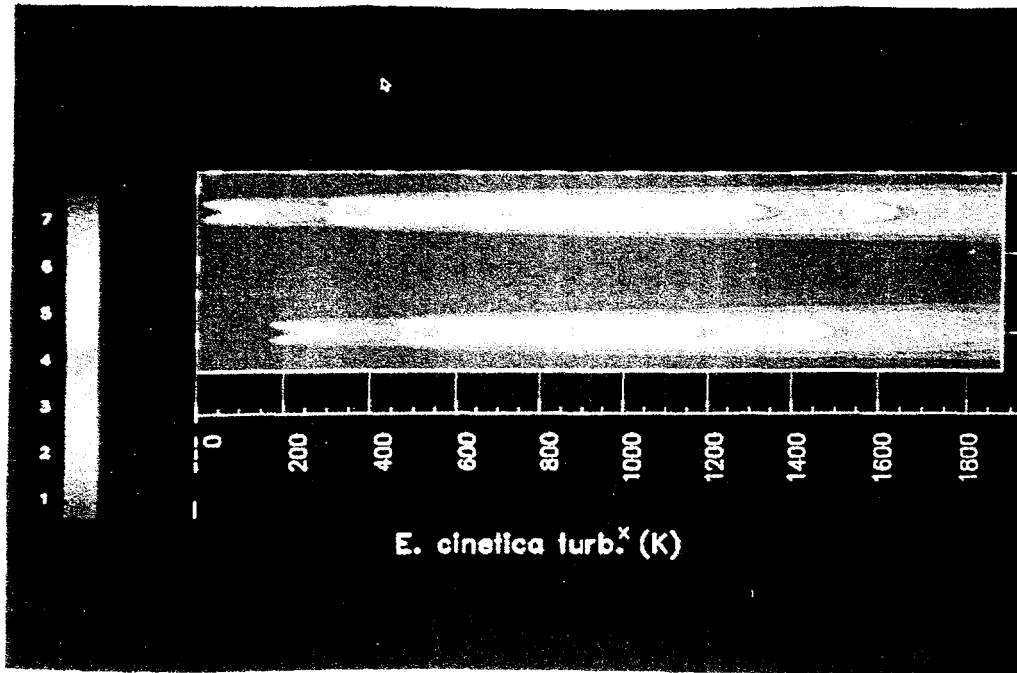
Figure 5.4 *Contour lines for the turbulent kinetic energy, k, in a horizontal plane containing the centers of all turbines for MW winds.*
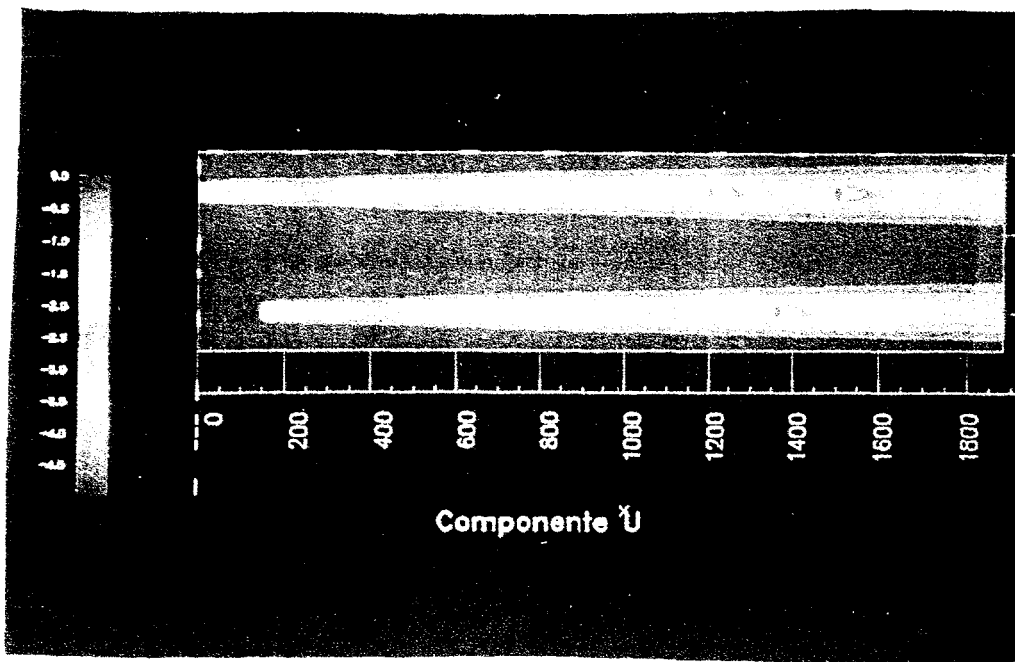
Figure 5.5 *Contour lines for the velocity deficit in a horizontal plane containing the centers of all turbines for NW winds.*
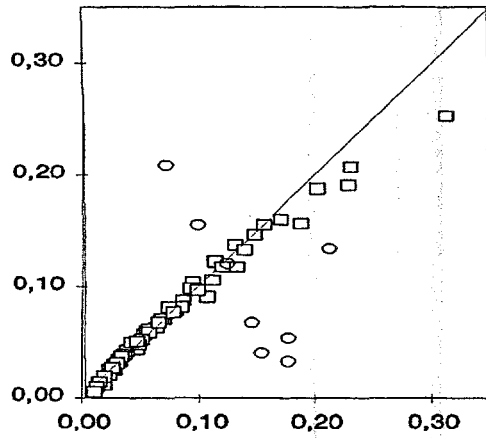
R_u (Analytical) = 0.176 s $^{-0.77}$ Ct $^{0.83}$ $I_{00}^{-0.63}$

Figure 5.6 *Speed deficit factor for 2nd turbine; row aligned in wind.*
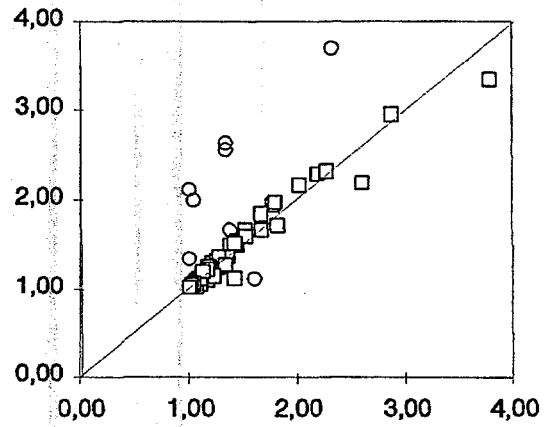
R_l (Analytical) = 1 + 0.045 s $^{-0.63}$ Ct $^{1.46}$ $I_{00}^{-1.82}$

Figure 5.7 *Turbulence increase factor for 2nd turbine;row aligned with wind.*
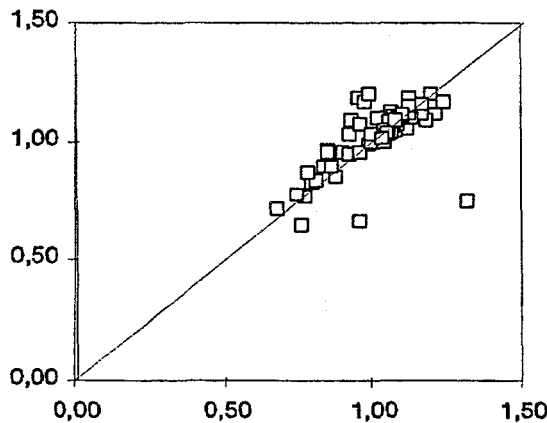
$$\frac{R_l^3}{R_e} = \frac{(1 + 0.045s^{0.63}Ct^{1.46}I_{00}^{-1.82})^3}{1 + 0.075s^{0.86}Ct^{2.64}I_{00}^{-2.77}}$$

Figure 5.8 *Scale of turbulence factor for 2nd tubine; row aligned to wind.*
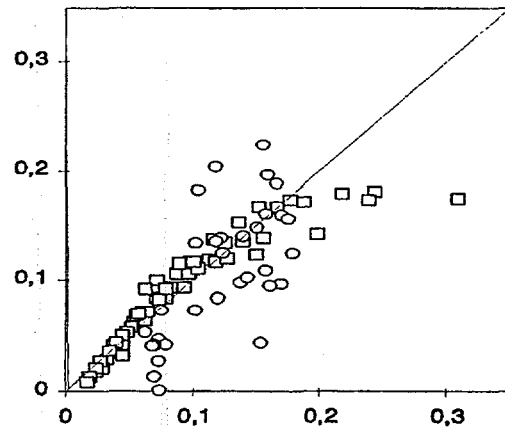
R_u (Analitycal) = 0.209 s $^{-0.67}$ Ct $^{0.69}$ $I_{00}^{-0.51}$

Figure 5.9 *Speed deficit factor for 3rd tubine; row aligned to wind.*
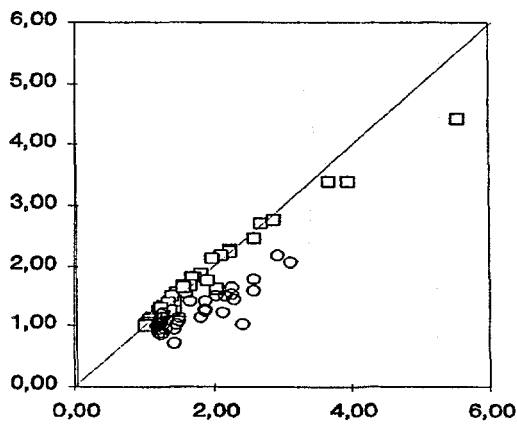
R_l (Analytical) = 1 + 0.072 s $^{-0.81}$Ct $^{1.13}$ $I_{00}^{-1.87}$

Figure 5.10 *Turbulence increase factor for 3rd turbine; row aligned to wind.*
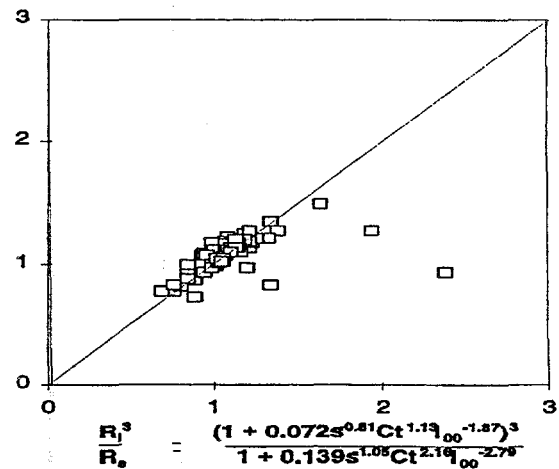
$$\frac{R_l^3}{R_e} = \frac{(1 + 0.072s^{0.81}Ct^{1.13}I_{00}^{-1.87})^3}{1 + 0.139s^{1.05}Ct^{2.16}I_{00}^{-2.79}}$$

Figure 5.11 *Scale of turbulence factor for 3rd turbine; row aligned to wind.*

32
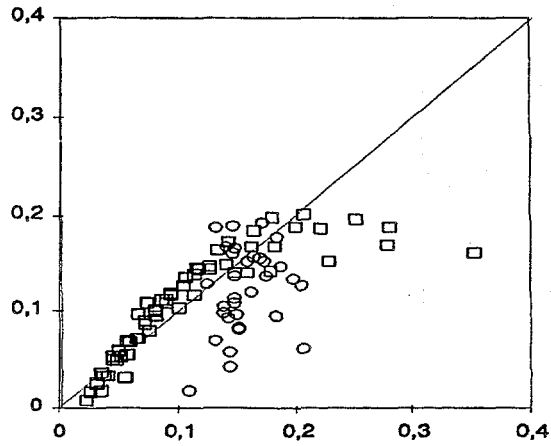
R_u (Analytical) = 0.245 $s^{-0.65}$ $Ct^{0.61}$ $I_{oo}^{-0.46}$

Figure 5.12 *speed deficit factor for 6th turbine; row aligned with wind.*
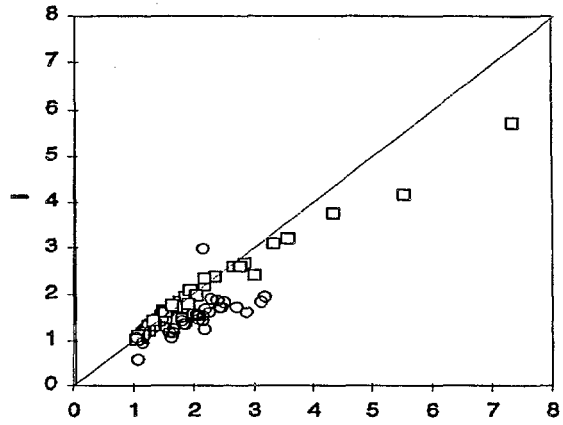
R_I = 1 + 0.103 $s^{0.96}$ $Ct^{0.88}$ $I_{oo}^{-1.91}$

Figure 5.13 *Turbulence increase factor for 6th turbine; row aligned with wind.*
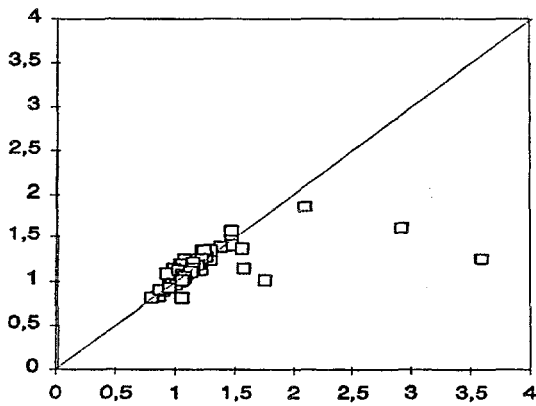
$$\frac{R_I^3}{R_o} = \frac{(1 + 0.103\ s^{0.96}Ct^{0.88}I_{oo}^{-1.91})^3}{1 + 0.21\ s^{1.33}Ct^{1.66}I_{oo}^{-2.88}}$$

Figure 5.14 *Scale of turbulence factor for 6th turbine; row aligned with wind.*
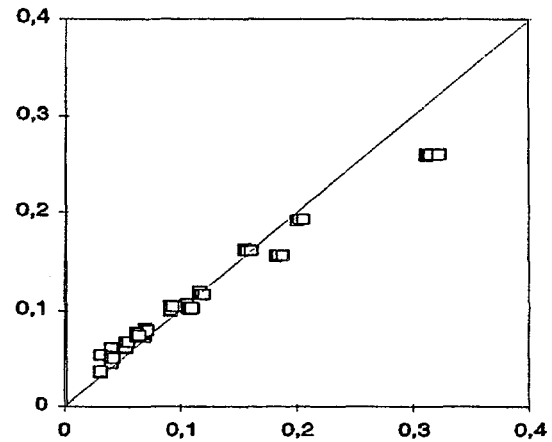
R_u (Analytical) = 0.136 $s^{-0.77}$(cos x)$^{0.77}$ $I_{oo}^{-0.63}$

Figure 5.15 *Maximum speed deficit factor for a plane upstream of 2nd turbine; row disaligned with wind.*
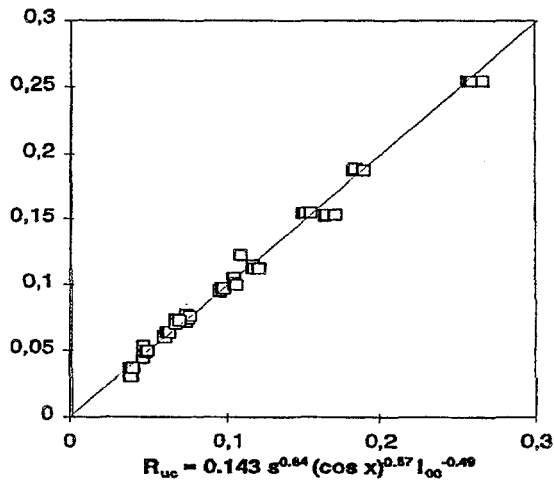
R_{uc} = 0.143 $s^{0.64}$ (cos x)$^{0.57}$ $I_{oo}^{-0.49}$

Figure 5.16 *Speed deficit at the centre of 2nd turbine; row disaligned with wind.*
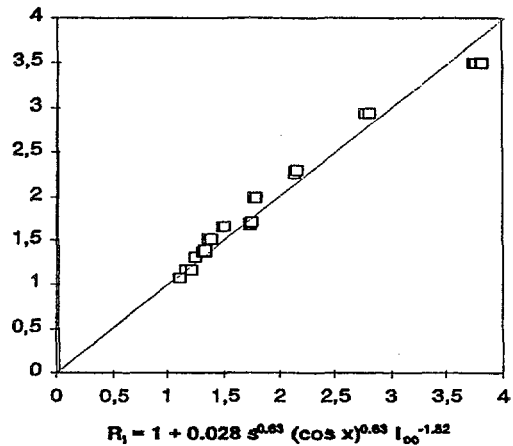
R_I = 1 + 0.028 $s^{0.63}$ (cos x)$^{0.63}$ $I_{oo}^{-1.52}$

Figure 5.17 *Maximum turbulence increase factor for a plane upstream of 2nd turbine; row disaligned.*
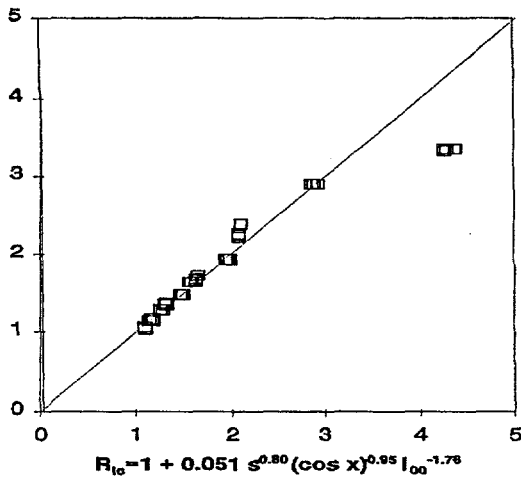
Figure 5.18 *Turbulence increase factor at centre of 2nd turbine; row disaligned.*

$$R_{ic} = 1 + 0.051\ s^{0.80}(\cos x)^{0.95}\ I_{00}^{-1.76}$$
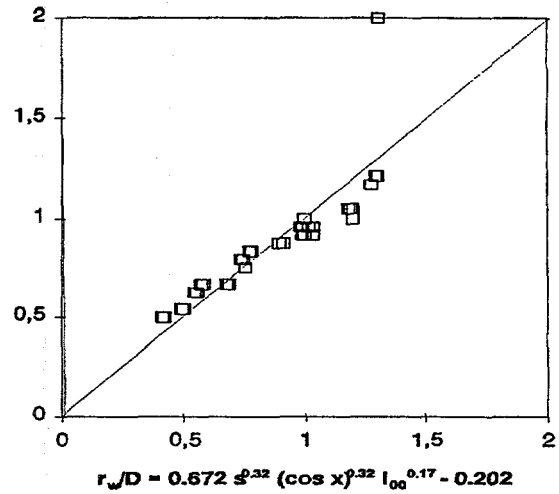
Figure 5.19 *Non-dimensional half-width of wake upstream of 2nd turbine; row disaligned.*

$$r_w/D = 0.672\ s^{0.32}(\cos x)^{0.32}\ I_{00}^{0.17} - 0.202$$
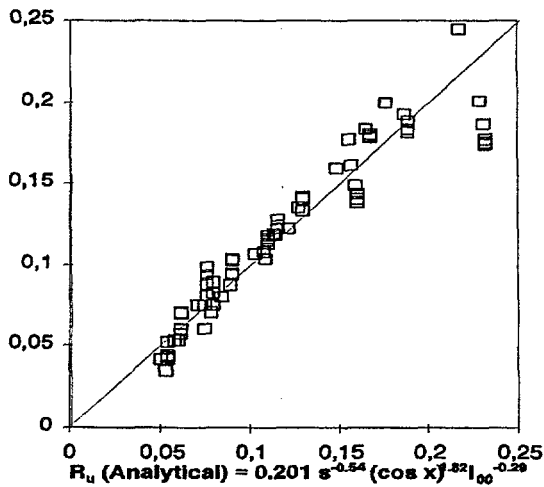
Figure 5.20 *Maximum speed deficit factor for a plane upstream of 3rd turbine; row disaligned.*

$$R_u\ (\text{Analytical}) = 0.201\ s^{-0.54}(\cos x)^{1.82}\ I_{00}^{-0.29}$$
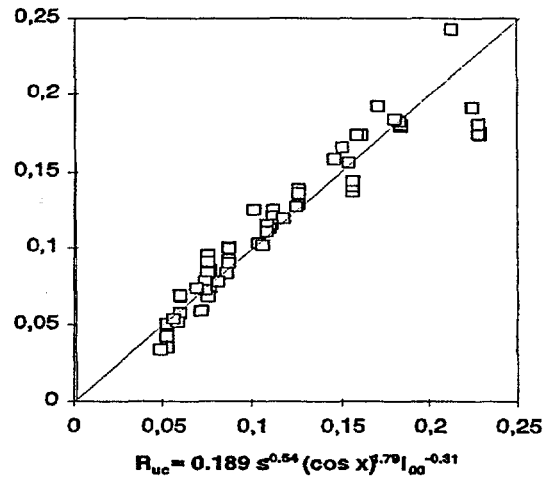
Figure 5.21 *Speed deficit factor at centre of 3rd wind turbine: row disaligned.*

$$R_{uc} = 0.189\ s^{0.54}(\cos x)^{1.79}\ I_{00}^{-0.31}$$
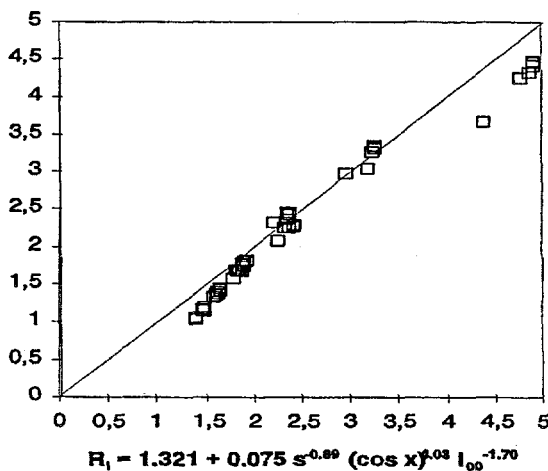
Figure 5.22 *Maximum turbulence increase factor for a plane upstream of 3rd turbine; row disaligned.*

$$R_i = 1.321 + 0.075\ s^{0.89}(\cos x)^{1.03}\ I_{00}^{-1.70}$$
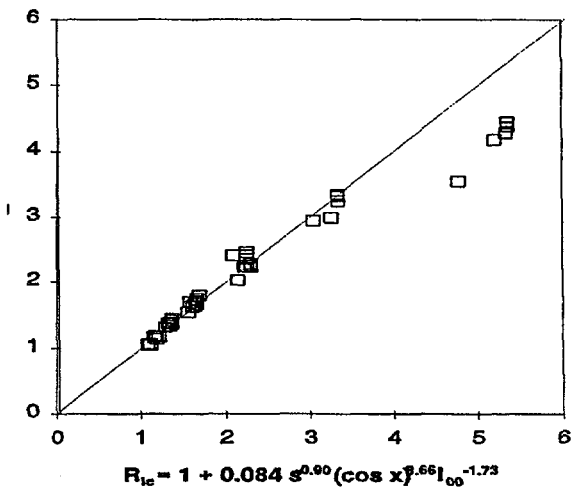
Figure 5.23 *Turbulence increase factor at centre of 3rd turbine; row disaligned.*

$$R_{ic} = 1 + 0.084\ s^{0.90}(\cos x)^{1.66}\ I_{00}^{-1.73}$$
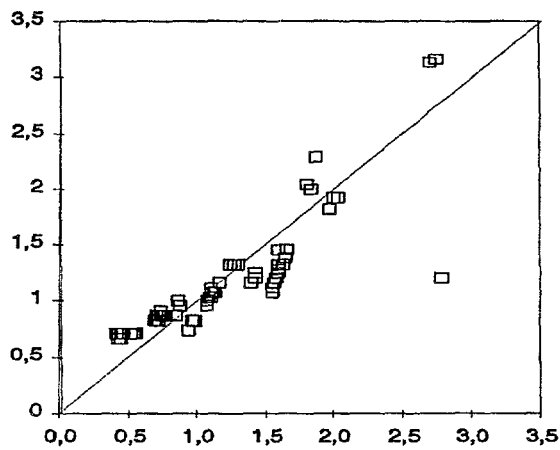
$$r_w/D = 0.638 \ s^{0.36}(\cos x)^{10.88}I_{00}^{0.022} - 0.584$$

Figure 5.24 *Non-dimentional half-width of wake upstream of 3rd turbine; row disaligned with wind.*
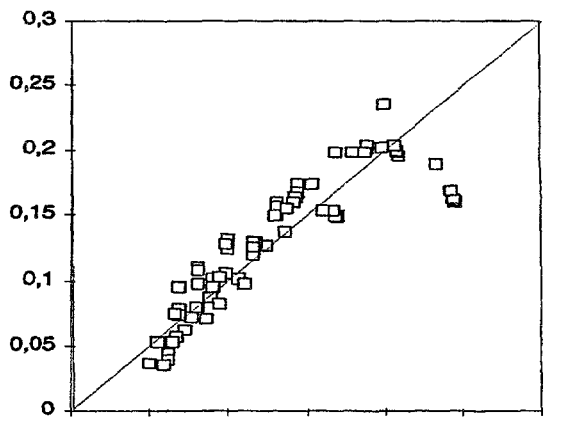
$$R_u \ (\text{Analytical}) = 0.255 \ s^{-0.53}(\cos x)^{7.32}I_{00}^{-0.23}$$

Figure 5.25 *Maximum speed deficit factor for a plan upstream of 6th turbine; row disaligned with wind.*
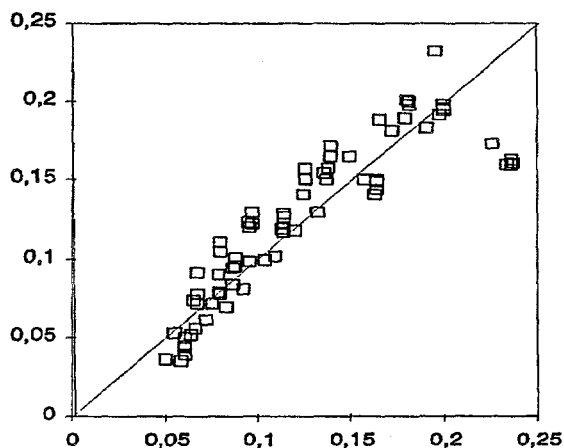
$$R_{uc} = 0.237 \ s^{0.52}(\cos x)^{7.88}I_{00}^{-0.24}$$

Figure 5.26 *Speed deficit factor at centre of 6th turbine; row disaligned with wind.*
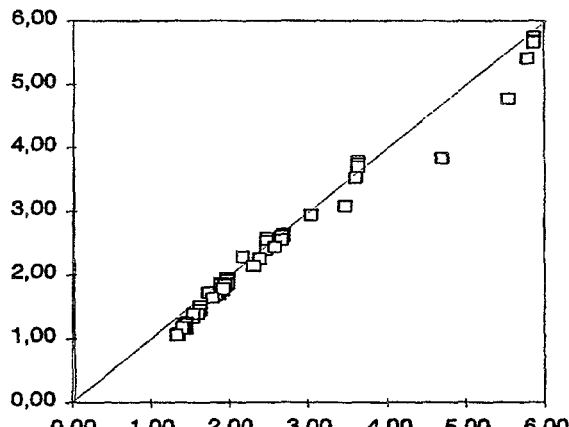
$$R_I = 1.255 + 0.106 \ s^{0.96}(\cos x)^{7.39}I_{00}^{-1.70}$$

Figure 5.27 *Maximum turbulence increase factor for plane upstream of 6th turbine; row disaligned with wind.*
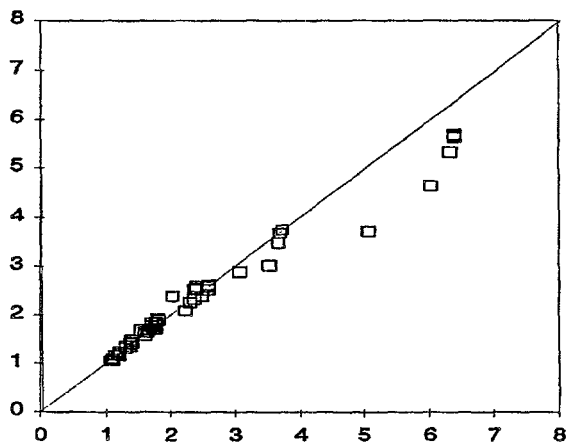
$$R_{Ic} = 1 + 0.113 \ s^{0.96}(\cos x)^{7.03}I_{00}^{-1.74}$$

Figure 5.28 *Turbulence increase factor for centre of 6th turbine; row disaligned with wind.*
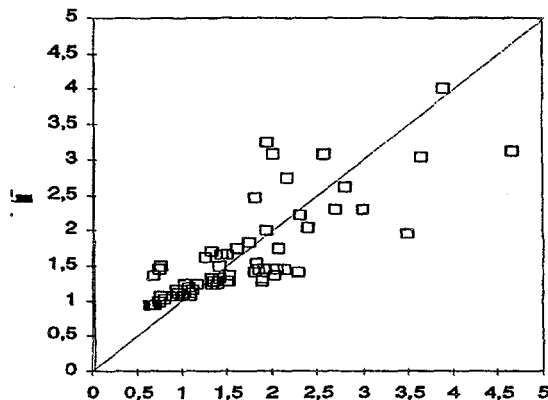
$$r_w/D = 0.725 \ s^{0.31}(\cos x)^{18.88}I_{00}^{-0.07} - 0.662$$

Figure 5.29 *Non-dimensional half-width of wake upstream of 6th turbine; row disaligned with wind.*
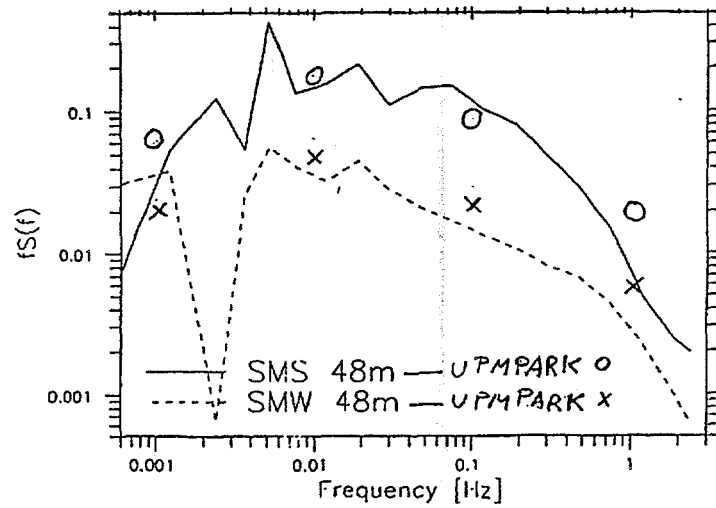
Figure 5.30 *Turbulence spectra at 48m. Comparison of model and experiments.*
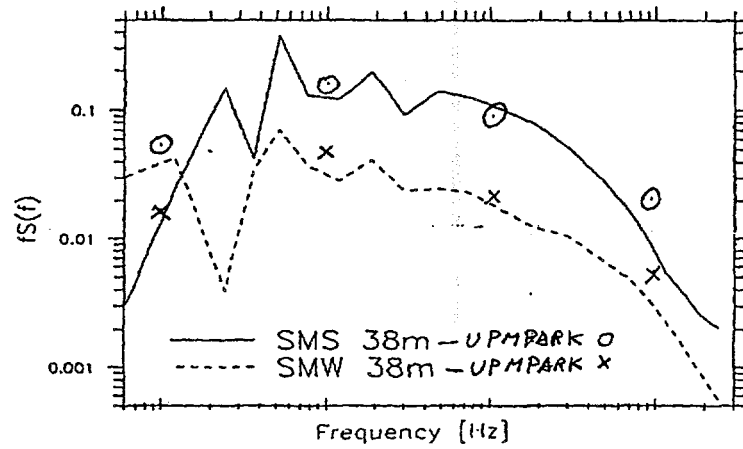
Figure 5.31 *Turbulence spectra at 38m. Comparison of model and experiments.*
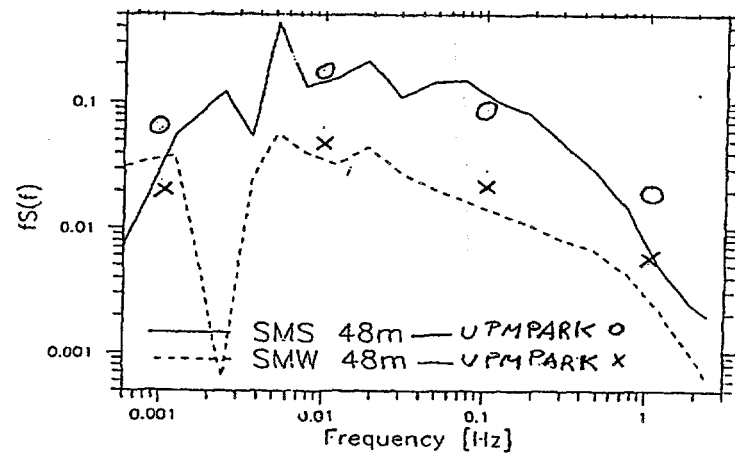
Figure 5.32 *Turbulence spectra at 7m. Comparison of model and experiments.*

Table 5.1 *Coefficients and exponents for speed deficit factor, R_u; row aligned with wind.*

	Turbine 2	Turbine 3	Turbine 6
A	0.176	0.209	0.245
a	-0.77	-0.67	-0.65
b	0.83	0.69	0.61
c	-0.63	-0.51	-0.48

Table 5.2 *Coefficients and exponents for turbulence increase factors, R_I; row aligned with wind.*

	Turbine 2	Turbine 3	Turbine 6
B	0.045	0.072	0.103
d	-0.63	-0.81	-0.96
e	1.46	1.13	0.88
f	-1.82	-1.87	-1.91

Table 5.3 *Coefficient and exponents for increase factor of dissipation of turbulent energy, R_ε; row aligned with wind.*

	Turbine 2	Turbine 3	Turbine 6
C	0.0757	0.1391	0.2101
g	-0.8615	-1.056	-1.3315
h	2.6456	2.1658	1.6996
j	-2.7714	-2.7934	-2.8813

Table 5.4 *Coefficients and exponents for maximum speed deficit factor, R_{umax}; row disaligned with wind.*

	Turbine 2	Turbine 3	Turbine 6
A	0.136	0.201	0.255
a	-0.77	-0.54	-0.53
b	-0.77	1.82	5.32
c	-0.63	-0.29	-0.23

Table 5.5 *Coefficients and exponents for speed deficit factor at turbine centre, R_{uc}; row disaligned with wind.*

	Turbine 2	Turbine 3	Turbine 6
A'	0.143	0.189	0.237
a'	-0.64	-0.54	-0.52
b'	-0.87	1.79	4.89
c'	-0.49	-0.31	-0.24

Table 5.6 *Coefficients and exponents for maximum turbulence increase factor, R_{Imax}; row disaligned with wind.*

	Turbine 2	Turbine 3	Turbine 6
E	1.0	1.321	1.255
B	0.028	0.075	0.106
d	-0.63	-0.89	-0.96
e	-0.63	4.032	7.39
f	-1.82	-1.70	-1.70

Table 5.7 *Coefficients and exponents for turbulence increase factor, R_{Ic}; rows disaligned.*

	Turbine2	Turbine3	Turbin6
B'	0.051	0.084	0.113
d'	-0.80	-0.90	-0.98
e'	-0.95	3.66	7.03
f'	-1.76	-1.73	-1.74

Table 5.8 *Coefficients and exponents for half width, R_w; row disaligned.*

	Turbine2	Turbine3	Turbine6
D	-0.202	-0.584	-0.662
C	0.672	0.638	0.725
g	0.32	0.36	0.31
h	0.32	-10.88	-18.68
j	0.17	0.022	-0.07

6 SEA CLIMATE AND TURBULENCE

6.1 Introduction

The wind field at an offshore site will be somewhat different than wind fields at common land sites. The sea surface roughness is typically much smaller than the corresponding land surface roughness, and consequently the mean wind speeds increase, and the turbulence levels decrease compared with a land site. The stability statistics will typically also be different on the sea, with a mean atmospheric stability slightly on the stable side, whereas over land we see slightly unstable conditions on the average.

For near coastal conditions, we will see increased sea roughness, and also internal boundary layers for offshore flows, i.e. the flow 'remembers' the upstream conditions some time after having passed the border between the high land roughness and the low sea roughness, see Figure 6.1.
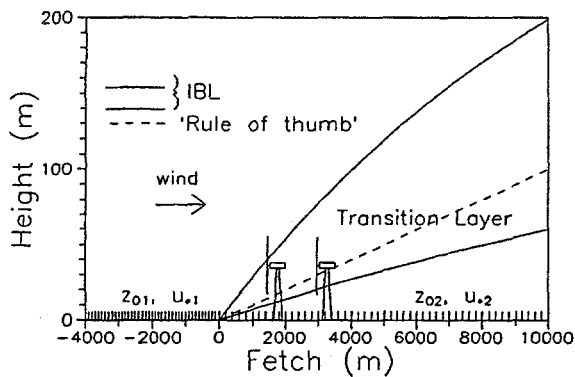
Figure 6.1 *Internal boundary layers developing after a sudden change in surface roughness.*
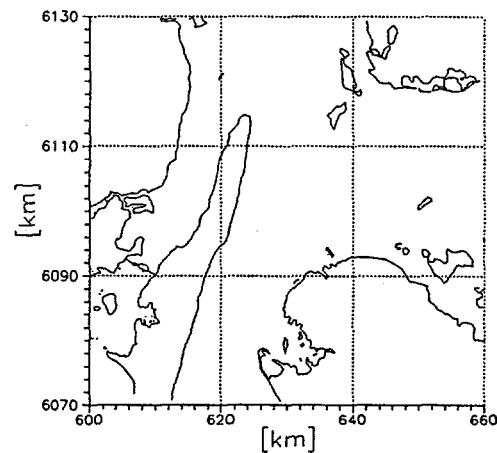
Figure 6.2 *60km * 60km map of the surroundings of the Vindeby Wind Farm, which can be found in the lower right corner of the center square on the map.*

The surroundings of the near-coastal Vindeby site are shown in fig. 6.2, which covers a 60 km * 60 km area (for a close-up, see Figure 3.1). The upstream conditions for the site are quite direction dependent and can be characterized by:

0-90°   More than 20km water fetch but the measurements at the sea masts will be influenced by wakes from the wind farm.

90-235°   Short water fetch, 2 - 5km.

235-315° 15-20 km water fetch.

315-360° More than 50 km water fetch, but measurements at sea masts are influenced by wakes from wind farm.

The predicted mean wind field (as a climatic average) using WASP, Troen and Petersen (1989), Barthelmie et al (1996), is shown in Figure 6.3, where the mean wind speed at hub height was predicted along a line perpendicular to the coastline, showing a gradual decrease by some 13% moving 5 km inland and an increase of the same magnitude moving 5 km offshore. There are indications both from this site and other sites in the Baltic Sea that the actual acceleration of the flow offshore, occurs at a slightly slower rate, probably caused by internal boundary layers growing slower than predicted by WASP, due to increased stability over the sea.
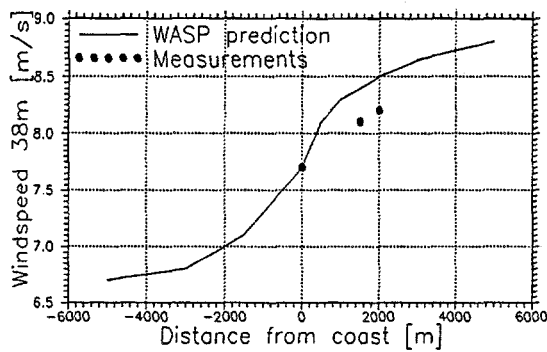
Figure 6.3 *Predicted variation of average wind speed using WASP. The three points shown represent measurements from the three Vindeby masts.*
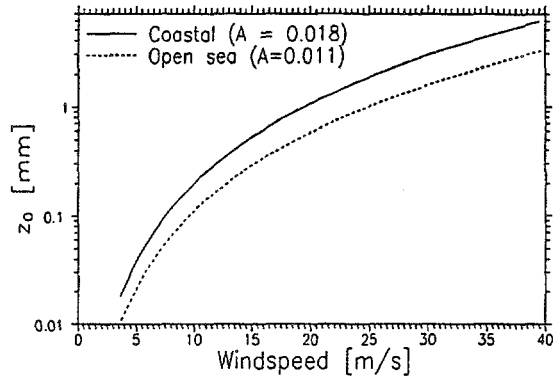
Figure 6.4 *Roughness lengths calculated using the Charnock relation, for open sea and coastal condition.*

6.2 Sea surface roughness lengths

Over land, the surface roughness can usually be assumed to have a constant value (as long as the vegetation does not change) with values varying from 0.01m to 0.1m for the types of terrain of interest for wind energy purposes.

At sea the situation is much more complicated. The roughness is very small at low wind speeds but increases then rapidly with increasing wind speed. A very simple description of this behavior was derived by Charnock (1955) and is still in widespread use:

$$z_o = A \frac{u_*^2}{g} \tag{6.1}$$

where z_o is the surface roughness, u_* the surface friction velocity, g acceleration of gravity and A a constant.

In near-neutral conditions the wind speed varies logarithmically with height

$$U = \frac{u_*}{\kappa} \ln\frac{z}{z_o} \tag{6.2}$$

where z is the height over ground and κ the von Karmann constant.

Using the logarithmic wind profile, (6.2), to eliminate u_*, we obtain

$$z_o = \frac{A \kappa^2}{\ln^2(\frac{z}{z_o})} U^2 \tag{6.3}$$

From this implicit equation for z_o it is obvious that we have a very rapid variation of the roughness with wind speed.

Normally accepted values for the "constant" A are 0.011 for open ocean and a somewhat higher value 0.018 for near coastal conditions. These values then result in a variation of roughness length over two orders of magnitude for a normal range of wind speed variations: Roughness lengths 10^{-5} - 0.001 m (4-25 m/s), see Figure 6.4.
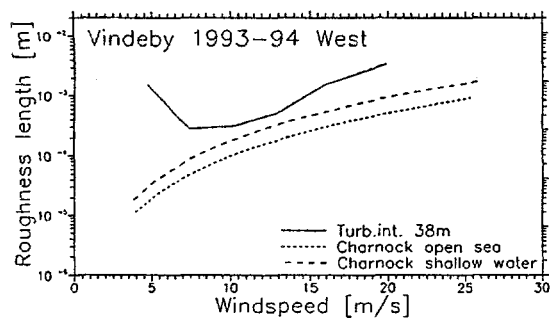
Figure 6.5 *Measured roughness length (turbulence intensity method) compared with results from Charnock relation.*
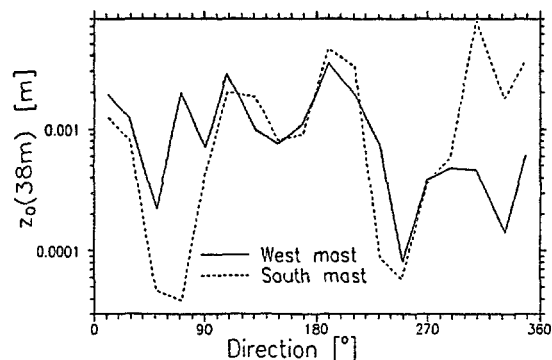
Figure 6.6 *Measured roughness lengths as a function of wind direction for the two offshore masts. The differences around 70° and 320° are due to different wake conditions.*

There are several different ways of calculating roughness lengths from data, Højstrup (1995), each with its own advantages and problems. We shall here employ a rather robust method for the derivation of roughness lengths from measurements of turbulence intensity.

The turbulence intensity, defined as the ratio of standard deviations of wind speed fluctuations to the average wind speed for averaging times of 10-30 minutes can be written as a function of the surface roughness only, for neutral conditions assuming that wind speed standard deviations vary proportionally to u_* (the constant of proportionality very conveniently happens be about 2.5 canceling out the von Karmann constant which is 0.4):

$$I = \frac{\sigma_u}{U} = \frac{\sigma_u}{u_*} \frac{k}{\ln(\frac{z}{z_0})} \approx \frac{1}{\ln(\frac{z}{z_0})}$$

(6.4)

The result of this exercise for the Vindeby site (only neutral data) is shown in Figure 6.5, which also illustrates one of the problems by this method, the roughness length seems to increase at low wind speeds, which to some extent is due to instationarities and stability effects that become increasingly important for the magnitude of the measured turbulence intensity as wind speed decreases (for other possible explanations for higher roughnesses at low speeds, see Wu (1994)). For higher wind speeds we see the data increasing as the theory predicts, albeit at a somewhat higher level than predicted, indicating that the conditions at Vindeby are more rough than the Charnock-coastal prediction indicates.

In Figure 6.6 we have calculated the roughness lengths, using the turbulence intensity method as function of direction for the two offshore masts, and as expected we see quite low values down to less than 0.1mm for the long water fetch directions (south mast 40-80°, both masts at WSW), values of a few millimieters for wind directions where the flow came over land surfaces a few km upstream. The differences between results from the two masts at ENE and NW is due to wake conditions influencing the measurements. The data in this figure consisted of about one years measurements at hub height (38m), with all wind speeds less than 5 m/s neglected.

In Figure 6.7 is shown a set of plots taken from Højstrup et al (1994) where the flow direction is offshore for the Vindeby site, such that the two offshore masts see different fetches, about 1.5km and 2km. Measurements are shown on the left and results from a simple model, Højstrup (1981), are shown on the right. The measurements are averages over eight 30 minute runs. We see the flow accelerating, and the turbulence levels decreasing as it moves out over the water surface.
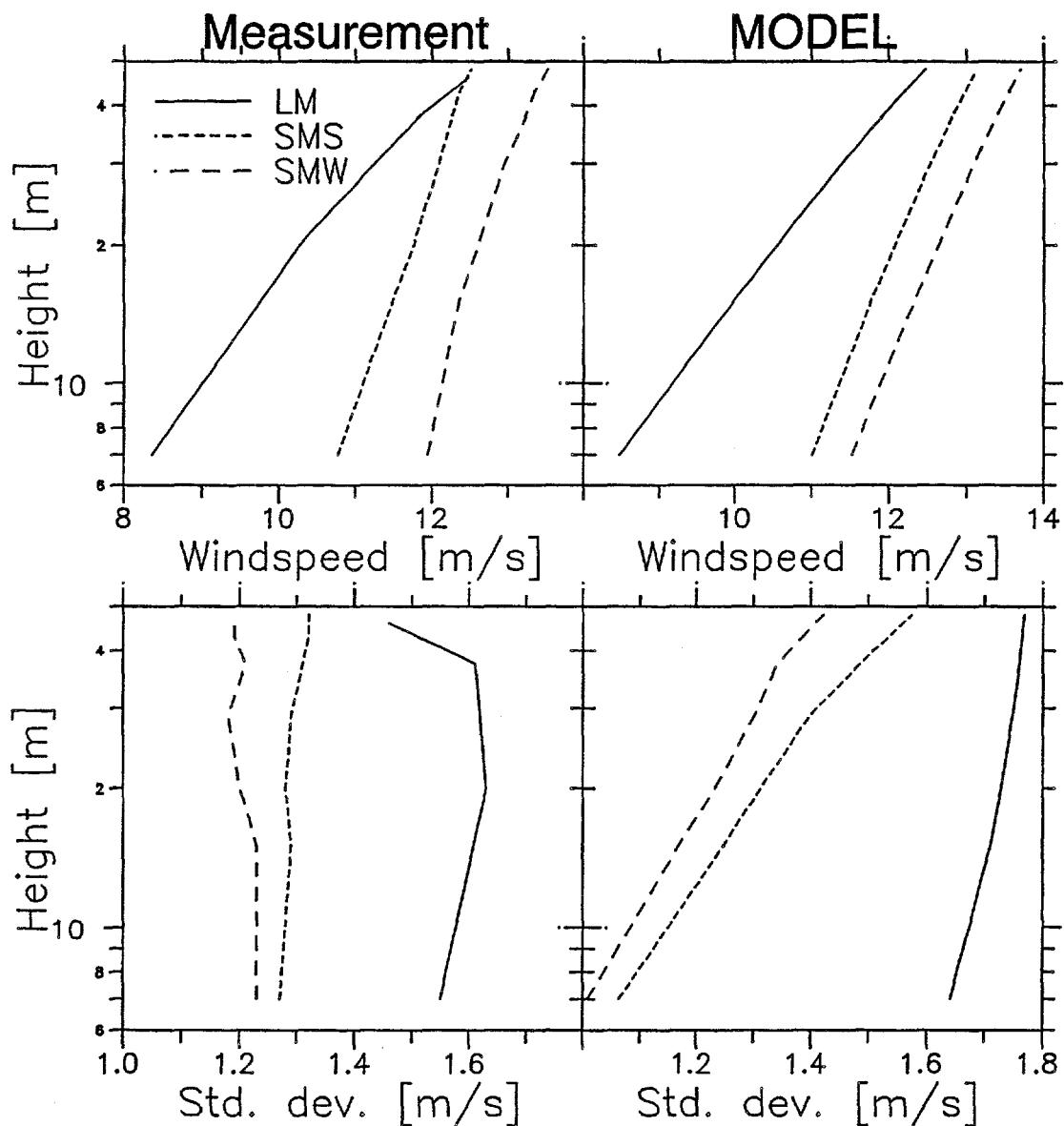
Figure 6.7 *Profiles of wind speed and turbulence from measurements (left) and simple model (Højstrup 1981) for offshore flow.*

6.3 Turbulence levels

The turbulence levels will increase with wind speed because the roughness increases with wind speed. This phenomenon is illustrated in Figure 6.8. showing average values of turbulence intensities from different heights at the West mast as a function of wind speed with wind from the West sector (neutral conditions). As expected, we see the turbulence intensity increase with wind speed towards values comparable with over land values for high wind speeds, and decreasing with increasing height.

Figure 6.9. shows the standard deviations of wind speed fluctuations from hub height at all three masts for wind speeds larger than 5 m/s, and for all wind directions. In order to compare the results from the three masts, we have made a linear fit to the data from each mast, which is shown in Figure 6.10., where we see that there is very little difference between the two offshore masts, showing average turbulence intensities of about 9%, whereas the land mast is somewhat higher, at approx. 11%. For comparison are also shown lines denoting the
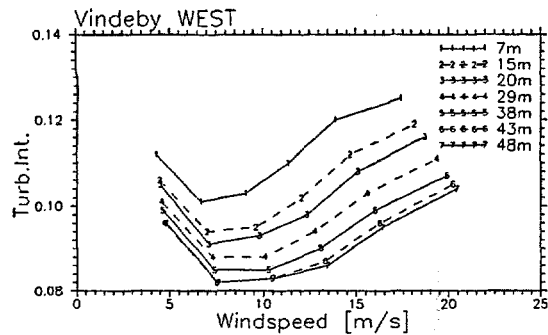
Figure 6.8 *Turbulence intensities as a function of wind speed for the West mast, for westerly winds, neutral conditions.*
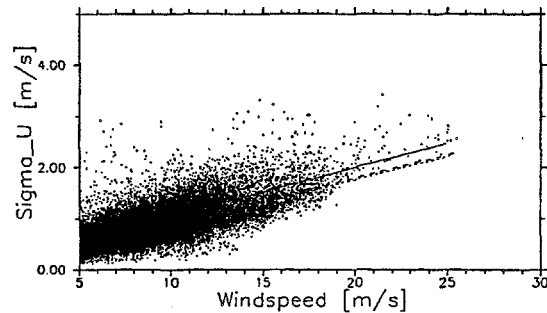
Figure 6.9 *Standard deviations of wind speeds from all three masts for one year.*
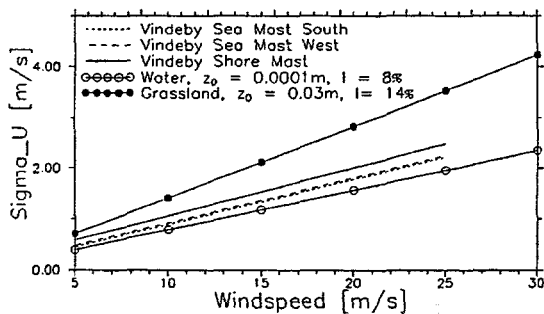
Figure 6.10 *Linear fits to the data in fig. 6.9. Also shown are predicted values for a 'normal' roughness length (0.03m) and for a very small roughness length (=0.0001m)*
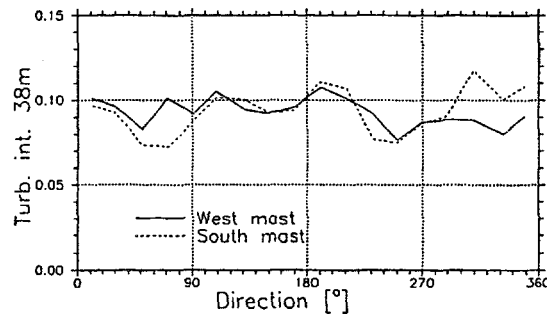
Figure 6.11 *Turbulence intensities as a function of wind direction for the two offshore masts. The differences around 70° and 320° are due to different wake influences.*

expected values for a water surface (8%), and for a land surface (14%), so we conclude that the turbulence at the offshore masts is slightly increased on the average because of the proximity of land, and the turbulence on the land mast on the coastline is of course decreased because the flow is from the smooth sea for a significant portion of the time.

The turbulence intensity as a function of direction is shown in Figure 6.11, where we see the expected low values (8%) for the long water fetch directions, and about 10% for flow from land. As for the roughness lengths, the differences at ENE and NW are due to differences in the wake influences on the two masts.

6.4 Length scales in free flow and in wakes

We see a great variation in the length scales of atmospheric turbulence, mainly due to stability effects, as shown in Figure 6.12, where we have used the spectral formulations of (Højstrup (1982), Højstrup (1990), Olesen et al (1984)). This is maybe better illustrated by Figure 6.13, where the length scales have been calculated for all of the available time series from the Vindeby site. The three frames show data from (top to bottom) the land mast, the South mast and the West mast. Each curve shows the number of occurrences of length scale within each bin, with one curve for each height on the mast in question. We note the following:
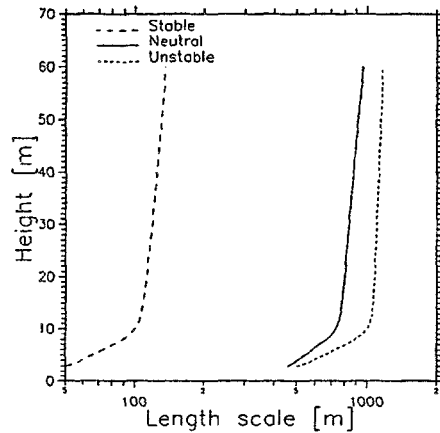
Figure 6.12 *Sketched prediction of the variation with height of turbulence length scale for different stability categories.*
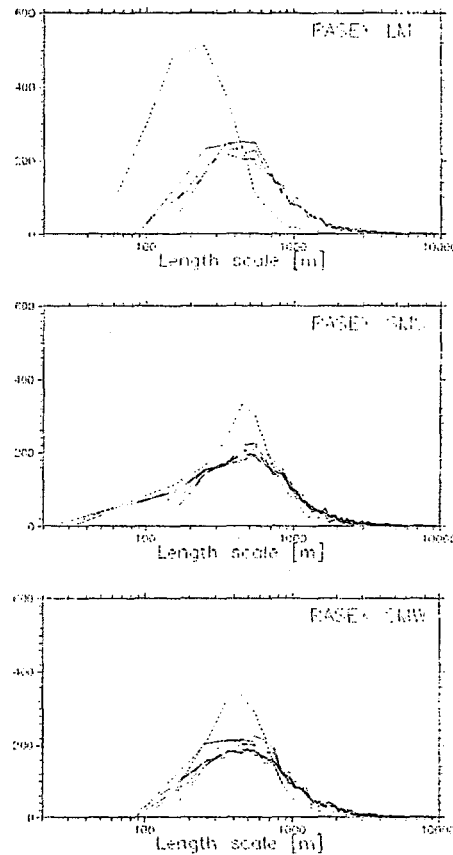

Figure 6.13 *Distribution of length scales for all heights at each mast. The lowest height (7m) is indicated by a dashed line.*

- Length scales vary from tens of meters to several km.

- All heights from 15m and up show similar behavior. The only height that is different is the lowest level (7m) where we see significantly smaller length scales.

- South mast has larger number of very small length scales, attributed to the multi-wake situations seen from this mast.

The average length scales varies with direction as measured in the RASEX experiment with 3D sonic anemometers which is shown in Figure 8.9, where we see shorter length scales for flow from land compared with flow from the sea. In order to further highlight this behavior, we have selected all available neutral time series in the speed interval 7-11 m/s, in 10° sectors around 180° and 300°. from which we very clearly see a decreased length scale on land at 180° (Figure 6.14a) increasing towards the sea, but still much lower than for the corresponding Figure 6.14b for NW-flow.

Downstream of a wind turbine wake, shear layers are created, with typical dimension of a few rotor diameters. These shear layers create turbulence at much smaller length scales than we see in free flow turbulence, which in turn will decrease the overall length scale measured in the wake (Højstrup 1993). One example is shown in figs. 6.15a-c, showing the profiles of wind speed, turbulence and length scales for the South mast downstream of a multi-wake situation.
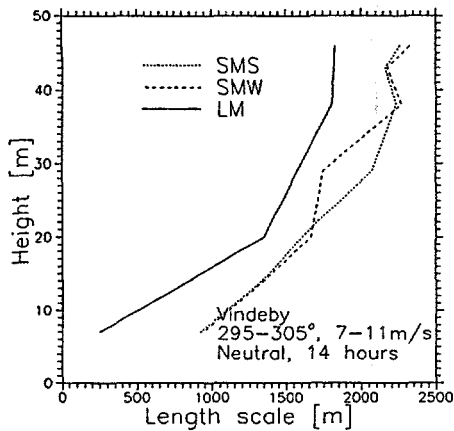
Figure 6.14a *Length scales for onshore flow. 14 hours of data were available from the selected direction. Neutral data, and wind speeds between 7m/s and 11m/s.*
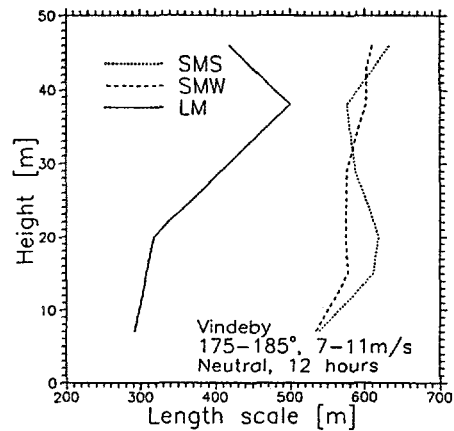
Figure 6.14b *Length scales for offshore flow. 12 hours of data were available from this sector.*
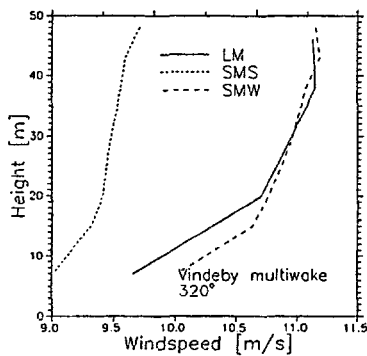
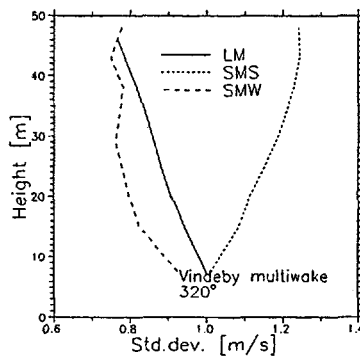**Figure 6.15a** *Wind profiles for a multiple wake situation.*

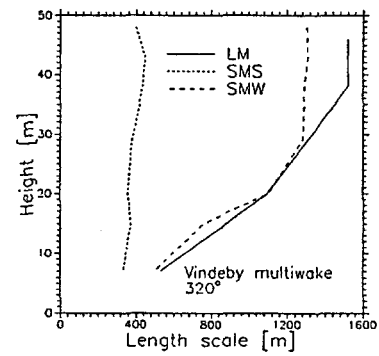**Figure 6.15b** *Profiles of standard deviations of wind speed fluctuations for a multiple wake situation.*

Figure 6.15c *Profiles of length scales derived from velocity spectra from a multiple wake situation.*

We very clearly see the velocity deficit, the increased turbulence levels and the decreased length scales. Furthermore in Figure 6.16 we have taken all multi-wake cases in the speed interval 7-11 m/sec and averaged the length scales, and we see the same behavior, although here we only see a decrease in length scale of a factor of 2, compared with the factor four decrease in the previous case, due probably to the averaging of a large number of profiles.

The shift towards larger length scales is also illustrated in Figure 6.17, which shows the power spectra of velocity signals at 38m from all three masts in a stationary four hour long multi-wake situation. We can very clearly see that the maximum input of energy in the wake spectrum originates around 0.1 Hz, corresponding to a length scale of about 100m, comparable to the cross wind dimensions of the wake. We also note that we see excess energy in the spectrum over a fairly wide frequency range. The response of the cup anemometers deteriorates above the half-power point of 0.8 Hz, causing the spectrum to drop faster than the anticipated -2/3 power-law.
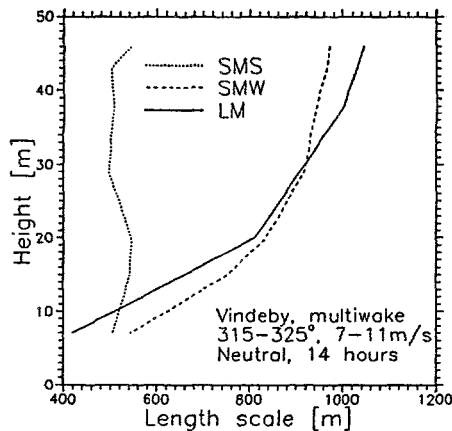
Figure 6.16 *Profiles of length scales in a multiple wake. The data represents an average of 14 hours of data taken within ±5° of the center of the wake. Near-neutral conditions.*
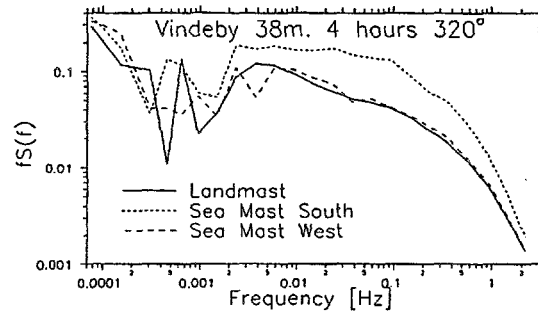
Figure 6.17 *Velocity spectra at hub height computed from a four hour time series. Note the similarity between the land mast and the sea mast west and the increased variance moved towards higher frequencies at sea mast south.*

6.5 Extreme wind speeds

On the basis of two years of data, we have attempted to extrapolate the data to get the anticipated 50 year maximum wind speed. The results have to be treated with some caution, because of the amount of extrapolation in question. The extrapolation has been done on the basis of the monthly maximum 30-minute average values, and the resulting 50 year maximum 30-minute average value is predicted to be about 37 m/s for all three masts (see Figure 6.18).

The 2 second gust value can be obtained from the 30 minute value (Højstrup and Tammelin 1996):

$$U_{2sec} \approx U_{30min} + 3\sigma_u \tag{6.5}$$

where σ_u is the standard deviation of wind speed fluctuations at 37 m/s. Assuming that the high wind speeds come from the sea, and applying the Charnock relation with a constant $A = 0.018$ we get a standard deviation of 4.1m/s (see Figure 6.19), extrapolating the deviation between data and model from Figure 6.19 (data are 13% higher at 20m/s), we get a standard deviation of 4.6m/s resulting in a 2 second gust value of approx. 51 m/s. This result must be treated with some caution, taking into account the amount of extrapolation involved.
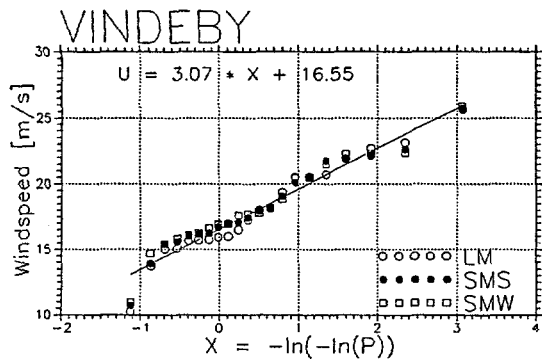
VINDEBY

$U = 3.07 * X + 16.55$

Windspeed [m/s] vs $X = -\ln(-\ln(P))$

LM
SMS
SMW

Coastal (A = 0.018)
Open sea (A=0.011)

Turb.int. [%] vs Windspeed [m/s]

Figure 6.18 *Ordered monthly maximum 30 minute averages from the 38m level at the three masts. Most of the maxima stem from Westerly wind directions.*
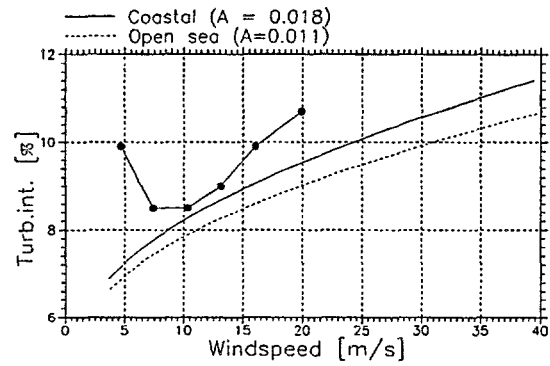
Figure 6.19 *Standard deviations of wind speed fluctuations as a function of mean wind speed using the Charnock relation to calculate roughness lengths. Also shown are measurements, which show somewhat higher values.*

7 STRUCTURAL MODELLING AND THE EQUIVALENT STRESS CONCEPT

In the present section we analyze by means of an aeroelastic computer code how different types of loads reflect in dynamic response of the wind turbine structure, and we present the concept of equivalent stress which has proven very useful in fatigue analysis.

The concept of *equivalent loads* is employed extensively in the analyses following in section 8. Loads are measured with strain gages at a number of structural components. The measured strain is converted into bending moments, which in turn are processed to provide simple statistics (maximum, minimum, mean and standard deviations) and so called load spectra resulting from "rain-flow counting". To make analysis of large quantities of data possible the load spectra are condensed into single numbers, equivalent load widths. Inhere, the basic principles of computation and addition of equivalent widths (*ew* or *s*) from different load cases is outlined.

The *characteristics of the loads* on a wind turbine operating in a single or multiple wake situation are different from loads on a stand alone wind turbine, and some of these differences can be identified through analysis of measured loads and wind field parameters. However, in a wake situation the wind turbine loads are caused by a more complex combination of wind field parameters. It is often difficult to identify and separate the individual wind field parameters and the effect on the loadings from measurement analysis alone. In order to support the analysis of the measurements, aeroelastic load calculations are carried out in this section. Some of the primary changes in the wind field in a wake situation compared to a free inflow situation are investigated with special focus on the influence on fatigue loads of the wind turbine in the wake.

The aeroelastic code HawC used for the load simulations is briefly described, and the aeroelastic modelling of the Bonus 450 kW turbine is verified using the measured loads from a free inflow situation. In the preceding section, the effect on fatigue loads of two important wake phenomena are investigated. These phenomena are mean shear across the rotor disc and increased turbulence.

7.1 Equivalent-Load concept and summation of s

Linear Damage Hypothesis

Stresses less than the ultimate stresses may cause failure of the employed material when repeated more or less frequently. The effect is called fatigue loading. If applying a load which is sinusoidal in shape and constant in frequency and amplitude ($s/2$) the material will fail after a number of cycles (n); in general: the more cycles the smaller stress amplitude is needed for the material to fracture. These sets of stresses and corresponding number of cycles before failure are found experimentally and denominated S-N or Wöhler curves:

$$n_{fat} = n_{fat}(s) , \quad s = f_s(n_{fat}) \tag{7.1}$$

For series of sinusoidal loads with different amplitudes and frequencies the damage relative to the strength is evaluated by the Palmgren-Miner sum

$$\Delta = \sum_{i=1}^{N} \frac{n_i(s_i)}{n_{fat}(s_i)} \tag{7.2}$$

where $n_i(s_i)$ is the number of cycles at stress range s_i and $n_{fat}(s_i)$ is the number of cycles at the same stress range that would cause fatigue. N is the number of discrete ranges applied. Failure is assumed to occur when the sum (7.2) exceeds 1. The quantity $n_i(s_i)$ is called the (inverse) load spectrum. When - as in the real world - the stress variations are not neat consecutive series of sinusoidal, but any arbitrary function the load spectrum $n_i(s_i)$ is calculated from a "rainflow counting" algorithm , which is found to represent fatigue mechanisms well. Thus, for a given structure the sustainability to fatigue is evaluated by an estimated or experimentally derived representative load spectrum for the whole design lifetime, e.g. 20 years, of the structural component considered.

It should be noted that in addition to the levels of stress variation, the mean of the loading may influence the fatigue effect considerably. This is ignored in the present context, where the goal is to devise a method of identifying relevant load cases and adding these in a rational manner, resulting in limited number of load cases for design use.

Equivalent Width Concept

Using a fixed number of reference cycles, n_t (here chosen to be equal to the integrated number of range cycles $n_t = \Sigma n_i$, which in turn is close to the number of rotor rotations during the considered 1800 sec periods), the concept equivalent width may be introduced:

$$\Delta = \sum_{i=1}^{N} \frac{n_i}{n_{fat}(s_i)} = \frac{n_t}{n_{fat}(s_e)}, \quad s_e = f_s(\Delta^{-1} n_t) \tag{7.3}$$

i.e. the equivalent width is the width that creates the same partial damage as the real stress sequence when applied the integrated number of cycles, Σn_i.

Combination of Equivalent Widths, Simplified S-N Curve

For convenience the simplified S-N curve is introduced:

$$n_{fat} = \frac{k}{s^m} \quad \Leftrightarrow \quad s = \left[\frac{k}{n_{fat}}\right]^{\frac{1}{m}} \tag{7.4}$$

where k and m are constants dependent on the applied materials[1]. Equivalent widths, $s_{e,j}$, for N time series - each with the probability p_j - is weighted as follows:

$$\Delta = \sum_j^N \frac{n_t}{k} s_{e,j}^m p_j = \frac{n_t}{k} s_e^m \Rightarrow s_e = [\sum_j^N p_j \, s_{e,j}^m]^{1/m} \tag{7.5}$$

The equivalent width is sensitive to a number of different parameters and the principle of weighing is the same as for separate time series:

$$s_{e,j} = s(x_1, x_2, \ldots\ldots) = s(x_i) \tag{7.6}$$

where the parameters x_i are wind speed, wind direction, turbulence intensity, turbulence scale etc. Interpreting data and modelling flow in wind farms the main task is to map/model the function (7.6).

Denominating the joint probability frequency distribution of the x_i's $p = p(x_1, x_2, \ldots\ldots) = p(x_i)$ the summation may be written in integral form:

$$s_e = \left[\int_1 \int_2 \cdots \int_K p(x_i) \, s(x_i)^m \, dx_1 dx_2 \ldots dx_K \right]^{\frac{1}{m}} \tag{7.7}$$

A relevant questions: why use the equivalent stress concept when partial damages summarize so much more simple? Because the needed increase in the load carrying capability of a structural component is proportional to the increase in equivalent stress. This means that if new load conditions yield an equivalent stress x per cent larger than under another set of load conditions then the sectional modulus of the considered structural component must also be increased x per cent, i.e. load carrying capability is linear in equivalent stress. Thus, the equivalent stress is in better correspondence with intuition than lifetime consumption.

---

[1]For steel the exponent m is of the order 5, for fiber glass 10-12.

Evaluation of idealized cases

We evaluate first three simple cases which will be useful for the data analysis. Thus, we take one parameter at a time:

$$s_e = \left[\int p(x)s(x)^m dx \right]^{\frac{1}{m}} \tag{7.8}$$

i.e. other parameters than the one considered are assumed fixed. The distribution of the parameter, $p(x)$, on which the equivalent stress depends, is assumed to be satisfactorily described by either the Weibull or the Normal distribution or a rectangular distribution. The integrated fatigue loading will be a function of both mean μ and variance σ^2 of x. In the following we device formulas to determine the "equivalent mean", μ_e, i.e. values of the parameter that would yield the same integrated fatigue loads as the distributed parameter.

Depending on the parameter considered, fatigue loads are assumed linear in x, $s(x) = \alpha(\beta + x)$, depending on x as $s(x) = \alpha x^h$, or having a "bell-shape" modelled by an exponential function. The integral (7.8) is evaluated for these functions combined with the mentioned distribution functions.

Normal Distribution and $s(x) = \alpha(\beta + x)$

When the parameter (as e.g. turbulence σ_u with fixed wind speed) has a Normal distribution

$$p(x) = \frac{1}{\sigma\sqrt{2\pi}} \exp[-\tfrac{1}{2}(\frac{x-\mu}{\sigma})^2] \tag{7.9}$$

where μ and σ are mean and standard deviation, respectively, and the sensitivity of equivalent load to the parameter is

$$s(x) = \alpha (x + \beta) \tag{7.10}$$

we get the integrated equivalent load from:

$$s_e^m = \alpha^m \int_{-\infty}^{\infty} (x+\beta)^m p(x) dx \tag{7.11}$$

The integral is evaluated in **Appendix A**. Thus, with the slope of the S-N curve of m we get

$$S_e = \alpha \, r_m = \alpha \, \mu_o \, r_e \tag{7.12}$$

where $r_o = 1$, $r_1 = 1$, $r_2 = 1 + \sigma_*^2$ and

$$r_m = [r_{m-1}^{m-1} + (m-1) \, \sigma_*^2 \, r_{m-2}^{m-2}]^{1/m} \tag{7.13}$$

For small values of $\sigma_* = \sigma/\mu_o$ an approximation to (7.13) is

$$r_e \simeq (1 + \tfrac{1}{2}(m-1)\sigma_*^2) \tag{7.14}$$

The equivalent mean of the parameter is

$$\mu_e = \mu_o \, r_e = (\mu+\beta) \, r_e \tag{7.15}$$

The principles are exemplified in Figure 7.1, where equivalent widths of blade root bending moment are plotted as function of wind speed. The equivalent width is seen to increase with wind speed rather linearly with considerably scatter. The regression analysis gives a standard uncertainty around the line of $\sigma_s = 2.3$ kN and with

$\sigma_* = \sigma_s/s_e$ it is found by means of (7.15) that $r_e = 1.02\text{-}1.04$, being largest for small wind speeds. Thus the effective equivalent width is 2-4% larger than what is found simply by averaging. For the (low) value of m applied in the following analysis r_e is close to unity and is consequently ignored. For large ms this correction factor must be taken into account.

Rectangular distribution and bell-shaped s(x)

Next, we consider the case where the frequency distribution is rectangular, $p(x) = constant = 1/(2a\beta)$, $x \in [-a\beta, +a\beta]$ and the equivalent stress depends on a parameter, e.g. wind direction, as an exponential:

$$s(x) = c \; [1 + \alpha \; \exp(-(\frac{x}{\beta})^2)] \qquad (7.16)$$

by

$$s_e^m = (\frac{c^m}{2a\beta}) \int_{-2a\beta}^{2a\beta} (1 + \alpha \; \exp[-(\frac{x}{\beta})^2])^m dx \qquad (7.17)$$

Figure 7.1 *Equivalent width, s_e (ew); regression line $s_e = 1.96u + 6.91$, $\sigma_s = 2.3$.*

The equivalent stress over the interval $[-a\beta, a\beta]$ is given

When combining s's from different wind directions, it is practical to find an "equivalent width", $2b_e\beta$, of the bell. The derivation is shown in **Appendix A**, the exact result as well as an approximate expression are

$$b_e = \frac{\sqrt{\pi}}{2} \; \frac{\sum_{i=1}^{m} \begin{bmatrix} m \\ i \end{bmatrix} \frac{\alpha^i}{\sqrt{i}}}{\sum_{i=1}^{m} \begin{bmatrix} m \\ i \end{bmatrix} \alpha^i} \approx \frac{2 + \sqrt{m} \; \alpha^{1.25}}{2 + m \; \alpha^{1.25}} \qquad (7.18)$$

Figure 7.2 shows the principle of replacing an observed bell-shaped wake with a rectangular shaped wake. It is seen that for a material with a steep SN-curve (large m) the wake actually appears more narrow, since the maximum becomes increasingly important.

In Figure 7.3 the equivalent wakes are shown for different relative peak heights. It is seen that the smaller the relative peak the broader is the equivalent wake.

Figure 7.2 *Equivalent, rectangular wakes for m=5 (broad) and m=12.*
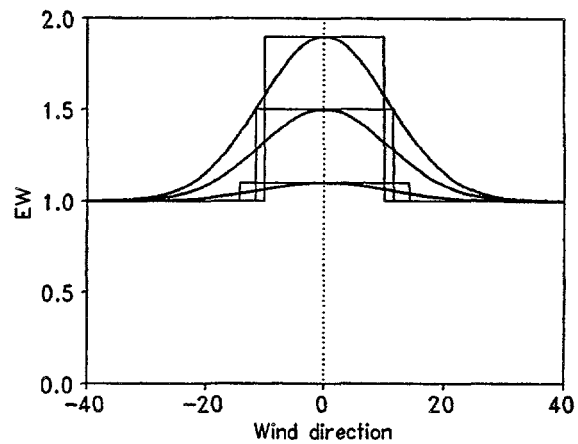
Figure 7.3 *Equivalent wakes for different relative peak heights (α), m=5.*

Similar expressions for correction factor and equivalent width are developed in **Appendix A** for a Weibull distribution and a equivalent width $s(x)=\alpha x^h$. The results are summarized in table 7.1 together with expressions for the cases treated above.

7.2 The aeroelestic model

The computer program applied is the aeroelastic code HawC, Thirstrup Petersen (1990). The model is basically a finite element model developed as a special-purpose wind turbine model. The model's compuational substructures of nacelle and rotor makes it unique compared to general purpose finite element programs, because these usually do not offer a satisfactory modelling of rotating substructures.

The structural model is based on 2-node prismatic beam elements, each note with 6 degrees of freedom, corresponding to 3 translations and 3 rotations. The wind turbine structure is subdivided into 3 substructures, the tower, the shaft/nacelle and the rotor. The shaft/nacelle and the rotor are described as rotating substructures, coupled to each other and to the tower. An example of a typical division of the wind turbine into finite elements is shown in Figure 7.4.

Both the elastic deformations -including rotations - and the bearing restrained rotations at the coupling nodes are taken into account in the expressions for the inertia loads on the substructures. Distributed loads on the elements (inertia, aerodynamic and gravity) are consistently transformed to the nodes. This results in a complete coupled dynamic model for the response of the wind turbine to external loading described by a set of discrete, nonlinear, ordinary differential equations with time varying coefficients, comprising the equations of motion, which arranged as a matrix equation has the general form
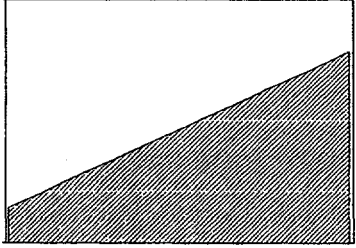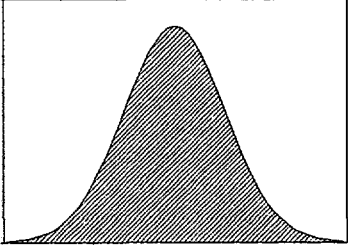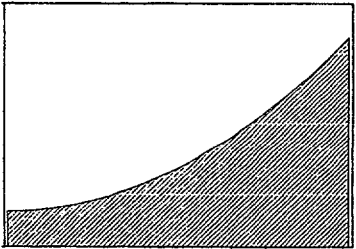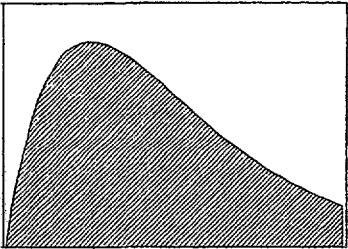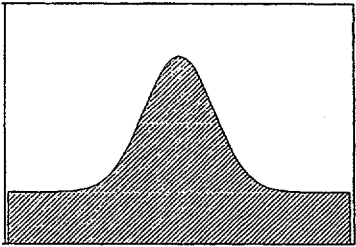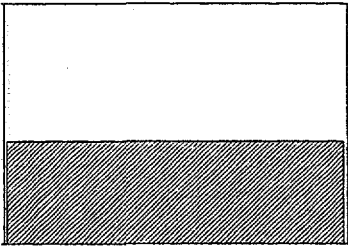
SENSITIVITY FUNCTIONS $s = s(x)$	FREQUENCY DISTRIBUTION $p = p(x)$	SUMMED EQUIV. STRESS $s_e^m = \int s(x)^m p(x)dx$
$s(x) = \alpha\,(\beta + x)$ Turbulence Shear Turbulence scale 	$p(x) = \dfrac{1}{\sigma\sqrt{2\pi}}\exp(-\tfrac{1}{2}(\dfrac{x-\mu_o}{\sigma})^2)$ $\mu_o = \mu + \beta$ 	$s_e = \alpha\,\mu_o\,r_e,\quad r_e{=}r_m$ $r_o{=}1,\ r_1{=}1,\ r_2^2{=}1+\sigma_*^2,\ \sigma_*{=}\sigma/\mu_o$ $r_m = [r_{m-1}^{m-1} + (m-1)\sigma_*^2 r_{m-2}^{m-2}]^{1/m}$ For small σ_*: $r_e \simeq (1+\tfrac{1}{2}\sigma_*^2 (m-1))$ $x_e = \mu_o r_e = (\mu+\beta)r_e$
$s(x) = \alpha\,x^h$ Mean wind speed 	$p(x) = (\dfrac{k}{A})(\dfrac{x}{A})^{k-1}\exp(-(\dfrac{x}{A})^k)$ $\mu = A\,\Gamma(1+\dfrac{1}{k})$ 	$s_e = \alpha\,\mu^h\,r_e$ $r_e = \dfrac{\Gamma(1+(mh)/k)^{1/m}}{\Gamma(1+1/k)^h}$ $x_e = \mu\,r_e^{1/h}$
$s(x) = c\cdot[1 + \alpha\,\exp(-(\dfrac{x}{\beta})^2]$ Wind direction (Wake conditions) 	$p(x) = constant$ 	Equivalent width: $2\,b_e\,\beta$ $b_e = \dfrac{\sqrt{\pi}}{2}\left[\dfrac{\sum_{i=1}^m \binom{m}{i}\dfrac{\alpha^i}{\sqrt{i}}}{\sum_{i=1}^m \binom{m}{i}\alpha^i}\right]$ Simple fit: $b_e = \dfrac{3 + \sqrt{m}\,\alpha^{1.25}}{3 + m\,\alpha^{1.25}}$

Table 7.1. *Summary of conversion formulas for equivalent loads.*

(7,20)

$$[M]\{\ddot{x}\} + [C]\{\dot{x}\} + [K]\{x\} = \{F\}$$

Where *[M]* is the mass matrix, *[C]* is the combined structural damping and Coriolis/gyroscopic matrix, *[K]* is the combined structural, geometrical and inertia stiffness matrix, *[F]* is the force vector composed of terms originating from aerodynamic, gravity and inertia loads, and *{x}* is the vector of translations and rotations.

The aerodynamic loads are derived by use of a quasi-steady theory, based on combined blade element and momentum theory. A dynamic stall model based on work by Øye (1991) is used in the load calculations. The model for aerodynamic load calculation is fully aeroelastic, the influence of the elastic deformations on the aerodynamic force being accounted for. The free-wind vector is composed of a deterministic part including wind shear and tower interference, and a stochastic component, generated according to Mann (1994).
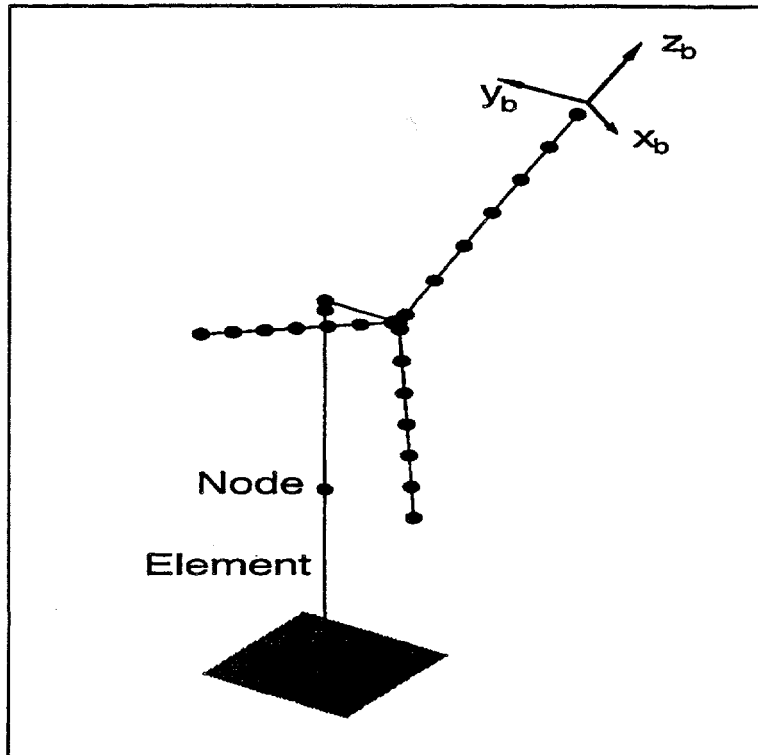
Figure 7.4 *Finite element model of the wind turbine.*

This turbulence simulation method, Mann (1994), is based on a model of a spectral tensor for atmospheric surface layer turbulence at high wind speeds, corresponding to neutral stratification. The model assumes that the turbulence homogeneous in space but it allows non-isotropic turbulence and also includes the influence of shear. The model delivers a full three-dimensional turbulence field.

The wind shear is described by either a log- or a power-law or alternatively, the shear field might be predefined through definition as a vector field on a planar grid perpendicular to the mean wind direction at hub height, which is read from a file. The tower interference is taken into account by use of a potential flow model.

The equations of motion of the wind turbine are solved each time step, resulting in sets of time series of selected loads.

7.3 Modelling the bonus 450 kW wind turbine

The data for the Bonus 450 kW wind turbine are provided by Bonus A/S and the data for the blades by the blade manufacturer LM Glassfiber A/S. The main parameters for the wind turbine are given in Table 7.2.

The airfoil data are based on 2D data for the actual profiles. These data have been modified in order to be able to match measured mean flapwise bending moment and electrical power curve under ideal conditions.

The structural dynamics of the turbines at Vindeby are measured at stand still and the natural frequencies are used to adjust the mass and stiffness distributions of the aeroelastic model so that the correct natural frequencies are applied. The measured and simulated natural frequencies are given in Table 7.4.

Table 7.2 *Main data for the 450kW Bonus wind turbine.*

Parameter	Value
Rotor diameter	35.0 m
Hub height	35.0 m
Rotor rotational speed	35.2 rpm
Tilt	4°
Blade type	LM 17HHT
Blade length	16.0 m
Profiled blade length	14.0 m
Cord length (root/tip)	1.40/0.48 m
Twist	11°
Profiles	NACA 63200 (modified)

Table 7.3 *Measured and simulated natural frequencies at stand-still (1P=0.58Hz).*

Parameter	Measured (Hz)	Computed (Hz)
1st tower bending (cross-wind)	0.90	0.92
1st tower bending (along-wind)	0.94	0.93
1st asymm. rotor/tower torsion (yaw)	1.78	1.78
1st asymm. rotor/2nd tower bending (tilt)	1.97	1.98
1st symm. rotor, flapwise	2.20	2.19
1st asymm. rotor, edgewise	3.27	3.26

Table 7.4 *Measured and simulated natural frequencies at stand-still (1P=0.58Hz).*

Parameter	Measured (Hz)	Computed (Hz)
1st tower bending (cross-wind)	0.90	0.92
1st tower bending (along-wind)	0.94	0.93
1st asymm. rotor/tower torsion (yaw)	1.78	1.78
1st asymm. rotor/2nd tower bending (tilt)	1.97	1.98
1st symm. rotor, flapwise	2.20	2.19
1st asymm. rotor, edgewise	3.27	3.26

Load measurements from a free inflow situation are used for a verification of the modelling of the Bonus 450 kW turbine. Binned statistics of the electrical power, flapwise bending moment and yaw moment from a wind direction of 253° to 258° are compared to simulated loads in Figure 7.8, Figure 7.9 and Figure 7.10.

In the chosen wind direction range, the 4W turbine is operating in free inflow, and data from this turbine are used. The measured loads are 30 minutes values while the simulations are carried out in 5 minute periods. In

order to compensate for this, the turbulence intensity in the simulations is increased with the ratio of the turbulence spectrum integrated from 1/300 Hz (frequency corresponding to 5 minutes) and 1/1800 Hz (30 minutes), respectively. Still some differences between simulated and measured extreme values of the electrical power can be seen. The reason for this is, that the electrical power is sensitive to low frequency turbulence, and the correction of the turbulence intensity in the simulations do not change the low frequency part of the turbulence. Furthermore, the damping of the drive train system could be assumed too high. However, the overall agreement between the measurements and simulations is good.

Aeroelastic Modelling of a Turbine Operating in Wake

In general, the characteristics of the loads on a wind turbine operating in the wind farm flow environment are significantly different from the loads on a stand alone turbine. The differences are caused by several changes of the wind field; the mean wind speed in a wake is reduced, the variance of the wind speed is increased and the overall structure and characteristics of the turbulence field are altered (presumably also spectra and coherence). Previous measurements have indicated that increased loads on a turbine in wake primarily are due to two changes in the wind field. In Thomsen et al (1994) the loads in wakes at a distance of 3.8D (spacing of the turbines are 3.8 times the rotor diameter) show a significant deterministic character, caused by the wind speed shear across the rotor. A very clear 1P variation of the flapwise blade bending moment is seen for the wake situation, due to the blade passing in and out from higher and lower wind speeds. This is also the condition for measured loads presented by Poppen and Dahlberg (1992). In this case, measurements are presented for spacings of 5D, 7D and 9.5 D, and the deterministic character of the loads is most significant for the 5D spacing. In another study, Thomsen et al (1993), the loads on a turbine in a complex terrain wind farm have been investigated. The spacing in the wind farm is 6.5D, and the character of the loads in wake is similar to the character of the loads on the turbine in free inflow, but at a higher turbulence level.

This could indicate, that in some cases the fatigue loads on turbines in wake operation are primarily caused by the wind shear across the rotor, and in other cases, the loads are mainly due to increased turbulence intensity. This suggests that the spacing of the turbines in combination with the turbulence originating from the terrain roughness could be the parameters competing on which is the most important. This is a very simplified consideration, and in wake situations the loads will be caused by combinations of these phenomena as well as others. However, in the following, this hypothesis will be tested by investigation of the sensitivity of the loads to shear and turbulence.

Load sensitivity to mean shear

In order to investigate the load sensitivity to mean shear across the rotor a simplified approach is followed. The vertical and horizontal mean wind speed variations are modelled as linear shear over the rotor. The shear is described as the maximum mean wind speed difference across the rotor, A, and this parameter is varied from $A = 1.5$ m/s to $A = -1.5$ m/s with steps of 0.3 m/s. The mean wind speed at hub height is 10 m/s, the turbulence intensity is 7% and only purely vertical or horizontal shear is investigated. The influence of shear on the loads is illustrated as accumulated power spectra of the flapwise bending moment and yaw moment in Figure 7.11 and Figure 7.12. In Figure 7.13, the sensitivity of shear to the equivalent loads is illustrated. The fatigue loads are presented as damage equivalent load ranges calculated using an equivalent number of load cycles corresponding to 1P. In the on-line analysis of the measurements the equivalent load ranges have been stored for a Wöhler curve exponent of $m=5$ only, and that exponent is used in the analysis of the simulated loads, as well.

As expected, the shear across the rotor results in increased energy at 1P for the flapwise blade bending. The shear is causing increased deterministic content of the load due to the passage in and out of higher and lower wind speeds, similar to the effect of a yaw error. The shear does not change the energy at zero frequency or at other harmonics of the blade passage frequency than 1P. No influence of the shear on the yaw moment is seen, Figure 7.12. This load is primarily caused by the lack of coherence across the rotor, which is not influenced by the average shear across the rotor. The influence on the blade load from the vertical and horizontal shear is not identical. This is due to the different interference with the tower shadow and the tilt of the rotor of these two types of shear. The difference in the flapwise equivalent load for the different shear is maximum 25% while the influence on the tilt and yaw moments is smaller and properly caused by the statistical

scatter in the load predictions.

Load sensitivity to turbulence

The load sensitivity to turbulence is found from a series of aeroelastic calculations with different turbulence intensities. The turbulence intensity is varied from 4% - 20%, the mean wind speed is 10m/s in all calculations, and the time duration of the simulations are 300 seconds. The results are given in ? as fatigue equivalent load ranges for the flapwise bending-, tilt- and yaw moment. All loads are highly sensitive to turbulence. Twice the turbulence intensity - e.g. from 10% to 20% - would cause the rotor loads (tilt- and yaw moments) to increase with a factor of nearly two, and the flapwise slightly less than a factor of two, due to a relatively higher deterministic content. In Figure 7.15 and Figure 7.16 the differences in the loads are illustrated as accumulated power spectra from the calculations with turbulence intensity of 8% and 16%, respectively. The primary difference in the blade load is seen at zero frequency and for the 1P frequency and higher harmonics. For the yaw moment (which is similar to the tilt moment), the primary difference is seen at zero frequency and harmonics of 3P. The difference in total accumulated power spectrum - which in the present case is equal to the variance of the signals - reflects the high sensitivity of equivalent loads to turbulence.

In order to investigate the characteristics of the loads on a turbine in wake, a number of measured time series are analyzed. The overall trend in all analyzed time series is the same, and only results from one of these time series are presented here. The actual time series is measured when the 4W unit is subject to free inflow (wind direction is 255°) and the 5E turbine operates in the 9.6D single wake of the 4W turbine. The free wind speed is measured 9.6D upwind of the 4W turbine.

The free wind speed is 10.8m/s, and the free turbulence intensity is 6.3%. The wind speed in the wake situation is not measured but can be estimated from the mean value of the electrical power of the turbine in wake. The mean power of the 5E turbine is 205 kW and from the power curve the corresponding mean wind speed can be found to be approximately 9.5m/s, i.e. a wind speed deficit of 1.3m/s which seems reasonable, see section 8. Concerning the turbulence intensity in the wake situation, an approach described by Frandsen and Christensen (1980), Madsen and Frandsen (1984) and outlined by Thomsen and Petersen (1992) is applied. Below stall, assuming that the wind over the rotor contribute equally to the power output, the instantaneous power output can be approximated as

$$p(t) \approx p_o + \frac{a}{\pi R^2} \cdot \int_0^R \int_0^{2\pi} (u(r,\theta,t) - U_o) \, r \, dr d\theta, \quad a = \left[\frac{dP}{dU} \right]_{U=U_u} \tag{7,21}$$

where U_o is the mean wind speed, $u(r,\theta,t)$ the instantaneous wind speed at rotor coordinates (r,θ) and a the slope of the power curve $P=P(U)$ at U_o. Thus, the variance of power output is from:

$$\sigma_p^2 = \int_0^\infty S_p(\omega) \, d\omega = a^2 \int_0^\infty S_u(\omega) \, H^2(\omega) \, d\omega \tag{7,22}$$

where S_u is the point power spectrum of wind speed as e.g. modelled by von Karman, and H is what could be called the rotor filter:

$$S_u(\omega) = 0.475 \, \sigma_u^2 \, \frac{c_u h/U_o}{[1 + (c_u h/U_o)^2 \omega^2]^{5/6}}, \quad H^2(x) = \frac{2+x^2}{(2+0.55x^2)(1+x^2/0.55)}, \quad x = \frac{\gamma R}{U_o}\omega \tag{7,23}$$

where c_u is a constant (≈ 10) and γ is a constant related to the lateral coherence of the along-wind component of wind speed. It is seen from (7,23), that the wind spectrum scales with $c_u h/U_o$, and the filter function with $\gamma R/U_o$, but since in general terms rotor diameter is proportional to hub height, h, and the coherence parameter should be assumed to follow the turbulence-scale parameter c_u, we should expect the integral (7,22) as a first order approximation to be independent of wind turbine size:

$$\sigma_p = B \, a \, \sigma_u \tag{7,24}$$

In general it is found that $B=0.8-0.9$. Using the Vindeby measurements of the free wind speed standard deviation and the standard deviation of the electrical power of the wind turbine in free inflow, the constant B can be found for this turbine to be 0.82. Having found this constant, and assuming the same constant for the

turbine in wake, the turbulence intensity in the wake can be calculated using the above relation to a value of 14.2%. However, more details and direct measurements on wake turbulence is presented in section 8.

It is now assumed, that the shear has a minor influence on the loads for the turbine in the wake situation, and therefore only the wind speed reduction and increased turbulence intensity are taken into account. Two aeroelastic calculations are carried out, one for the free inflow situation, and one for the wake situation. The resulting loads are presented as accumulated power spectra in Figure 7.17, Figure 7.18 and Figure 7.19 for both measurements and simulations in free inflow and wake, respectively. In Table 7.5 the equivalent load ranges are given for the time series.

In the comparison of the accumulated power spectra of the loads it is seen, that the main features of the measured loads for the turbine in wake are included in the simulation in the wake situation. For the flapwise blade load in particular, the characteristics of the measured loads in free inflow and in wake is reflected in the simulations. In the accumulated power spectra for the measured rotor loads, a small amount of energy is observed at 1P. This is

Table 7.5 *Measured and computed equivalent load ranges for selected time series. All equivalent load ranges correspond to 1P and m=5.*

Parameter	Measured		Computed	
	Free-inflow	Wake	Free-inflow	Wake
Flap [kN]	27.7	57.8	23.7	50.4
Yaw [kN]	39.0	75.1	32.1	62.4
Tilt [kN]	39.5	88.3	32.1	68.1

either due to mass- or aerodynamic imbalance of the rotor: one blade with a different pitch setting than the other two blades. This is not included in the simulations, and accordingly no 1P energy content is observed for the simulated rotor loads. The main characteristics for the rotor loads are reproduced in a convincing way even though some discrepancies are seen in the total accumulated power spectra. These discrepancies are more pronounced in the fatigue analysis of the time series, Table 7.5. Even for the free inflow case, the simulated equivalent loads are smaller than the measured loads. For the flapwise blade the equivalent load range from the simulation is 14% smaller than the measured value, for the yaw moment 18% smaller and 19% smaller for the tilt moment. Approximately the same is observed for the wake case; flapwise load is underestimated by 13%, yaw 17% and tilt 23%. In the evaluation of these differences, it is necessary to have in mind the statistical variation of the equivalent load range in general. As will be shown later on, if measurements in the free inflow situations are selected at the same turbulence level and at the same wind speed, the variation of the equivalent load range can be expected to be very high. Variations of 20% is often seen for the measured equivalent load range at the same operational conditions. The same can be seen for simulations, where the main cause for the statistical scatter is the random seed parameter in the generation of the wind turbulence time series. In the present investigation, the sensitivity of equivalent load ranges to random seed is not analyzed, but previously this has been done, Thomsen et al (1996), and a variation of 10-15% can be expected for simulations. Having these values for the statistical scatter in mind, the results from the fatigue analysis of the selected time series seems acceptable.

To investigate the statistical scatter of the fatigue loads for the present measurements, a large number of measurements are analyzed in the following. This would furthermore give information on the fatigue loads at other wind speeds than 10 m/s. Measurements are selected in the wind direction range 253°-258°, where the situation is similar to the situation for the selected time series discussed earlier. The 4W turbine operates in free inflow, and the 5E turbine operates in a single 9.6D wake.

In Figure 7.20, Figure 7.21 and Figure 7.22 the comparison of measured and simulated equivalent loads is illustrated for the flapwise bending moment and the tilt and yaw moments.

The free turbulence intensity is 6-8% for the measurements. The simulations are carried out in three cases. The first corresponds to the free inflow situation, and the second and third case correspond to a wake situation. These wake calculations are performed with inclusion of a wind speed deficit and a turbulence intensity of I=16% and I=12-13%. For the latter, 13% is used at lower wind speeds, and the turbulence intensity is decreasing to 12% at the highest wind speed. This value for the turbulence intensity is found from an analysis of the wind field in a wake. In both wake cases (I=16% and I=12-13%), the wind speed deficit is found from

an analysis of the measured wind in a wake situation (i.e. at another wind direction, causing the wind mast to be in a single 9.6D wake).

All three equivalent loads are simulated well in free inflow, but for the wake case, it seems that the turbulence intensity of 16% should be used in the calculations in order to be able to predict the loads at lower wind speeds. At higher wind speeds (>13m/s), the calculations based on 16% turbulence overpredict the measured loads, and the calculations with a turbulence intensity of 12% fit well with measurements. Thus, if the loads on a turbine in wake operation should be predicted using this very simple approach, where the only wake phenomena included are the wind speed deficit and increased turbulence intensity, the turbulence intensity at the lower wind speeds must be set to a higher value than can be measured in the wake.

The variation of the measured loads in the wake situation is significantly higher than the variation of the measured loads in the free inflow situation. This could be due to variation in the wind field parameters not included in this investigation, e.g. turbulence spectrum, coherence etc. These parameters could furthermore account for the discrepancies between the simulated and measured loads at the low wind speeds.

7.4 Summary of load sensitivity analysis

Two characteristic wind field parameters have been investigated for a wind turbine operating in a wake situation. These parameters are wind speed shear and turbulence intensity. The load sensitivity to the parameters has been investigated, and in general the sensitivity to shear is low, while the sensitivity of the turbulence intensity is high. A detailed investigation based on time series analysis has indicated that the turbulence intensity is the main parameter causing the loads to increase in the wake situation. Aeroelastic load calculations have been performed, and it has been found that the characteristics of the measured loads in some cases can be simulated well if only wind speed deficit and increased turbulence intensity is included. This means that the characteristics of the wind field in the wake situation is similar to the characteristics of the wind field in free inflow as far as wind turbine response is concerned. Some discrepancies are seen in the simulation of equivalent loads for lower wind speeds, though. From the analysis of the wind field in a wake situation, an average turbulence intensity of approximately 13% at 6-9 m/s was used in the aeroelastic load calculations, and doing so the loads are underpredicted. Aeroelastic calculations with a turbulence intensity of 16% gives satisfactory agreement with measured loads for this wind speed interval. The results given here apply for the relatively high spacing (9.6D) of turbines, and in case of lower turbine spacing other phenomena in the wake may be of importance.

The investigation has been based on a specific wind turbine type in a particular wind farm. However, it is important whether the results apply in general to the load case of wind turbines in wake-operation or whether the applicability is more or less restricted to the present case. Thus the question is whether the results may be exptended to other component loads, wind turbine separations and other types of wind turbines.

The main findings concerning the wake wind field characteristics are increased turbulence intensity, reduced mean wind speed, reduced turbulence length scale and increased horizontal and vertical shear in the wake situation. All these parameters influence the wind turbine loads through the aerodynamical forces on the blades, mainly in the flapwise direction, and thus all other fluctuating sectional loads (rotor, nacelle, tower, etc.) in the turbine. It seems resonably to assume that all loads caused by the fluctuating inflow to the blades changes in a wake situation in a similar way as the flapwise load. Differences will exist in the frequency contents but the picture will be the same: tilt- and yaw moments behave quite similar to flapwise bending, see also section 8.

Futher arguments for the general applicability of the results of the data analysis are offered in the following section.
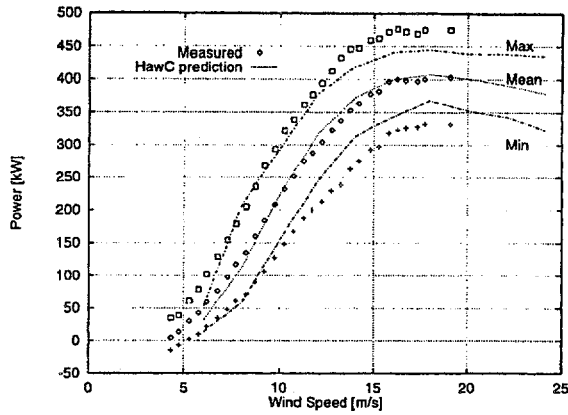
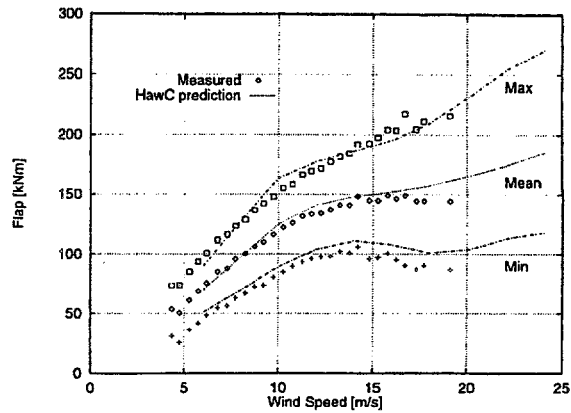**Figure 7.8** *Statistics of electrical power, free flow.*

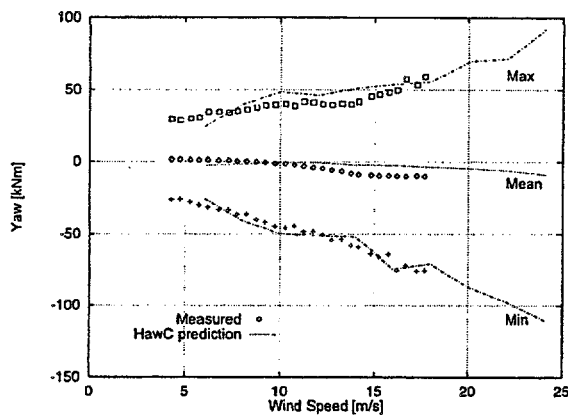**Figure 7.9** *Statistics of flapwise bending moment, free flow.*

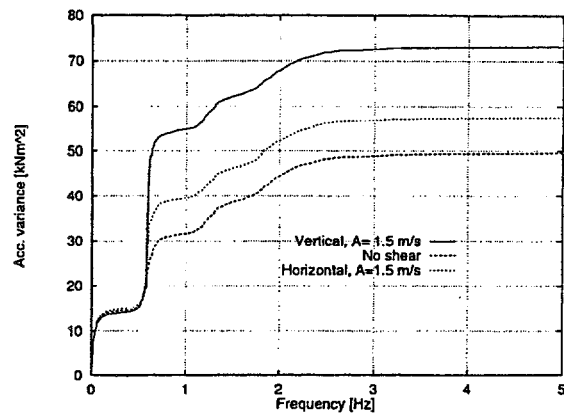**Figure 7.10** *Statistics of yaw moment, free flow.*

Figure 7.11 *Influence of vertical and horizontal linear shear to accumulated power spectrum, flapwise bending.*
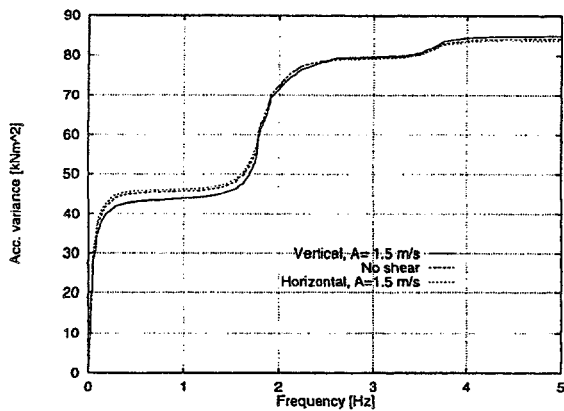

Figure 7.12 *Influence of vertical and horizontal linear shear on accumulated power spectrum, yaw moment.*
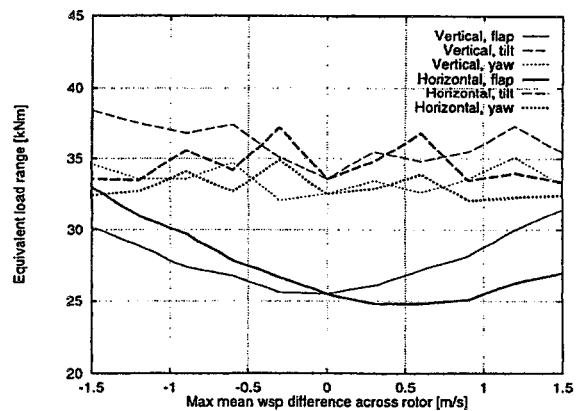

Figure 7.13 *Sensitivity of vertical and horizontal linear shear to fatigue loads.*
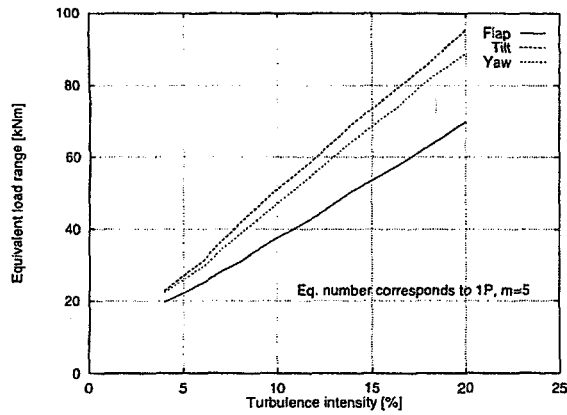
Figure 7.14 *Sensitivity of fatigue equivalent loads to turbulence intensity.*
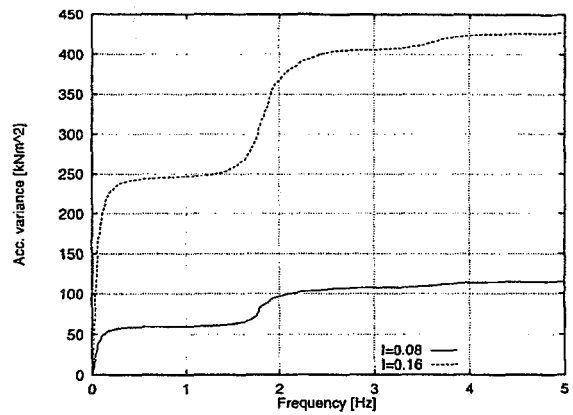
Figure 7.15 *Influence of turbulence intensity on accumulated power spectrum, flapwise bending.*
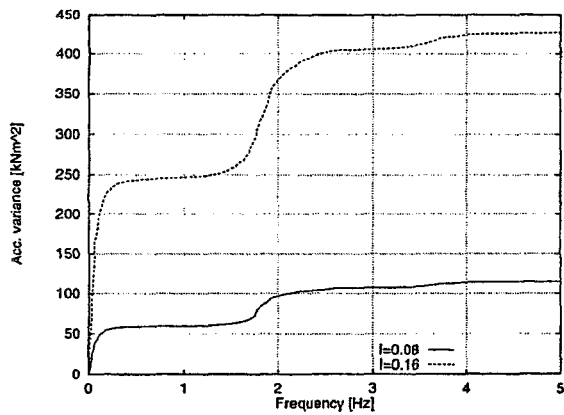
Figure 7.16 *Influence of turbulence intensity on accumulated power spectrum, yaw moment.*
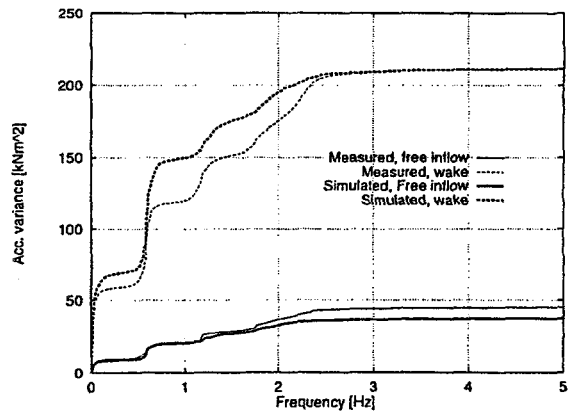
Figure 7.17 *accumulated flap power spectrum for selected run, free wind (10.8ms⁻¹), turbulence intensity 6.3%.*
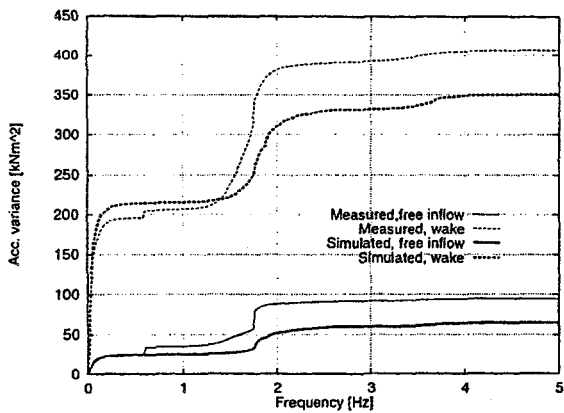
Figure 7.18 *Accumulated yaw power spectrum for selected run, free wind 10.8ms⁻¹, and I=6.3%.*
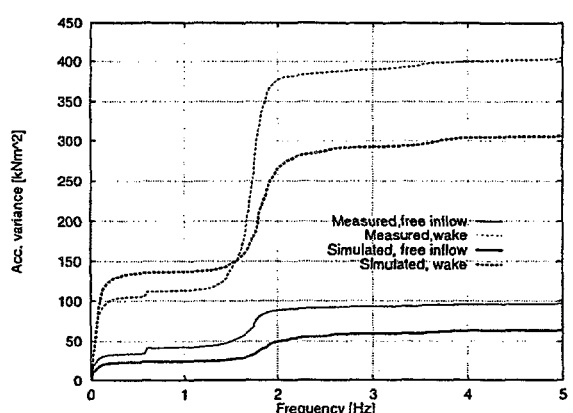
Figure 7.19 *Accumulated tilt power spectrum for selected run, free windspeed 10.8ms⁻¹, and free turbulence intensity I_o=6.3%.*
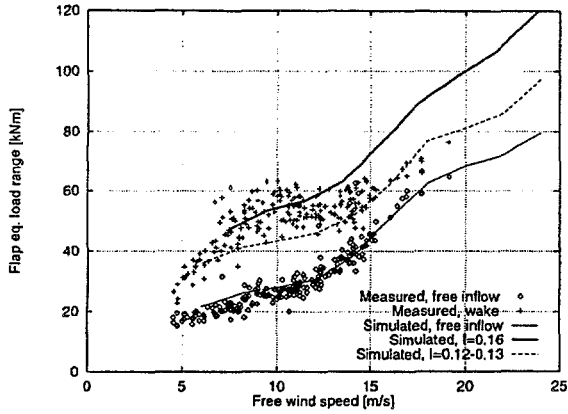
Figure 7.20 *1P equivalent load ranges for flapwise moment, measured and computed.*
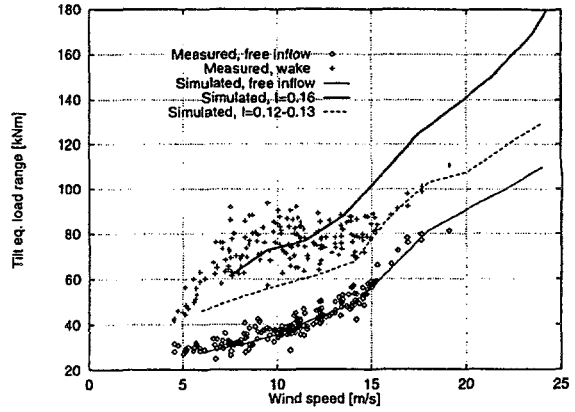
Figure 7.21 *1P equivalent load ranges for tilt moment, measured and computed.*
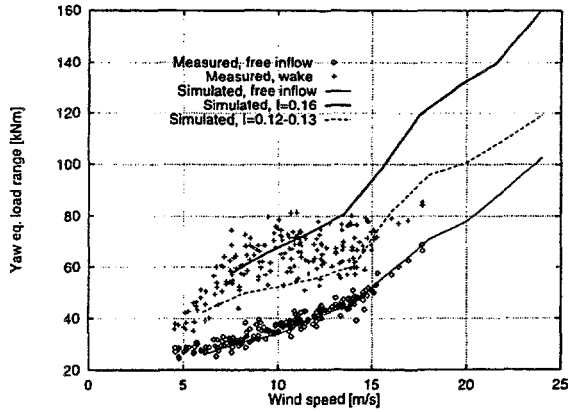
Figure 7.22 *1P equivalent load ranges for yaw moment, measured and computed.*

8 FATIGUE LOADING

In the previous section we analyzed the sensitivity of wind turbine loads to various special specific load cases and found that turbine response may be modelled quite well provided the loads are well known - and that the combination of loads (turbulence, horizontal and vertical shear, turbulence scale etc.) must be expected to be complicated in wind turbine wakes. In this section we concentrate on trying to obtain an overall picture of the load-wise consequences of placing wind turbines close to other wind turbines, offshore and to the extent possible with the available data onshore. Presently, this can only be done at the expense of the completeness/details of modelling.

8.1 Method of data analysis

Engineering structures must be designed to - throughout their design lifetime - withstand ultimate stresses *and* repeated (smaller) stresses, fatigue loading. While ultimate stresses occur once or a few times during the target lifetime, fatigue life consumption is constantly accumulated. Wind turbine "fatigue response" is sensitive to a range of parameters as shown in the previous section and further analyzed in this section. However, from section 7 we know that turbulence is a primary factor and it may be argued that from a statistical point of view turbulence can represent other parameters: in the unobstructed flow field in neutrally stratified atmosphere both vertical shear and turbulence are proportional to wind speed, and under wake conditions turbulence and speed deficit (and thus horizontal shear) are proportional to the wind turbine thrust coefficient C_T. While this on the one hand makes it difficult to separate the effects, it does on the other hand imply that a turbulence parameter may correlate well with loads. We did try, though with poor result, to correlate fatigue loads with shear and standard deviation of e.g. wind direction. As stated, the reason may be the coinciding changes of these parameters with turbulence, possibly reinforced by the large wind turbine separations ($>8.6D$) in the Vindeby Wind Farm.

Thus, we center on the along-wind turbulence component, σ_u, and the free flow mean wind speed at hub height, U, as (only partly) independent parameters causing fatigue. In other words, seeking the loadwise impact of the machines being placed close together we assume that turbulence is a good representative for load generating factors in the free flow as well as in wake flow. The analyses to follow aim at verifying simple physical models or empirical expressions for turbulence, mean wind speed and equivalent widths and the inter-connection of these parameters, by means of the data available. We seek to evaluate the fatigue loading as function of annual mean wind speed and turbulence of a machine exposed to the free flow and exposed to the flow inside a wind farm.

The objective of the analysis is to quantify the increase or decrease in fatigue loading caused by wind farm effects offshore. Therefore, there is little emphasis on absolute measures of fatigue life of this wind farm.

Seeking simplicity we looked for one structural load, which represents well most turbine loads under most load conditions. The flapwise blade bending moment seems to fulfil that requirement, see later in this section, and in the analysis the **flapwise blade bending moment** has been chosen for the more detailed investigation. So when nothing else is stated the equivalent load referred to is the equivalent load of flapwise blade bending of the machines 4W and 5E, Figure 8.1.

Analyzing the equivalent loads - as well as other loads - a considerable "scatter" of the data is noticed. In many cases it is not possible to identify the reason for the scatter; is it caused by the large separation between met tower and wind turbine, real changes in load conditions or the method of data analysis (e.g. rainflow counting)? There are indications, that the scatter is due to the large separations of met towers and turbines, and we thus counter, if necessary, this problem by averaging of the ½hourly statistical data over 5-10 data sets.

The met towers have for most heights two sets of anemometers, mounted on booms pointing in opposite directions (NE and SW) to avoid wake effects from the met towers themselves. When nothing else is stated the anemometer least affected by the met tower is chosen for the analysis. Also, when not specifically stating elsewise we use **the free stream wind speed at hub height, 38m,** as reference wind speed, U, for the various
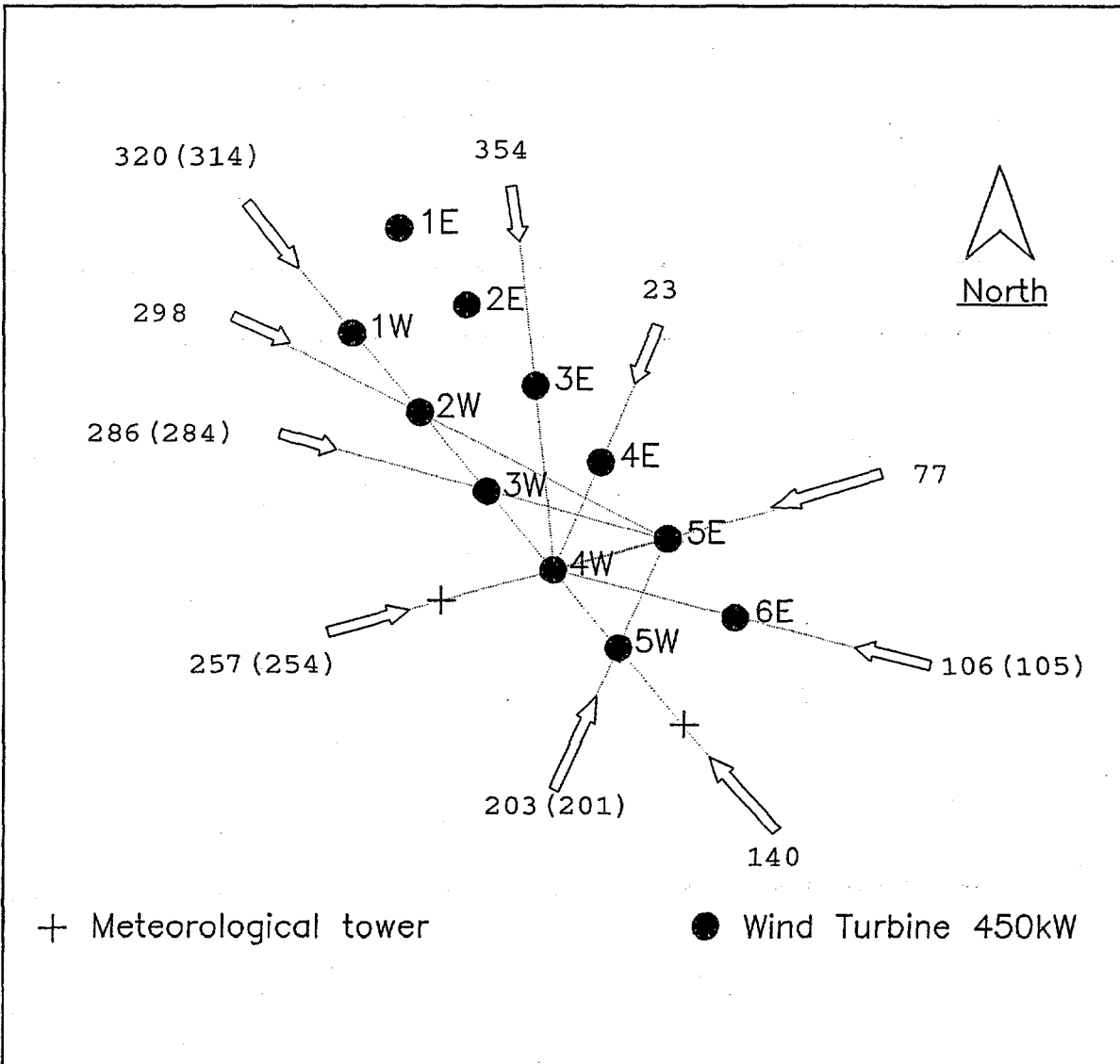
Figure 8.1 *Map of the Vindeby Wind Farm showing the wind directions, where one or both instrumented wind turbines are in the wake of one of the other machines.*

analyses. Further, all wind speeds and turbulence used for the analysis are measured at hub height. There are reasons for choosing a higher reference level, see section 5; however, hub height has been chosen out of tradition for using that height.

The dynamics - fatigue load spectrum as well as standard deviation - of the structural components of the wind turbines depend on wind direction as illustrated in Figure 8.2, where equivalent widths for flapwise bending of blades are shown as function of wind direction. In the figure, the equivalent width, s - also denominated ew in the figures - has been smoothed of 9 ½hour estimates. For westerly wind directions ($230°$ to $300°$) the 4W turbine unit, see Figure 8.1, and for easterly directions ($340°$ to $120°$) the 5E unit is not in the wake of other wind turbines, and s is basically constant though with some variability. Notably, s increases for both machines from the approximate direction $140°$ to $220°$, for the 5E unit with a wake condition from 5W superimposed.

It is seen from Figure 8.2, and found from more detailed analysis that s of the 5E unit is 10% higher the s of the 4W unit. The difference may reflect a real structural difference or just a calibration offset in one of the sensor sets. In any case, the difference is of less importance to the present analysis. Consequently, in the analysis we have adjusted the s of the 5E unit with a factor of 0.9 to make loads on the instrumented machine units directly comparable.
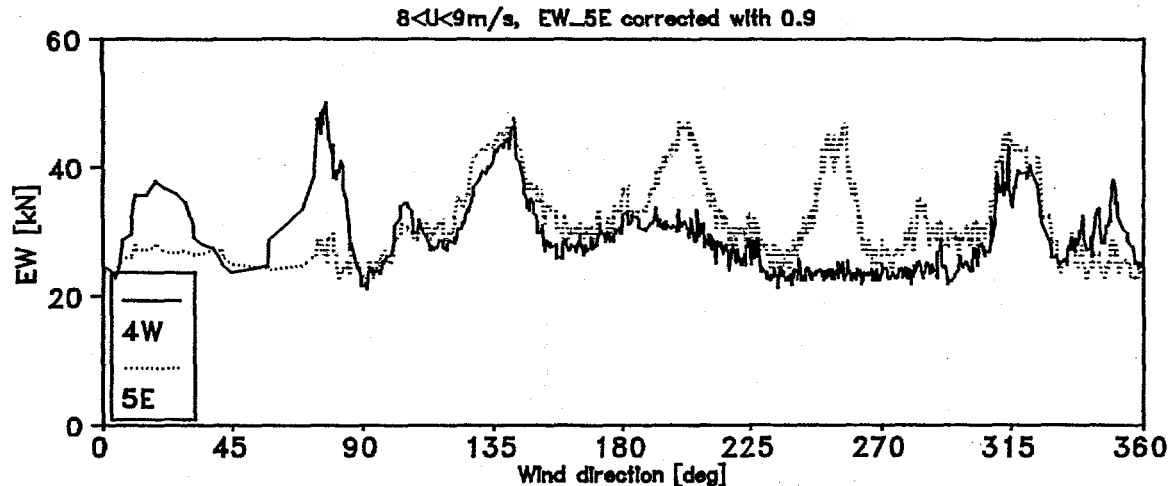
Figure 8.2 *Equivalent widths of flapwise bending moment of the instrumented units 4W (full line) and 5E.*

In the following we first disregard wake effects by choosing load situations without obstructing turbines and investigate how fatigue loads are altered on a stand alone wind turbine when moving from land to offshore. Two different approaches are applied. Secondly, the turbulence and the equivalent load "wake shapes" - i.e. the change of turbulence and equivalent load across the wake of one or more wakes - are analyzed. Thirdly, we investigate as far as it is possible maximum turbulence levels in the wake. Fourthly, we analyze maximum equivalent load under wake conditions.

Performing these analyses, we also try to devise more general expressions for the quantities involved, valid for other wind turbine separations and other ambient turbulence.

Following these basic analyses, we briefly investigate how well flapwise blade root bending moment represent other structural loads on the wind turbine. And finally, we present an extrapolation of the results to other wind farm configurations (separation and no. of rows) than the one investigated.

8.2 Free-flow fatigue loads

The sensitivity analysis of section 7 more or less pointed to proportionality between turbulence and dynamic response (standard deviations and equivalent loads). Disregarding possible response amplification at structural eigenfrequencies that observation makes sense directly for the standard deviation of response quantities. For the equivalent load the same would be expected if the turbulence scale is unchanged. Here, we shall further investigate the dependency of s to U and turbulence.

As it was seen in Figure 8.2, there is a distinct increase in s for wind directions from the land side of the wind farm. This is also illustrated in Figure 8.3, where s and standard deviation of flapwise blade bending from a narrow wind speed and turbulence range are plotted as function of wind direction. It is seen that the simple standard deviation is little - if at all - affected by the nearby land provided the turbulence intensity is the same as when wind comes from the open sea. This is not directly the case for fatigue loading: there is a distinct maximum around wind directions 180-200° azimuth from north, the average level being some 30-40% higher than when wind comes from the west.

The ratio of s and standard deviation for wind from water and water/land (and wake condition) is shown as function of wind speed in Figure 8.4, also indicating that s is relatively larger than standard deviation, at least for lower wind speeds when the wind field is affected by the nearby land. This could indicate, see Figure 8.9, that the smaller turbulence length scale (shorter time scale) from the land side causes a larger s simply by speeding up the process even though the load amplitudes - represented by the standard deviation - is unchanged. Thus, if the turbulence time scale, at a fixed observation height, is a function of surface roughness then

structural response could be different over water and land, even having the same turbulence level (and high turbulence levels over water is frequently seen if the atmosphere is thermally instable).

These observations also point to an important conclusion, namely that winds of southerly directions - despite to 2km distance to shore - represent onshore load conditions with a surface roughness of approx. 0.01m quite well. This is utilized to make reference to onshore load conditions.
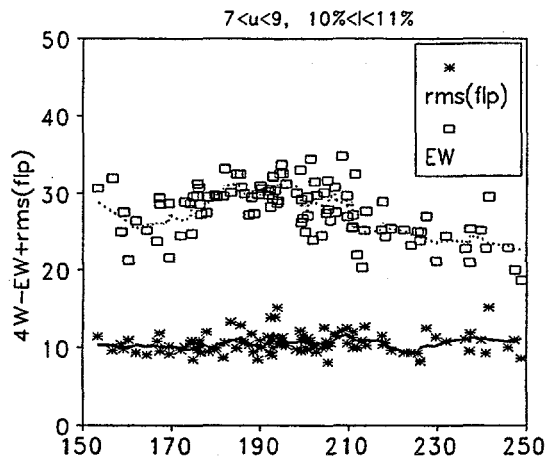
Figure 8.3 *Equivalent width and σ_{flp} as function of wind direction; wind from land.*
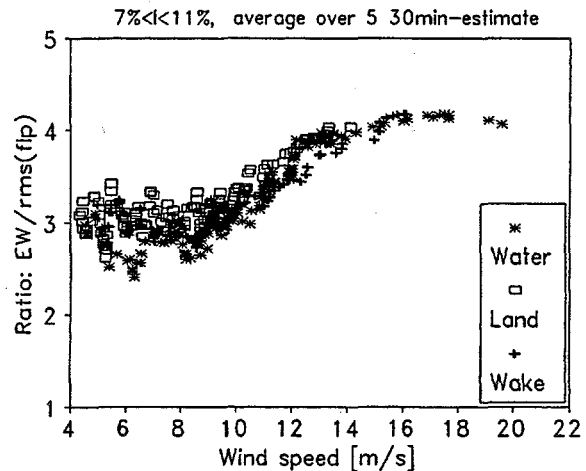
Figure 8.4 *Ratio (ew/σ_{flp}) as function of wind speed for wind from water, land and under wake condition.*

In the following we will perform two different sets of analyses, one where we apply regression analysis separately to data with purely westerly winds and to data with purely southerly winds, and one where we use azimuthal or otherwise averaged values of s and σ_u for sets of different wind speeds.

Separate analysis of data for wind over water and wind over land

Wind over water, pure offshore case: In Figure 8.5, s of 4W for a narrow band of westerly wind directions are plotted as function of wind speed. In the selected wind direction, the upstream fetch is water for at least 20km. The turbulence intensity varies considerably, see section 6, especially for lower wind speeds; at 8-10m/s the average turbulence intensity at wind turbine hub height h=38m is I=7.5% corresponding to a surface roughness of 10^{-4}m for neutrally stratified atmosphere.
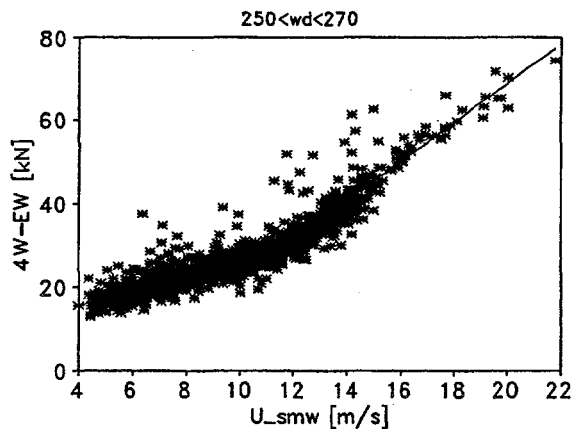
Figure 8.5 *Equivalent widths from unobstructed westerly wind direction; approx 1300 ½hour values.*
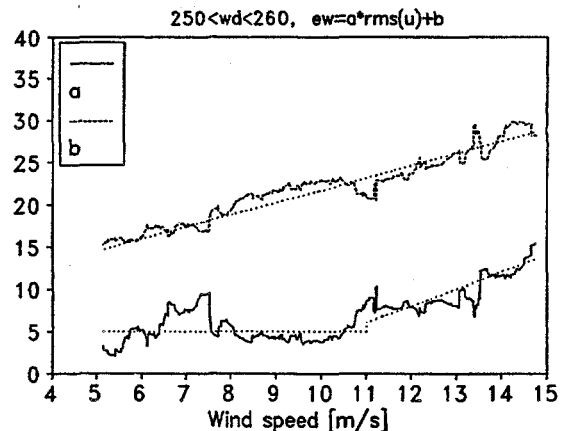
Figure 8.6 *Regression analysis, free wind from west.*

Linear regression analysis has been performed on the data of Figure 8.5, identifying dependency of s on σ_u and mean wind speed U. It was done the following way: the data - including s, σ_u and U - were sorted by increasing U, and the linear regression analysis was performed on the first 60 data sets with σ_u as the independent variable and s as the dependent variable:

$$s = a \cdot \sigma_u + b \tag{8.1}$$

Thus, a and b are determined from the analysis. Then data set no. 1 is dropped and no. 61 is included and the regression analysis is repeated etc. This way the two constants are determined as functions of U, see Figure 8.6. It is seen that the term not depending on σ_u is well approximated by $b=1.45(U+5)$ and the coefficient to σ_u by $a=5$ when $U<11$m/s, and $a=2(U-8)$ for $U>11$m/s, the result being an expression for equivalent width of the flapwise blade root bending moment as function of σ_u and U:

$$s_{water} \approx \begin{cases} 5\sigma_u + 1.45(U+5), & U < 11 \\ 2(U-8.5)\sigma_u + 1.45(U+5), & U > 11 \end{cases} \tag{8.2}$$

Though the dependency of σ_u in the real world deviates from the model, it is clear the for $U>11$m/s the dependency is steadily increasing.

Table 8.1 *Free-flow condition, statistics of s, wind direction and s-dependency of vertical shear, $250 < wd < 260$.*

Wind speed	s		wd		shr		
range (m/s)	m_s	σ_s	m_{wd}	σ_{wd}	m_s	σ_s	a_s
4-6	17.1	2.8	4.8°	4.8°	0.60	0.43	3.35
6-8	21.2	2.8	4.2°	2.2°	0.78	0.54	2.67
8-10	24.6	2.5	3.8°	1.8°	1.02	0.59	0.65
10-12	27.5	3.3	2.8°	2.1°	1.81	0.58	-2.04
12-14	35.1	4.3	3.7°	1.4°	1.34	0.52	-1.57
14-16	44.8	5.1	3.8°	1.5°	1.53	0.50	-3.01
16-18	56.0	4.6	3.9°	1.3°	1.72	0.28	0.82

The standard deviation of s for fixed U is of the order 10%, see Table 8.1; thus according to Eq. (7.14) and with a SN-curve slope of $m=5$ the (mean) equivalent width of (8.2) must be correct with a factor of $r_\varepsilon = 1 + \frac{1}{2} \times (5-1) \times 0.1^2 = 1.02$. If applied in actual design calculations such correction should be made. In the present analysis, where we merely look for differences in s we will in the following neglect the correction as it is of minor importance, especially for small values of the SN-curve exponent m.

Also shown in the table is mean and standard deviation of wind direction (wd) and vertical shear (shr). It was tried to establish correlation between wind direction and s and shear and s, the result being rather poor correlation. An interesting observation is that equivalent width seems to decrease with increasing shear for high wind speeds, right column of Table 8.1.

Wind from land: Figure 8.7 and Figure 8.8 represent the same analysis as for westerly "offshore winds", but this time for winds from the south, i.e. with a flow structure formed over land, and seemingly only to a lesser extent affected by the 2km water passed on the way to the turbines. In Figure 8.7, also the regression line corresponding to wind from the west is shown, clearly illustrating the higher fatigue loading in southerly wind directions.
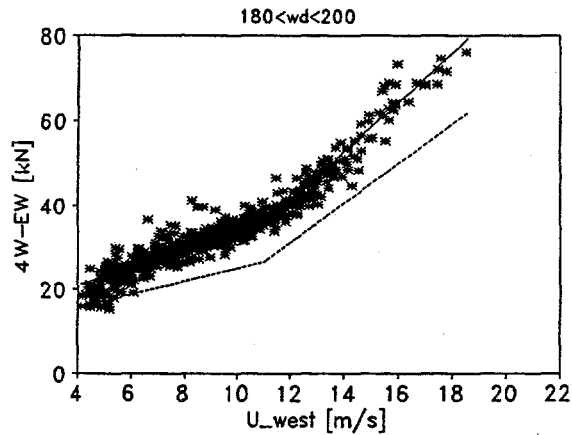
Figure 8.7 *Wind from land, distance to land approx. 2 km; number of points approx. 600 ½ hour values.*
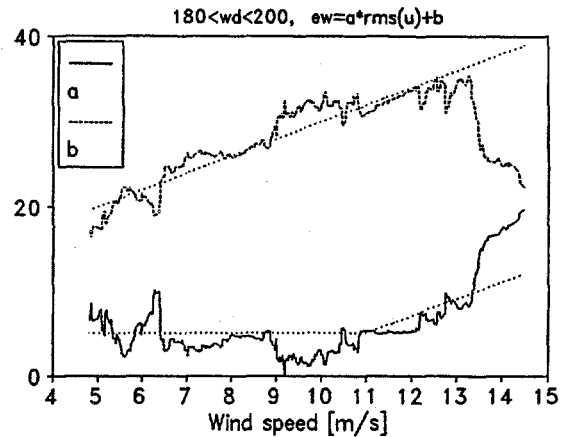

Figure 8.8 *Regression analysis, wind from land.*

The "running" regression analysis shown in Figure 8.8 results in the following model for equivalent stresses:

$$S_{land} = \begin{array}{ll} 5\sigma_u + 1.45(U+5), & U < 11 \\ 2(U-8.5)\sigma_u + 2(U+5), & U > 11 \end{array} \qquad (8.3)$$

with an upper limit of approx. 75kNm. As was the case with wind from west, there is a considerable variation in parameters a and b. However, the general picture seems to be the same: the parameter not dependent on turbulence increases steadily, while the σ_u-dependent term basically is the same as for wind from west - constant for lower wind speeds and from a certain wind speed upward s increases wind speed. The difference between (8.2) and (8.3) is the non-σ_u dependent term which is considerably larger with wind from the south.
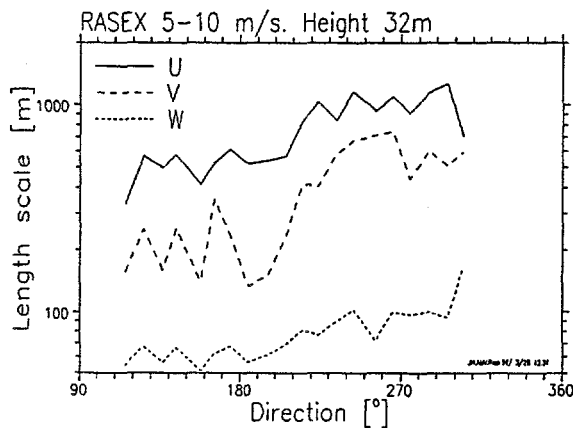
Figure 8.9 *Length scale of turbulence as function of wind direction.*
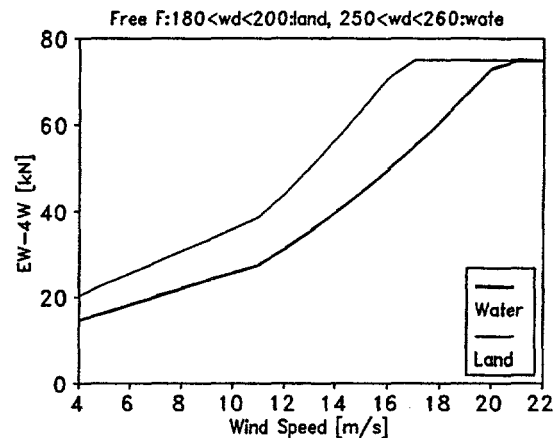
Figure 8.10 *The fitted equivalent width as function of wind speed, $I_{land}=12\%$ and $I_{water}=8\%$.*

The fits of s for wind from water, (8.2), and from land, (8.3), are plotted in Figure 8.10, Figure 8.12 for average turbulence intensities for the two wind directions. Applying the frequently used expression for turbulence intensity, $I= 1/ln(h/z_o)$, and assuming homogeneity, the turbulence intensity of 12% for wind from the land side is found to correspond to a roughness of $z_o=10^{-2}$m.
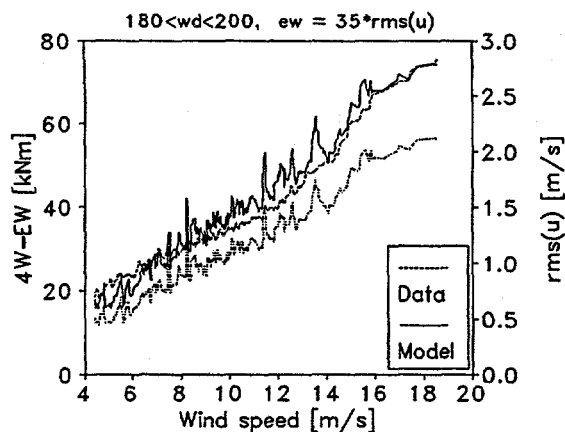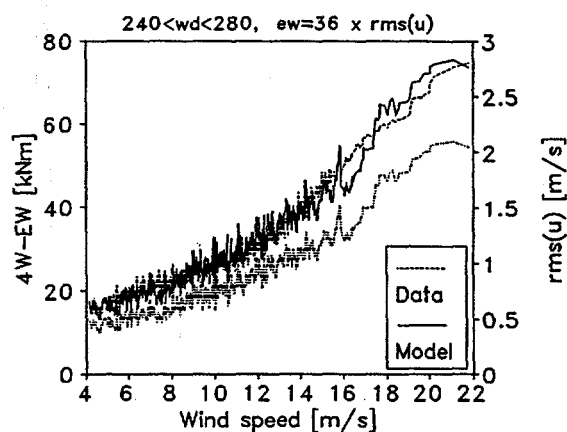
Figure 8.11 *Equivalent width of 4W from land, with σ_u model.*

Figure 8.12 *Equivalent width of 4W with wind from water, with σ_u model fit.*

While good end results are obtained with the analysis, the regression analysis does properly not reflect the physics: it appears that at a given, fixed wind speed fatigue response is basically not directly proportional to turbulence. This is most likely because the structure of turbulence under stable and unstable conditions is different from the neutral case and thus have different impact on loads.

Free flow loads using averaged values of σ_u and s

The above analysis was made using all corresponding, individual sets of (s, U, σ_u), also including stable and unstable flow conditions. Here, we now use averaged values of the data. The effect is primarily that strongly stable or unstable stratified cases are "averaged out". In Figure 8.11 and Figure 8.12 equivalent widths and σ_u are averaged over 10 ½hour values and plotted against wind speed at hub height, for wind from land and water, respectively. It is seen that the equivalent width rather neatly follow a simple curve $a \cdot \sigma_u$, where $a \approx 36$. This is much different from what obtained in the previous analysis, though end-results are similar.

Finally, a regression analysis is performed on azimuthal averaged values of s and σ_u in the transition between land conditions and water conditions, $wd = 180°\text{-}224°$. This way it is possible to obtain wind speed binwise regression lines, Table 8.2. An expression that fits the binewise regression lines of Table 8.2 has been found:

$$s = (24 - 0.25\ U)\ \sigma_u + (0.155U)^3 + 7.6 \tag{8.4}$$

Table 8.2 *Regression analysis on azimuthal bin values of s and σ_u, in land-water transition, $wd = 180°\text{-}220°$.*

U-bins	ew (s)
4-6 m/s	$22.9 \cdot \sigma_u + 7.6$
6-8 m/s	$22.4 \cdot \sigma_u + 8.6$
8-10 m/s	$21.0 \cdot \sigma_u + 11.1$
10-12 m/s	$19.8 \cdot \sigma_u + 12.4$
12-14 m/s	$2o.3 \cdot \sigma_u + 15.1$
14-16 m/s	$20.1 \cdot \sigma_u + 21.4$
16-18 m/s	$15.7 \cdot \sigma_u + 32.8$

Thus, if both this expression and the simpler $a \cdot \sigma_u$ are valid we may - indirectly - find the turbulence variation with wind speed over water as function of wind speed by equalizing the two:

$$\sigma_{u,water} \approx \frac{(0.155U)^3 + 7.6}{0.25U + 12} \tag{8.5}$$

This turns out to be a good approximation of turbulence under free flow conditions over water for wind speeds less than 16-18 m/s, matching the findings of section 5. It is concluded that under <u>neutral stratification</u> - and thus over long-term averages - the flapwise fatigue loading represented by the equivalent load is as a good approximation $36 \cdot \sigma_u$ for this particular machine.

Before turning to wake effects, the difference in fatigue loading on- and offshore on a single machine is compared. Applying The European Windatlas, Petersen and Troen (1989), see section 6, it is found that for constant geostrophic wind speed the difference in wind speed at hub height $h=38$m for terrains with $z_o=10^{-4}$m and $z_o=0.03$m (typical Danish farmland), respectively, is approx. 17% (see section 6 for more details) Thus, comparing fatigue loads in terrains with different surface roughness, also the difference in mean wind speed must be taken into account. The equivalent width is (numerically) calculated as

$$s_e = \left\{ \int_o^\infty s^m(u) \, f_w(u) \, du \right\}^{1/m} \tag{8.6}$$

where f_w is the Weibull distribution with shape parameter $k=1.8$, $s=36 \cdot \sigma_u$, $\sigma_{u,land}=0.14 \cdot U (= U/ln(h/z_o))$ over land and $\sigma_{u,water}$ is found from (8.5).

In Table 8.3 equivalent loads are given for two different annual mean wind speeds. The difference in the two wind speeds applied is 17%. In the right-most column the differences in equivalent loads are given. It is seen that for the same annual mean wind speed the difference in equivalent width is 22-25%, but with different turbulence.

Table 8.3 *Equivalent width for unit 4W with wind coming from west (water) and south (land), respectively; no wake effects.*

U_{year} (m/s)	A (m/s)	Water I_{water}	"Land" $(I=12\%)$	δ
8.80	9.89	$s_e=42.9$kNn	$s_e=56.0$kNm	-23%
7.38	8.29	$s_e=36.5$kNn	$s_e=51.1$kNm	-29%

The fatigue load-level for pure offshore conditions and for the wind from over land, $I=12\%$, are shaded in the table, showing an approx. 15% lower equivalent width for offshore conditions compared to onshore conditions with the same geostrophic wind speed distribution.

8.3 Wake fatigue loads

Wake shapes and widths

Figure 8.13 shows equivalent widths, s, of flapwise blade bending of unit 5E when more or less in the wake of unit 4W (i.e. single-wake condition), for wind speed between 8 and 9m/s. Also shown is the data smoothed over 7 ½hour estimates of s as well as the model-fit of expression (7.16). Though considerable scatter of the data it is seen that the "bell" model fits quite well. For the selected wind speed range the width parameter is $\beta=8°$ and the peak value of the modelled wake is $s_{peak}=c(1+\alpha)=30(1+0.7)=51$kNm.

Figure 8.14 shows measured values of s, smoothed curve for the data and the bell fit, in the rare 3-wake case of wind from the north-west. Also indicated is the equivalent wake, see section 7, to be applied when adding up fatigue loading for different wind directions. Interestingly, there seems to be less scatter in the data; however it is even more noteworthy that the peak value of s, $s_{peak}=c(1+\alpha)=25(1+0.9)=48$kNm, is about the same as

in the single-wake case. Also the wake width is only slightly - if at all - larger than in the single-wake case. This indicates, as was found in Frandsen et al (1996), that basically only the wakes of the nearest turbines contribute to fatigue life consumption.
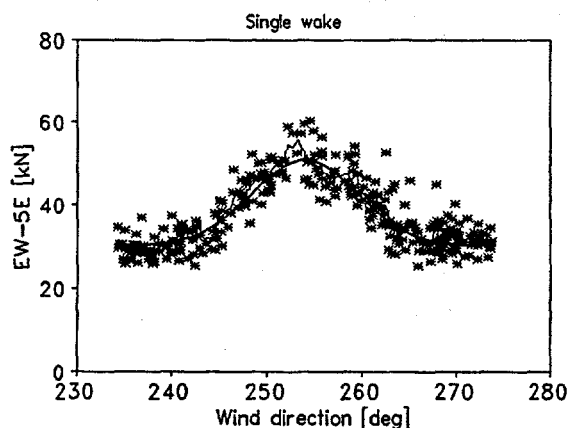

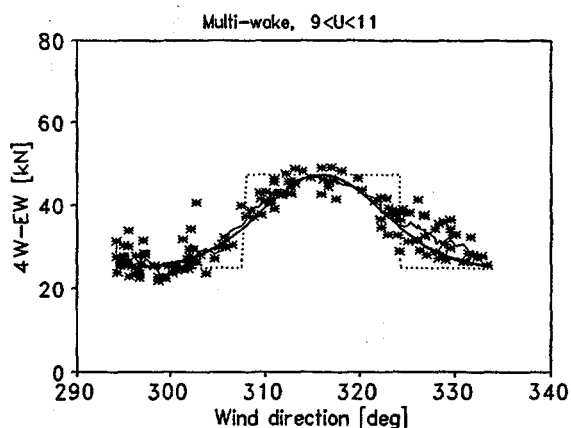**Figure 8.13** *Single-wake (4W), raw data of equivalent width, smoothed curve and model fit: c=30, α=0.7, β=8°.*

Figure 8.14 *Multiple wake, raw data, smoothed curve, fit: c=25, α=0.9, β=9°, and equivalent wake.*

In Figure 8.15 and Figure 8.16 smoothed curves of equivalent widths, 3 x σ_{flp} and turbulence intensity are given for single wake conditions (though double-wake for turbulence intensity) and 3-wake conditions, respectively. The single-wake curve is somewhat ragged due to few data points. Two things should be noted here: 1) for fixed wind speed, 9m/s < U < 11m/s, equivalent width and standard deviation of blade bending are nearly identical except for scaling, and 2) both follow the variation in turbulence intensity quite closely. *A priori*, this should not be expected since turbulence in measured in one point whereas flapwise blade dynamics are affected by flow parameters over the whole swept area of the rotor. Also, one could expect loads to be a function of partial wake conditions. However, horizontal shear in the wake and turbulence level are most probable correlated and it is therefore difficult to separate their effects on loading.

An explanation of the good correlation between turbulence and loads under wake conditions could be that the wake generating turbine produces a more fixed - though different - vertical shear and turbulence level as well as a more constant turbulence length scale.

With the wake conditions of Figure 8.13 to Figure 8.16 it was seen that the wake parameter $β$ is not dependent of the number of wind turbines upstream. With the data available it is also possible to investigate $β$'s dependency of wind speed and wind turbine separations (larger than 8.6·D). It is found that $β$ is basically constant, pointing to linear wake expansion. For smaller turbine separations, the wake width as experienced by a downstream observer is bound to be wider, see proposal in Table 8.4.
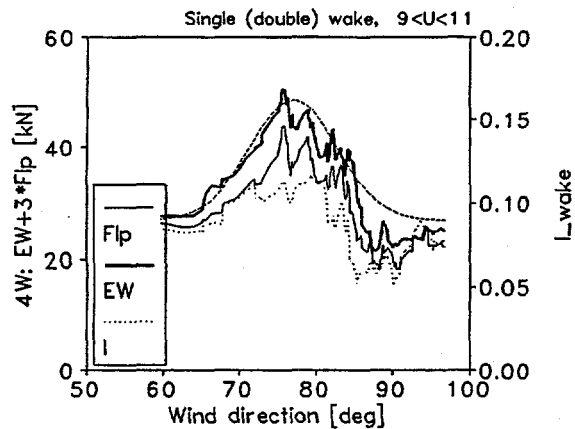
70

Figure 8.15 *Single wake 4W, double wake turbulence, smoothed curves; c=27, α=0.8 and β=8°.*
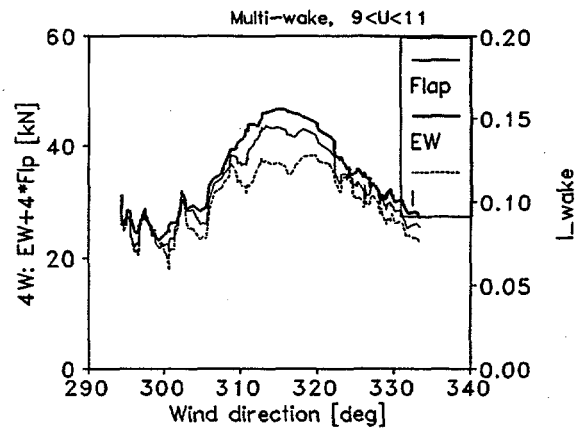
Figure 8.16 *Multiple-wake Smoothed curves of σ_{flp}, s and wake turbulence.*

Wake turbulence

The meteorological offshore towers have deliberately been placed so that their positions relative to the wind turbines correspond to imaginary wind turbine positions in a larger wind farm with unchanged distances between row and machines in the rows, see Figure 8.1. The southern tower (SMS) is exposed to multiple wake (wind turbine separations are $8.6D$) when wind direction (wd) is approx. 314°, single wake (turbine distance $9.6D$) when $wd \approx 23°$ The multiple wake turbulence may statistically be assumed to be same as the turbulence causing loads on 4W and 5E. The western tower (SMW) measures double wake (turbine distances $9.6D$) turbulence for $wd \approx 23°$ and $wd \approx 77°$ and single wake (turbine distance $15.5D$) for $wd \approx 105°$. Neither instrumented wind turbine unit 4W nor 5E are exposed to double wake turbulence, but for $wd \approx 105°$ the SMW tower measures turbulence which statistically should be identical to turbulence experienced by unit 4W.

In all, there are possibilities to measure wake turbulence as seen by the wind turbines, for turbine separations larger the $8.6D$.

Figure 8.17 shows wake turbulence for single wake and double wake, respectively. In the wind direction of Figure 8.17 there is no free flow reference wind speed; the indicated wind speed range measured in wake correspond to free flow wind speed of $6 < U < 10m/s$. Horizontal variation as well as center line turbulence for single and double wake are approximately the same. In Figure 8.18, turbulence is shown as function of wind direction for the 5-wake situation of wind from north-west. Comparing with Figure 8.17 is it seen (note that scales of ordinates are different) that wake amplitudes are not distinctly different.

In Figure 8.19, center wake hub height turbulence is plotted for single, double and multiple wake cases, the lower straight line corresponding to σ_u with fixed turbulence intensity of 0.075. In this presentation there is some differences between the three cases. A closer analysis have shown that these differences are due to different free flow turbulence. Several sets of wake turbulence data selected similarly as the data shown in Figure 8.19 to represent center line turbulence - a wind direction sector of $\pm 2°$ around the stipulated maximum was used - show that maximum wake turbulence, $\sigma_{u,wake}$ is the same whether there is one, two or several wind turbines upstream to for the wake. It is found that the following expression does match measured maximum wake turbulence well:
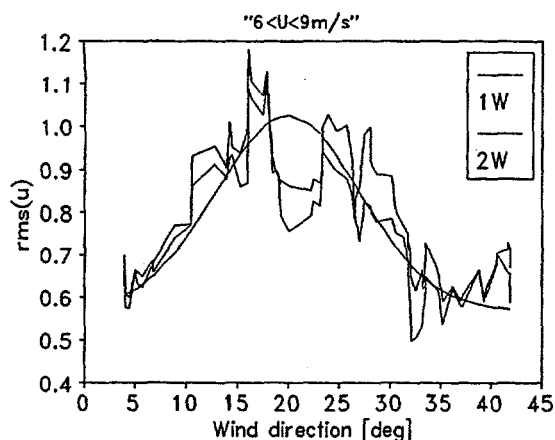
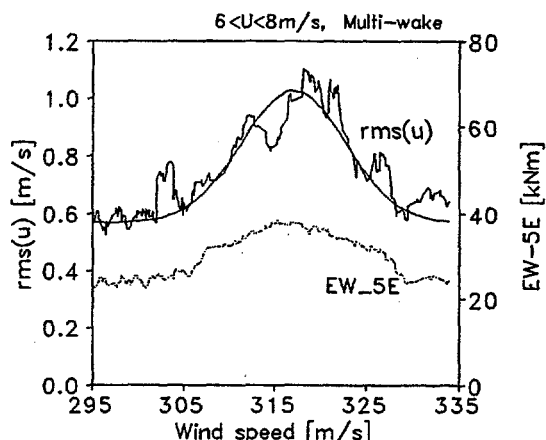**Figure 8.17** *Turbulence profiles for single (SMS) and double (SMW) wake, and fit.*

Figure 8.18 *Turbulence profile for 5-wake case, with fit and also showing s of unit 5E.*

$$\frac{\sigma_{u,wake}}{U} = \sqrt{\frac{1.2C_T}{s_t^2} + I_o^2} \tag{8.7}$$

where C_T is the (nearest) wake generating wind turbine's thrust coefficient, $s_t = x/D$ the non-dimensional turbine separation, and $I_o = \sigma_u/U$ turbulence intensity of the undisturbed flow field. This result is in fair agreement with the results referenced in section 4 and with the modelling results of section 5 for single wake, but not as good for multiple wake cases; however, (8.7) is in good agreement with a careful analysis of the Vindeby data and has a simple form which makes is well applicable in engineering calculations. Crespo and Hernandez (1992) argues that maximum turbulence in the near wake is 0.36; Højstrup (personal communication) states - based on experience from various wind farm measurements -

Figure 8.19 *Center-wake, hub height turbulence for single, double and multiple wake.*

that wake turbulence never exceeds 0.25. We apply in the following sensitivity analysis a maximum limit of (8.7) of 0.30 for small values of s_t exceeds that value.
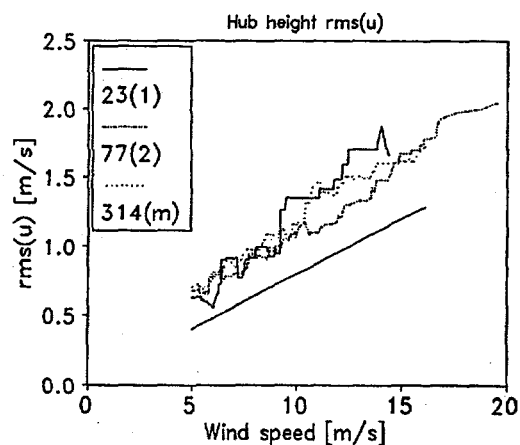
Maximum equivalent width under wake conditions

Previously it was seen, Figure 8.15 and Figure 8.16, that loads follow turbulence closely in the wake when wind direction changes, i.e. the "wake shape" of load and turbulence are more or less identical. We also found that equivalent loads in the free stream - under certain conditions - were proportional to turbulence, σ_u. The working hypotheses applied in the analysis has therefore been that maximum equivalent load in the wake is proportional to turbulence, as it is in the free stream.

Figure 8.20 to Figure 8.24 give center wake equivalent loads for single and multiple wake conditions, and for different wind turbine spacings. Also free stream turbulence (lowest curve, full line) as well as wake turbulence (when it is possible to measure it, full line) and modelled wake turbulence (broken line) are plotted in the figures.

First, it is worth noting how well the wake turbulence model work, both for different wind turbine separation, and for single and multiple wake cases.
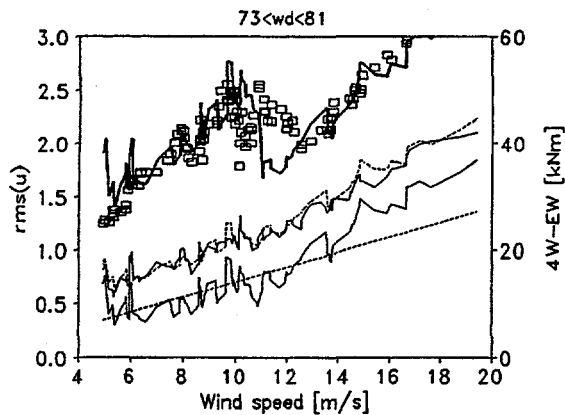
Figure 8.20 *Single wake on 4W; lowest curve are free-σ_u, wake-σ_u and wake-σ_u-model, respectively; data points are data and thick line model.*
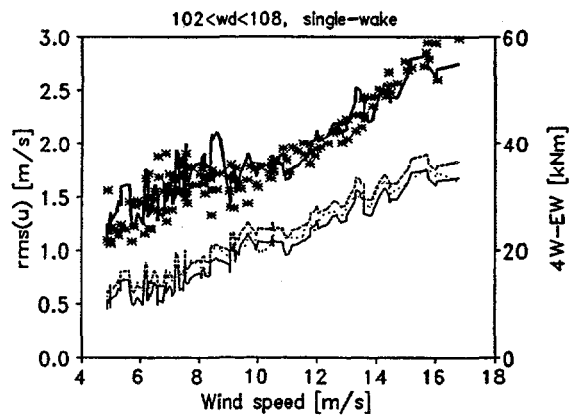
Figure 8.21 *single wake on 4W; lower curves are free-σ_u, wake-σ_u and wake-σ_u-model; points are data and thick line model of s.*
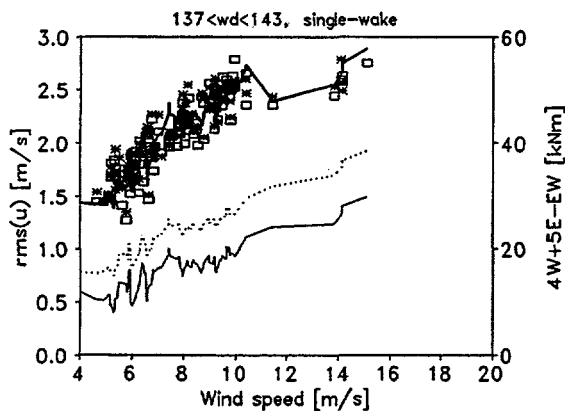

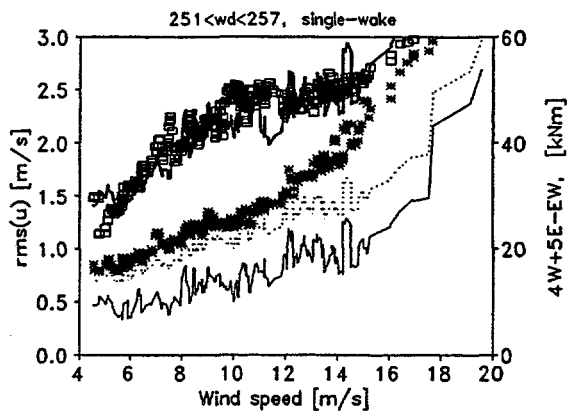**Figure 8.22** *As for last figure, for 4W and 5E; only modelled wake turbulence.*

Figure 8.23 *As last figure, but 5E in wake and 4W free; only modelled wake-σ_u.*
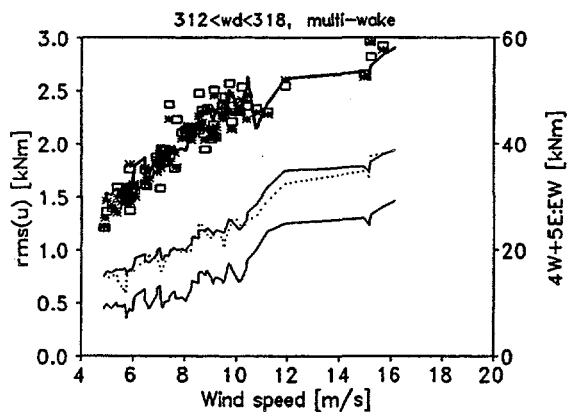

Figure 8.24 *As last figure, multi wake on 4W an 5E.*

Secondly, it is seen that equivalent loads in the wakes have a more complicated development with wind speed than was found for free stream conditions; for wind speeds up to about 10-12 m/s with wind turbine spacing 9.6D (Figure 8.20) and for 15D spacing up to 8-9 m/s (Figure 8.21) the equivalent loads increase with wind speed at a significant higher level than what was seen in the free stream. For wind speeds above 10-12 and 8-9 m/s, respectively, s drops off or at least levels out and continue upward at a lower level of increase. Looking at flapwise blade bending moment (no illustration is offered) this development with wind speed is even more pronounced. At this point we can only offer a qualitative explanation to the phenomena, namely that for low wind speeds, with large C_T/s_t^2, the structure of turbulence including turbulence scale and coherence are dominated by the turbulence generated by the wind turbine, and for higher wind speeds the turbulence structure becomes more identical to free flow turbulence.

The following expression fits data rather well:

$$ S_{wake} = 36 \left[1 + \frac{0.2}{1 + [0.1(\frac{I_o}{I_{add}})U]^{10}} \right] \sigma_{u,wake} \tag{8.8} $$

where $I_{add} = (I_{tot}^2 - I_o^2)^{\frac{1}{2}}$ is the wake added turbulence. The expression has the property that it approaches free flow conditions for $I_{add} \Rightarrow 0$ and increasing values I_{add} approaches a value of $43\sigma_u$ for the whole wind speed range.

As stated the expression fits well for the particular wind turbine type of which Vindeby Wind Farm consists, for wind turbine separations larger than 8.5D. Another wind turbine make may be expected to show different characteristics, if pitch and not stalled regulated. However, we assume that the formula can be applied for extrapolations to lower s_t. It is difficult to find suitable data to justify that assumption, though Poppen and Dahlberg (1992) report measurements of standard deviation of flapwise bending moments on 4 stall regulated wind turbines in Alsvik, Sweden, under conditions similar to Vindeby. The machines are sited so that it is possible to measure wake conditions for non-dimensional separations $s_t = 5$, 7 and 9.5. It is found that flapwise bending standard deviation follows fairly well the expression (8.7), scaled with an arbitrary constant.

A detailed linear regression analysis of wake fatigue loads are given in **Appendix C**. The expressions given there for equivalent loads in wake situations are more accurate for each individual wake case than what is given above. However, it was found important to produce a more general applicable expression, which we thus did, possibly at the expense accuracy.

8.4 Other loads and C_T

The validity of the analysis applying only flapwise blade bending moment depends on whether other loads display similar dependencies on the basic load input parameters, turbulence, wind speed and wind direction. Figure 8.25 shows equivalent loads of wind turbine unit 4W as function of wind speed for flapwise (Flp) and edgewise (Edg) blade bending, tilt (Tlt) and yaw (Yaw) bending, and tower base bending cross-wind (TMy) and along-wind (TMx). Edgewise blade bending equivalent load is as expected only moderately dependent on wind speed (and thus turbulence level). The remaining loads change quite similarly with wind speed variations.

Equivalent loads of tilt moment, yaw moment, along-wind tower moment, and flapwise blade bending are shown in Figure 8.26 for $7 < U < 10$m/s as functions of wind direction for the multiple wake case with wind from NW. The loads have here been normalized. It is seen that except for proportionality constants the different loads have identical behavior moving from no-wake to wake situation.

Therefore, it seems well justified to assume that the flapwise blade bending moment represents all loads - for the considered wind turbine - as far as fatigue loads are concerned.
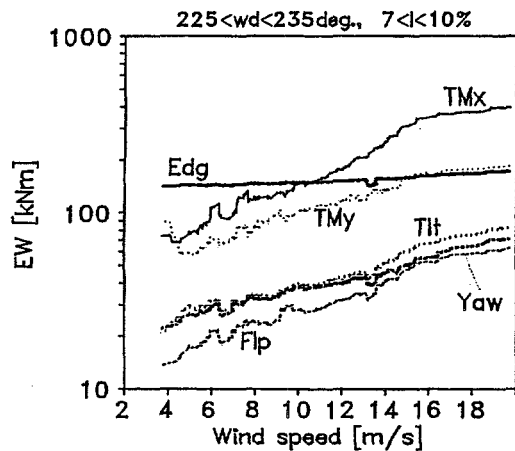
Figure 8.25 *Different loads as function of wind speed, free flow conditions.*
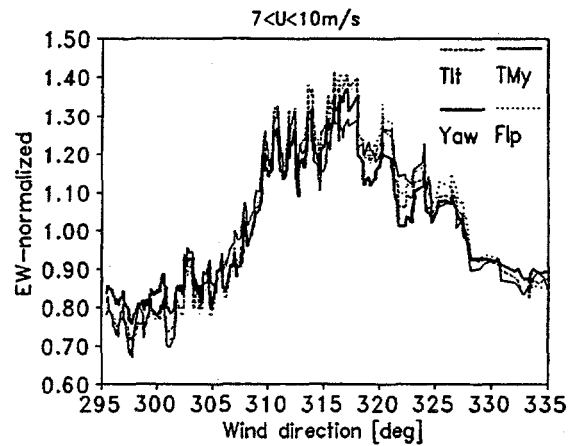

Figure 8.26 *Different loads as function of wind direction, multi-wake conditions.*

Mean values of the considered loads may display diverting characteristics, e.g. tilt and yaw mean levels could depend differently on horizontal shear than flapwise blade bending. However, this is of no consequence to fatigue loading.

For the modelling it is necessary to know the wind turbine thrust coefficient C_T as function of wind speed. Here, C_T has been found by means of the tower base bending moment, which is expected to fairly closely represent thrust. In Figure 8.27 rotor thrust for unit 4W is shown as function of wind speed. In absolute terms, it is difficult to trust the strain gage measurement, and the y-scale in the figure in arbitrary; however, in relative terms the experimental thrust - and thus C_T, also shown in the figure - curves appear reliable with little scatter of the 30 minute averages. The doubt of the absolute level makes it necessary to estimate the level, e.g. the maximum of C_T. Here, we choose $max\{C_t\}=1$ for the further considerations, while in section 5 another value has been chosen for reasons explained in that section.
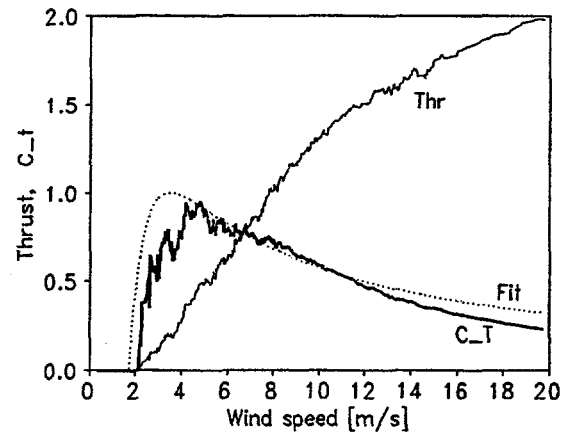

Figure 8.27 *Measured thrust (Thr) and C_t; units arbitrary.*

In pursue of a simple fit to the C_T curve we utilize the observation that the wake speed deficit measured seems constant (not dependent of wind speed) measured at the distance $8.6D$ downstream, $\Delta u(s=8.6) \approx 1$ m/s; thus, assuming that Δu is only a function of downstream distance, that $\Delta u = 1$ m/s at the distance $s=8.6$, and that $max\{C_t\}=1$ lead to the following expression for the thrust coefficient:

$$C_T = \frac{3.5(2U - 3.5)}{U^2} \tag{8.9}$$

As seen this curve is a good approximation although the fit drops off slower than the measured C_T curve for increasing wind speed. It is assumed that the fit to a good approximation can be applied for other machines than the Bonus machine of Vindeby.

8.5 Fatigue load modelling

The intention of the method of the data analysis chosen in this section is to model parameters of importance in

order to be able to extent the measurement results to other wind turbine configurations and separations. The models developed allow us to generalize results and thus to make statements of wake effects in broader terms than the specific wind farm configuration and the specific type of machine at Vindeby.

Table 8.4 summarizes the approximate expressions derived for the parameters needed for calculation of the final, integrated equivalent load. The derivation of each expression is explained previously, except for the wake width expansion, which is based on the observations of wake widths at 8-15D downstream measurements, an assumption of linear wake expansion (the Vindeby data do not allow verification) and simple geometrical considerations in the near wake. In general, the formulas are based on the Vindeby measurements, basic knowledge of atmospheric flow and structural response, basics from other wind farm measurements, and mathematical representation of more complicated physical realities. In the right column of Table 8.4 it is hinted - in order - the nature of origin of the formulas (empirical, physical).

The following assumptions have been applied:

- An important finding in the Vindeby measurements - as well as other measurements - is that only wakes of the machines in the immediate vicinity of the considered machine is of importance to fatigue loading. It is assumed that this finding extends to wind farms in general.
- Dynamic characteristics of flapwise blade root bending moment are in general a good representative for other wind turbine loads.
- The Bonus machine of Vindeby is response-wise a typical representative of present day wind turbines, and the results are valid also for other machines.
- Turbulence - standard deviation of along wind fluctuations of wind speed - is the main load parameter, in free stream and in wake(s). Other load factors such as horizontal and vertical flow shear in wake situations are possibly also of major importance, but these may be expected to be related to/proportional to turbulence, and thus be implicitly represented by the turbulence parameter.
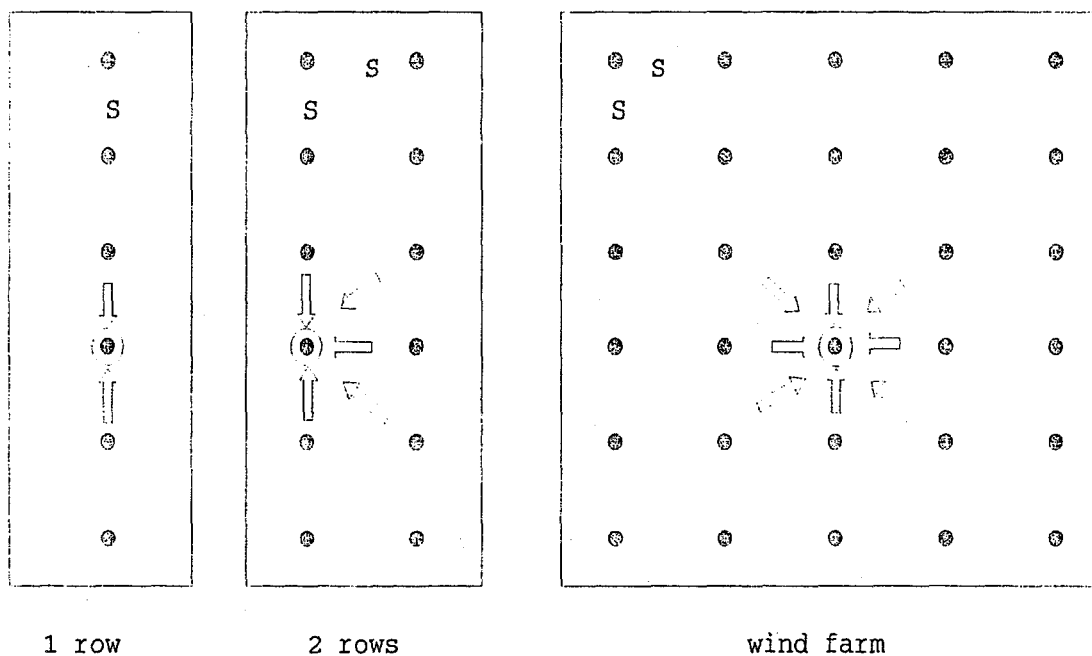

1 row   2 rows   wind farm

Figure 8.28 *3 of 4 considered wake configurations; spacings are equal in all directions.*

Parameter	Expression	Comments
Turbulence, on land	$\sigma_{u,land} = \dfrac{U}{\ln(h/z_o)}$	Physical. Generally accepted.
Turbulence, off-shore	$\sigma_{u,water} \approx \dfrac{(0.155U)^3+7.6}{0.25U+12}$	Empirical. Possibly only valid for shallow waters like Vindeby, though see also section 5.
Turbulence, wake(s)	$\dfrac{\sigma_{u,wake}}{U} = \sqrt{\dfrac{1.2C_T}{s_t^2} + I_o^2}$	Physical/Empirical. Fits well the Vindeby data; in agreement with some other experiments.
Thrust coefficient	$C_T = \dfrac{3.5(2U - 3.5)}{U^2}$	Empirical/Physical. Fits well Vindeby wind turbines; fits in general terms a number of other machines.
Wake "shape", all parameter	$x = c \left(1 + \alpha \exp\left(-\left(\dfrac{wd-wd_{max}}{\beta}\right)^2\right)\right)$	Empirical. Should be acceptable in general, possibly except for very small s. E.g. $\alpha_s = s_{wake}/c - 1$, $\alpha_{ou} = \sigma_{u,wake}/c - 1$, c is non-wake level.
Wake width expansion	$\beta = \tfrac{1}{2}\left(\tan^{-1}\left(\dfrac{1}{s}\right) + 10^o\right)$	Empirical. Fits for large s; is logical for smaller s.
Effective wake width	$2\,\beta\,b_e, \quad b_e \approx \dfrac{2 + \sqrt{m}\,\alpha^{1.25}}{2 + m\,\alpha^{1.25}}$	Mathematical. Should be generally acceptable.
Equivalent width, land and offshore	$s = 36\,\sigma_u, \quad for \quad s<75,$	Empirical/physical. Is turbine specific, though the same (with different constant) has been found for a number of other stall-regulated wind turbines.
Equivalent width in wake, land and offshore.	$s_{wake} = 36\left[1 + \dfrac{0.2}{1 + [0.1(\dfrac{I_o}{I_{add}})U]^{10}}\right]\sigma_{u,wake}$	Empirical. Is turbine specific; should apply (except for constants) to other stall-regulated machines.

Table 8.4 *Summary of analytical expressions derived from the Vindeby data, to be used for computation of "equivalent turbulence intensities".*

On basis of these assumptions, the expressions of Table 8.4 and an extra assumption that wind direction is uniformly distributed (for all wind speeds) it is possible to compute the "integrated" equivalent width under various conditions. We use the idealized wind farm layouts illustrated in Figure 8.28: 1) 1-wake situation, corresponding to two machines close one another (not shown), 2) a single row, 3) 2-rows similar to Vindeby, and 4) "wind farm conditions", which is regarded as one case since we found that the number of layers of wind turbines around the target wind turbine were of little or no consequence to fatigue loading. The number of wakes taken into account is illustrated in Figure 8.28.

Since α is a function of wind speed we find first the equivalent width of the (1m/s) wind speed bins;

$$S_{e,u} = \left\{ \frac{2i\beta(s_t)b_e)}{360} \cdot s_{wake}^m(s_t) + \frac{2j\beta(\sqrt{2}s_t)b_e}{360} \cdot s_{wake}^m(\sqrt{2}s_t) + \frac{360 - (2i\beta(s_t)b_e + 2j\beta(\sqrt{2}s_t))}{360} \cdot s^m \right\}^{\frac{1}{m}}$$ (8.19)

where for case 1) $\{i,j\} = \{1,0\}$, case 2) $\{i,j\} = \{2,0\}$, case 3) $\{i,j\} = \{3,2\}$ and case 4) $\{i,j\} = \{4,4\}$. Since we in this simplified approach assumed the wind speed Weibull distributed, with the same parameters, in all wind directions the final equivalent width becomes:

$$S_{e,tot} = \left\{ \int_o^\infty f_w \, s_{e,u}^m \, du \right\}^{\frac{1}{m}}$$ (8.20)

First, this result is applied to produce a table similar to Table 8.3, but here comparing loads on a machine in a 2-row configuration, offshore and onshore. The result is given in Table 8.5, where it is seen that for the same mean wind speed the equivalent load is 23-29% less offshore, the difference increasing for decreasing annual mean wind speed. If it is taken into account that mean wind speed is higher offshore than onshore for the same geostrophic wind, the difference decreases to 14%. Comparing this to the stand alone case, Table 8.3, we see that increased fatigue loading due to wind farm effects are slightly more pronounced at sea for the Vindeby configuration.

Comparing Tables 8.3 and 8.5 it is also seen that for $U_y = 8.8$m/s the difference in equivalent load for offshore free flow and offshore wake conditions with the Vindeby wind farm configuration is about 5%.

Table 8.5 *Equivalent loads, 2-row case, onshore and offshore.*

U_y (m/s)	$S_{u,tot}$ (onshore) (kNm)	$S_{u,tot}$ (offshore) (kNm)	Difference
8.80	56.9	44.7	-21%
7.38	52.2	38.8	-26%

Next we will apply the setup of models to estimate the total, integrated equivalent load for the four cluster configurations. Figure 8.29 show for the offshore case for an annual mean wind speed of 8 m/s. For approx $s_t > 8$-10 there are small wind farm effects for all considered cases. For $s_t < 8$-10, the wake effects increase and reach levels up 40% of free stream values for the "farm" case for separations of $4D$ and less than that for the other cases.

Figure 8.30 shows what we call the effective turbulence, I_{eff}, defined as the free stream turbulence causing the same fatigue life consumption on a stand alone unit as the wake effects cause on the machines in the wind farm. I_{eff} follows much the same pattern as s in the previous figure. Most notable in Figure 8.30 is that I_{eff} does not under realistic circumstances reach the presently internationally (IEC (1993)) applied reference turbulence intensity of 17%, when considering offshore installations.
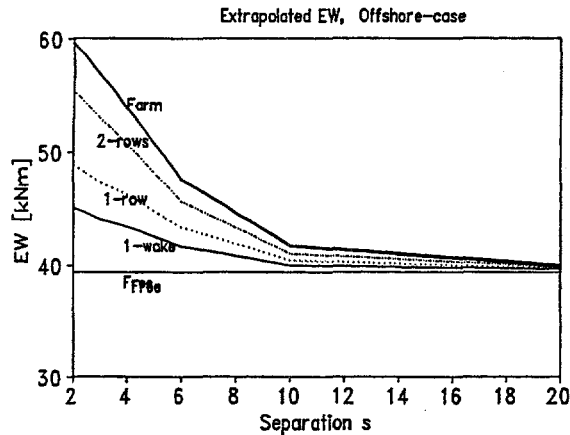
Figure 8.29 *s as function of wind turbine separation for offshore conditions; 4 machine configurations; Mean wind speed U=8m/s.*
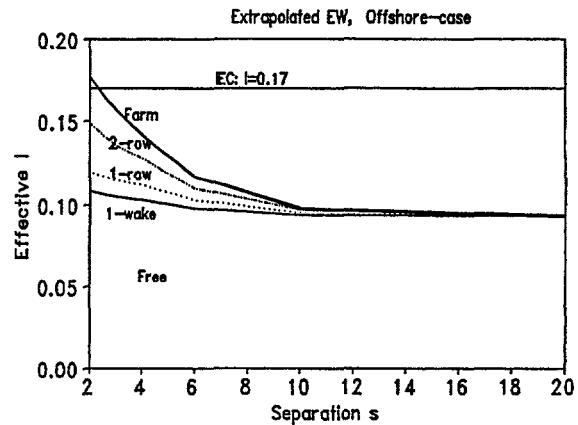

Figure 8.30 *Effective turbulence uncertainty giving the same s as integrated wake action; Mean wind speed U=8m/s.*

Finally, Figure 8.31 illustrates an attempt to point to future criteria for design of wind turbines for offshore as well as onshore. The figure shows *s* for case 4), the wind "farm" case, for offshore and onshore conditions (full lines), and a very simple model for the effective turbulence intensity to be applied. It is similar to the model applied for wake turbulence, inspired by a model, Emeis and Frandsen (1993) and Frandsen (1992), which results in expressions for speed deficit and turbulence. Her it has been given an even simpler form:

$$I_{eff} = \sqrt{\frac{0.4C_T}{s_r^2} + I_o^2} \qquad (8.21)$$

The curve fits of Figure 8.31 have been obtained simply by using an equivalent load of $s=36 \cdot I_{eff} \cdot U$ ($s<75$) and integrating as in (8.20). As seen the fits are excellent except for the smallest separations.

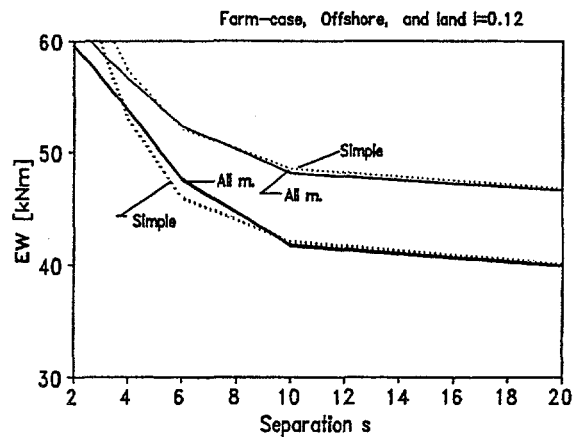Figure 8.31 *Comparison of integrated and simple models for farm-case, onshore and offshore; U =8m/s.*

The modelling presented above is based on data with rather large wind turbine separations, and scarce experimental evidence on dynamic loads for smaller separations. However, while in detail the complex of models are incomplete, we find that the end result is fairly reliable and may serve as input to preparation of future design codes.

Finally it is suggested that some efforts are invested in the near future to a) verify assumptions in more details, b) verify the sub-models, and b) to verify and possibly calibrate the models for small wind turbine separations. Also, it should be carefully considered whether - as expected - machines other than the stall regulated concept display basically the same behavior.

9 POWER PERFORMANCE MEASUREMENTS

The scope of this section is a little off the scope of the rest of the report, which is centered on loads on offshore wind turbines. Here, we try to use the ideal, unobstructed site to evaluate variations in energy production from the individual wind turbine units. Thus, measurements are presented and compared using the IEC committee draft version of a standard for power performance measurement techniques (IEC 1995) as far as possible.

Table 9.1. *List of category B uncertainty limits.*

Sensor	Accuracy	Uncertainty limits
Pressure		10^{-3}
	Drift (3 years)	$3 \cdot 10^{-3}$
Absolute temperature	Calibration	$< 10^{-3}$
	Linearity	$< 10^{-3}$
Temperature difference	Sensitivity	$0.025 \cdot 10^{-3}$
	Offset	$0.06 \cdot 10^{-3}$
Risø Power	Current transformers	$2 \cdot 10^{-3}$
	Power transducer	4.5 kW
Anemometer	Calibration	$2.5 \cdot 10^{-3}$
	Reference	$2.5 \cdot 10^{-3}$
Control system Power	Total (current transformers + transducer)	$< 20 \cdot 10^{-3}$

Only two of the wind turbines in Vindeby were extensively instrumented by Risø, including power measurements. However, the control systems of the wind turbines also provide power measurements. The control systems are supplied by the company KK-electronics. The local control systems of the wind turbines are connected to a remote control system at the utility SK-power. SK-power has used this system to collect data from all the wind turbines. The collected data are 30 second mean values of power and nacelle wind speed along with time and date on the local control systems.

As the remote control system is also used by the utility to supervise the wind farm the speed of data transfer has been limited. Thus, the 30 second mean values are only sampled every 5 minute. Moreover, the 30 second mean values of the power are based on fast samples in every 6th grid period, i.e. 20 ms measurements followed by 100 ms pause for calculation etc. These 30 second mean values are synchronized with the 30 min statistics of the Risø measurements and 30 min "mean values" of the power are calculated. Consequently, each 30 min "mean value" is based on typically 6 (30 min/5 min) 30 second mean values.

This procedure off course increases the uncertainty of each 30 min "mean value" compared to regular measurements. As the increased uncertainty is of category A according to the definition in the draft power performance standard (IEC 1995), the uncertainty can be reduced by measuring long enough.

The category B uncertainty limits of the involved instruments are listed in Table 9.1. The data are from Barthalmie et al (1994), except the power measurement data. The company KK-electronics states that they aim at a class 1 (1 %) uncertainty for the entire power measurement chain, but they only guarantee class 2. As KK-

electronics measures current and voltage and calculate power they have extremely small offset error, and therefore the error is assumed to be the same percentage for all power levels. Risø's power measurements use class 0.1 current transformers corresponding to 0.2 % error limit at 20 % according to IEC 185 (1987). The power transducer applied by Risø is class 0.5. According to IEC 688 (1992) this corresponds to 0.5 % of nominal power 900 kW, i.e. 4.5 kW uncertainty for all power levels.

The Vindeby version of the Bonus 450 kW wind turbine uses 700 V generators. Therefore, it has separate 400 V supply for the control system. The power transducers are mounted on the 700 V system and consequently they do not include the power consumption of the control system as it should according to the draft IEC standard (1995).

The temperature and pressure in hub height are used to normalize the measured power according to IEC (1995). The temperature is measured at each mast. The absolute value of the temperature is measured in 10 m height and the temperature differences between 10 m and 24 m and between 10 m and 47 m are measured. The hub height temperature is interpolated using these measurements. The pressure is measured in 3 m height on land only, and scaled to hub height according to ISO 2533 (1978).

The control system power measurements and the SMS wind speed measurements in 38 m height are used to generate the power curves of the turbines 1E, 2E, 3E, 4E, 5E, and 6E. The wind direction is limited to the interval between 40° and 90° measured on SMS in 43 m height. The power curves are shown in Figure 9.1 - Figure 9.6. The power measurements have been logged from 18 September 1995 to 31 January 1996. However, Risø's anemometers were switched and calibrated 26 October 1995. In the remainding 3 months approximately 2000 half hour values of Risø and control system measurements have been combined. However, most of the data was logged when the wind direction was between 90° and 140° where the variability in distance to land have significant influence on the wind speeds on SMS and at the turbines, respectively. Only approximately 200 values were in the wind direction interval from 40° to 90°.
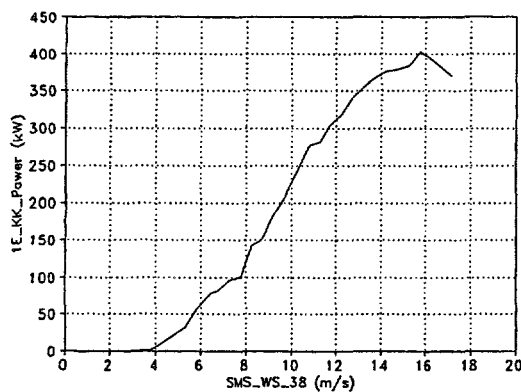

Figure 9.1. *1E power curve based on SMS wind speed and control system power measurements with wind directions from 40° to 90°.*
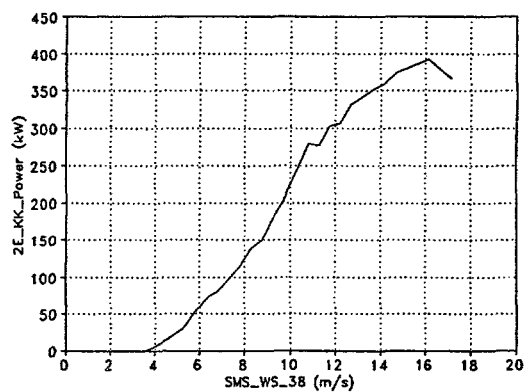
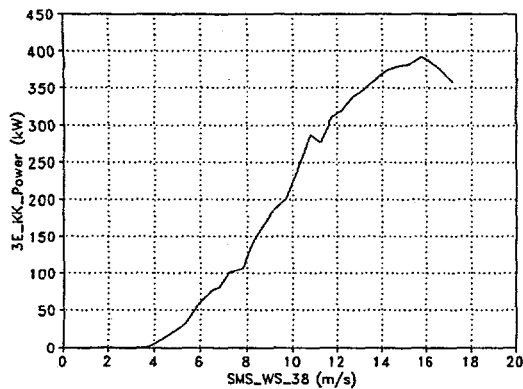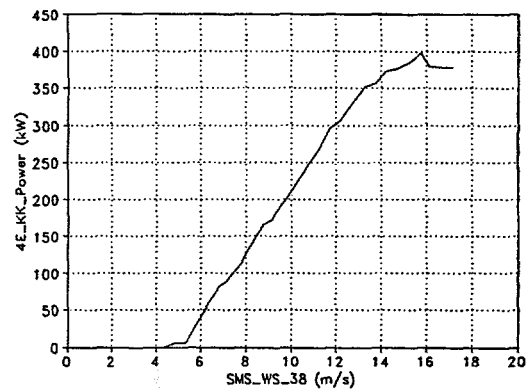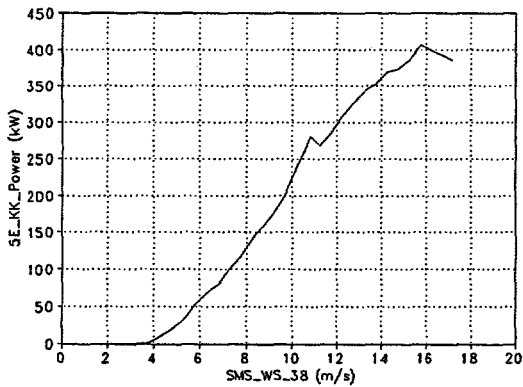**Figure 9.2.** *2E power curve based on SMS wind speed and control system power measurements with wind directions from 40° to 90°.*

Figure 9.3. *3E power curve based on SMS wind speed and control system power measurements with wind directions from 40° to 90°.*

Figure 9.4. *4E power curve based on SMS wind speed and control system power measurements with wind directions from 40° to 90°.*

Figure 9.5. *5E power curve based on SMS wind speed and control system power measurements with wind directions from 40° to 90°.*
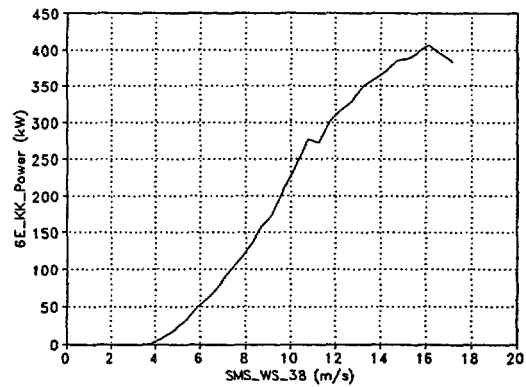

Figure 9.6. *6E power curve based on SMS wind speed and control system power measurements with wind directions from 40° to 90°.*

The estimated annual energy productions (AEPs) corresponding to the power curves are listed in Table 9.2. The AEPs are estimated according to IEC (1995) assuming a Rayleigh distribution with an annual average wind speed $U_y = 8$ m/s. In order to limit the uncertainties the estimates are limited to wind speed intervals with sufficient number of half hour "mean values" in each wind speed bin. The table also lists the category A uncertainties of the AEP estimates and the total number of half hour "mean values" in the selected wind speed intervals.

Note that 4E has a significantly smaller AEP than the other wind turbines. This is mainly due to the spike on all power curves except 4E in the bin from 10.5 m/s to 11 m/s.

A similar estimation is performed on the wind turbines 1W, 2W, 4W, 5W, and 1E based on the SMW wind speed measurements with wind directions from 240° to 300°. The amount of data from 3W was not sufficient. From the other turbines, approximately 150 half hour "mean values" were available. The power curves are

Table 9.2. *Estimated AEP based on control system power and SMS wind speed measurements with wind directions from 40° to 90°. The category A uncertainties (s) and the number (N) of half hour "mean values" are also listed.*

Turbine	3-10 m/s			3-12 m/s		
	AEP (MWh)	s (MWh)	N	AEP (MWh)	s (MWh)	N
1E	435.7	7.7	97	728.9	16.9	119
2E	426.8	6.6	108	717.7	13.6	129
3E	438.9	8.9	109	734.6	15.5	131
4E	397.1	6.8	100	671.0	14.2	116
5E	434.8	5.1	108	721.0	11.9	130
6E	421.0	5.9	107	711.0	10.7	129

Table 9.3. *Estimated AEP based on control system power and SMW wind speed measurements with wind directions from 240° to 300°. The category A uncertainties (s) and the number (N) of half hour mean values are also listed.*

Turbine	3-10 m/s			3-12 m/s		
	AEP (MWh)	s (MWh)	N	AEP (MWh)	s (MWh)	N
1W	420.7	5.2	119	688.5	5.9	133
2W	421.2	5.2	119	688.7	6.9	133
4W	420.1	4.6	119	689.6	5.6	133
5W	437.5	4.4	119	721.9	5.7	133
1E	428.2	5.5	119	702.9	8.4	133

shown in **Appendix B** and the AEP results are listed in Table 9.3.

Finally, the Risø measurements have been used to estimate the power curves and the AEPs of 4W and 5E. The power curves are shown in Figure 9.7 and Figure 9.8 and the AEPs are listed in Table 9.4. The wind speeds and direction intervals are the same as above, i.e. 240° - 300° SMW for 4W and 40° - 90° SMS for 5E.
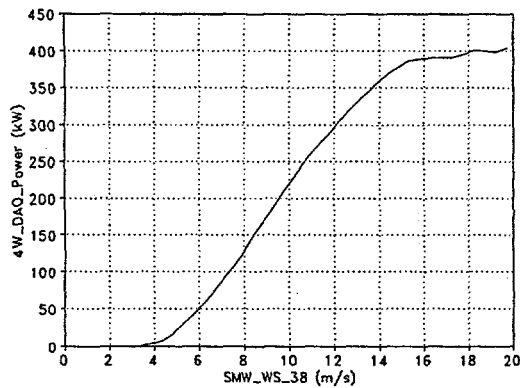
Figure 9.7. *4W power curve based on SMW wind speed and Risø power measurements with wind directions from 240° to 300°.*
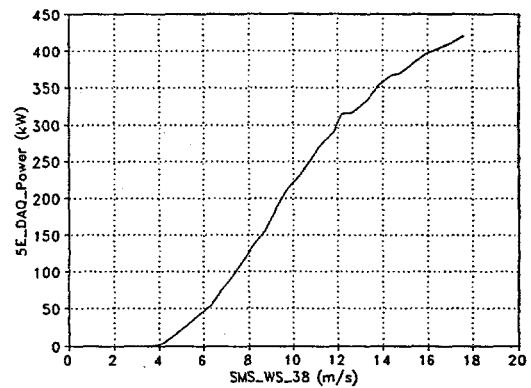

Figure 9.8. *5E power curve based on SMS wind speed and Risø power measurements with wind directions from 40° to 90°.*

The wind speed measurement on the two masts are compared in Figure 9.9 and Figure 9.10 using wind directions from 240° to 300° where both anemometers are free of mast and wind turbine wakes. Figure 9.9 shows data after October 1995, i.e. with the anemometers used to estimate the power curves in Figure 9.1 - Figure 9.6 and the AEPs in Table 9.2 and Table 9.3. Figure 9.10 shown data before October 1995, i.e. with the anemometers used to estimate the power curves in Figure 9.7 and Figure 9.8 and the AEPs in Table 9.4. It is seen that the south mast measures almost 1 % more than the west mast with both sets of anemometers. This could be due to boom effects.

The control system and the Risø power measurements are compared in Figure 9.11 and Figure 9.12. The measurements on 5E agree whereas Risø measures 1 % higher power than the control system on 4W. The control system on 4W is an older version than the other turbines, which could explain this difference. Adding 1 % to the AEPs of 4W based on control system measurements in Table 9.3 these AEPs agree with the estimates based on Risø measurements in Table 9.4. On the other hand, the AEPs of 5E in Table 9.2 are higher than in Table 9.4. This is probably because of the spike on the power curve in Figure 9.5. This should be accounted for in the category A uncertainty, but with only two measurements in a bin the "uncertainty of the uncertainty estimate" becomes important.

Table 9.4. *Estimated AEP based on Risø power and wind speed measurements. The category A uncertainties (s) and the number (N) of half hour mean values are also listed.*

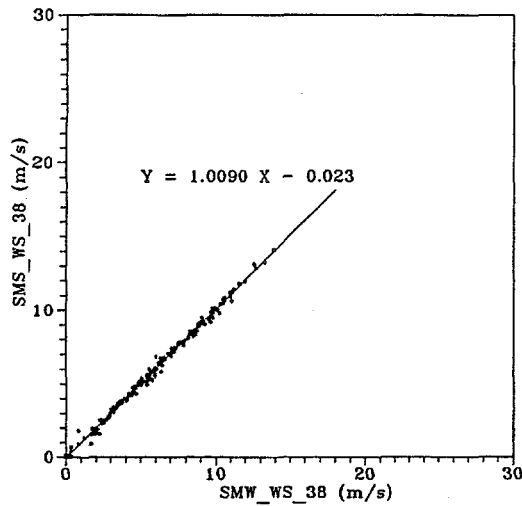| Turbine	3-10 m/s			3-12m/s		
	AEP (MWh)	s (MWh)	N	AEP (MWh)	s (MWh)	N
4W	429.5	1.1	1257	705.8	1.2	1634
5E	418.3	3.7	249	694.4	4.1	302

Figure 9.9. *Measured 30 min averages of wind speeds on SMS vs SMW with wind directions from 240° to 300° using data after October 1995.*
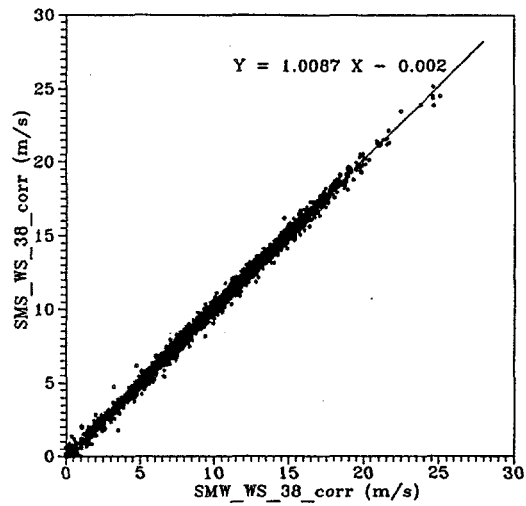

Figure 9.10. *Measured 30 min averages of wind speeds on SMS vs SMW with wind directions from 240° to 300° using data before October 1995.*
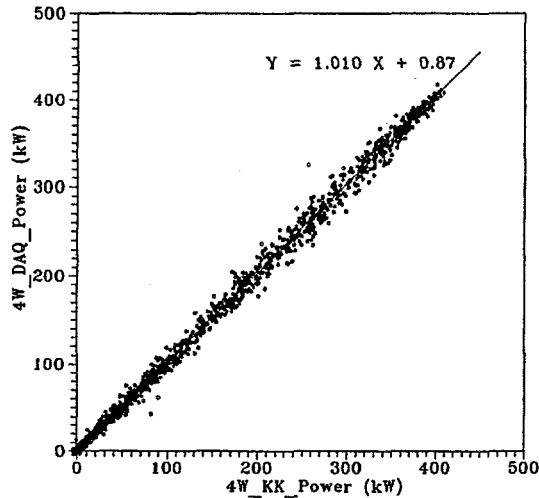

Figure 9.11. *30 min mean values of Risø power measurements versus control system measurements on turbine 4W.*
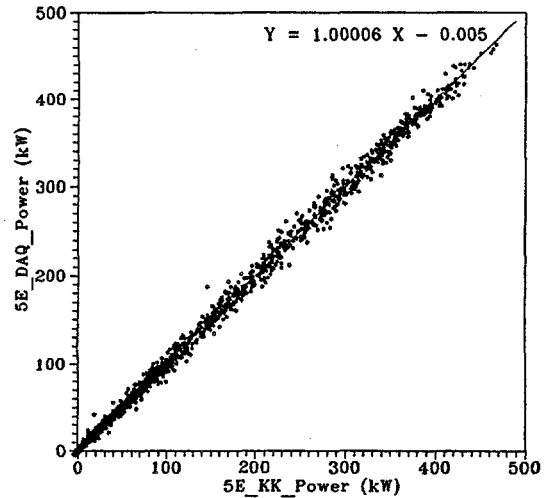

Figure 9.12. *30 min mean values of Risø power measurements versus control system measurements on turbine 5E.*

Having assumed $U_y = 8$m/s and using the power curve the largest contribution to AEP is from the wind speed bin from 11.5 m/s to 12 m/s. In this wind speed bin on SMW_WS_38 the standard deviation of the wind speed SMS_WS_38 in Figure 9.10 is 0.28 m/s. Using the slope on the power curve in Figure 9.7 this corresponds to a standard deviation of the power on 9.9 kW. Selecting the corresponding power interval (278.8 kW - 296.5 kW) of the Risø power measurement in Figure 9.11, the standard deviation of the control system power measurement is 12.2 kW.

The aim of this analysis has been to determine the difference between the power curves of examples of the same type of wind turbine. However, the number of mean values was too small to be conclusive on the issue. Variation in production from one machine to the next may be expected to be a few per cent; to pinpoint with significance differences of that size demands more data and lesser uncertainties than achieved in this experiment.

10 REFERENCES

Abramovich, G. N. (1963), "The theory of turbulent jets", MIT Press, Cambridge, Mass..

Ainslie, J.F. (1986), "Wake Modelling and the Prediction of Turbulent Properties," 8th BWEA Conference, 115-119.

Ainslie, J.F. (1988), "Calculating the Field in the Wake of Wind Turbines" Journal of Wind Engineering and Industrial Aerodynamics, 27.

Ainslie, J.F., U. Hassan, H.G. Parkinson and G.J. Taylor (1990), "A wind tunnel investigation of the wake structure within small wind turbine farms", Wind Engineering, 14, pp 24 - 28.

Alfredson, P. H., J.A. Dahlberg and F.H. Bark (1980), "Some properties of the wake behind horizontal axis wind turbines", Proceedings of the 3rd. International Symposium on Wind Energy Systems, Copenhagen.

Ansorgen, Th., M. Fallen, P. Günther, P. Ruth and T. Wolfanger (1994), "Numerical Simulation of Wake-Effects in Complex Terrain and Application of a Reynolds-Stress Turbulence Model". Proceedings of EWEC' 94.

Baker, R. W. and S. Walker (1985), "Wake velocity deficit measurements at the Goodnoe Hills MOD-2 Site", report No. BPA 84-15, January.

Barthelmie, R.J., M.S.Courtney, J.Højstrup, S.E.Larsen (1996): "Meteorological aspects of offfshore wind energy - observations from the Vindeby Wind farm. Submitted to Journ. Wind Eng. and Ind. Aerodyn.

Barthelmie, R.J., M.S. Courtney, J.Højstrup, and P.Sanderhoff (1994), "The Vindeby Project: a description", Risø-R-741(EN), Roskilde, Denmark, March.

Bossanyi, E. A., C. Maclean, G.E. Whittle, P.D. Dunn, N.H. Lipman and P.J. Musgrove (1980), "The efficiency of wind turbine clusters" Proceedings of the 3rd. International Symposium on Wind Energy Systems, Copenhagen.

Builtjes, P. J. (1978), "The interaction of windmill wakes" 2nd. Symp. of wind energy systems. Amsterdam. BHRA.

Builtjes, P. J. H. and P.E.J. Vermeulen (1982), "Turbulence in wind turbine clusters" Proceedings of the 4th International Wind Energy Conference, Stockholm.

Chacón, L. (1994), "Modelización por ordenador de parques eólicos", Engineer's degree project, E.T.S.I.I. Universidad Politécnica de Madrid.

Charnock, H. (1955): "Wind stress on a water surface". Quart. J. Roy. Meteor. Soc., 81, 639-640.

Cleijne, J.W. (1992), "Results of Sexbierum Wind Farm", Internal report of TNO 92-388, November.

Cleijne, J. W.; A. Crespo, S. Huberson, G.J. Taylor and S.G. Voutsinas (1993), "Wake and wind farm modelling", Final Report contract CEC JOUR-0087-NL (CEC). TNO-report 93-374.

Crafoord, C. (1979), "Interaction in limited arrays of windmills", Dept. of Meteorology, University of Stockholm, Report DM-26, March.

Crespo, A., Manuel, F. Moreno, D. Fraga and J. Hernández (1985), "Numerical Analysis of wind turbine wakes" Proc. of the Delphi Workshop on Wind Energy Applications.

Crespo, A. and J. Hernández (1986), "A numerical model of wind turbine wakes and wind farms." Proceedings of the EWEC ' 86, Rome, pp. 111 - 115.

Crespo, A., J. Hernández, E. Fraga, and C. Andreu (1988), "Experimental validation of the UPM computer code to calculate wind turbine wakes and comparison with other models," Journal of Wind Engineering and Industrial Aerodynamics, 27.

Crespo, A., J. Hernández, E. Fraga and C. Andreu (1988a), "Analysis of Wind Turbine Wakes", Final Report of CEC contract EN3W / 0020 / E(B).

Crespo, A. and J. Hernández (1989), "Numerical modelling of the flow field in a wind turbine wake", Proceedings of the Forum on Turbulent Flows, ASME meeting, La Jolla.

Crespo, A., F. Manuel and J. Hernández (1990), "Numerical modelling of wind turbine wakes", Proceedings of the ECWEC ' 90, Madrid, pp. 111 - 115.

Crespo, A. and J. Hernández (1991), "Parabolic and elliptic models of wind turbine wakes; application to the interaction between different wakes and turbines", The PHOENICS journal of Computational Fluid Dynamics, Vol. 4, n°2, pp. 104-127.

Crespo, A., J. Hernández, F. Manuel, J.C. Grau and L. Chacón (1993), "Full scale measurements in wind turbine arrays", Spanish contribution to the Final Report of the CEC Project, jour-0064. Edited by National Power, G.J. Taylor, appendix 4.

Crespo A., and J. Hernández (1993a), "Analytical correlations for turbulence characteristics in the wakes of wind turbines", Proceedings of ECWEC'93, pp. 436-439. Travemünde, Germany.

Crespo A., F. Manuel, J.C. Grau and J. Hernández (1993b), "Modelization of wind farms in complex terrain", Application to the Monteahumada Wind Farm, Proceedings of ECWEC'93, pp. 440-443, Travemünde, Germany.

Crespo A. (1993c), "Wake and wind farm modelling", Contribution to the Final Report contract CEC JOUR-0087-NL (CEC) . TNO-report 93-374.

Crespo A., L. Chacon, J. Hernández, F. Manuel and J.C. Grau (1994), "UPMPARK a parabolic 3D code to model wind farms". Proceedings of EWEC' 94.

Crespo A., and J. Hernández (1996), "Turbulence characteristics in wind-turbine wakes", Accepted for publication in the Journal of Wind Engineering and Industrial Aerodynamics.

Green, D.R.R. (1986), "Near wake wind tunnel studies", Loughborough Univ. of Techn. Dept of Mech. Eng., ETSU-WN-S040P1.

Günther, P., M. Fallen and T. Wolfanger (1993), "Numerical wake simulation of a HAWT considering topography and using a mesoscale turbulence model" Proceedings of ECWEC'93, pp. 448-450. Travemünde, Germany.

Emeis, S. and S. Frandsen (1992), "Reduction of horizontal wind speed in a boundary layer with obstacles", Boundary Layer Meteor., 64, 297-305.

Faxen, T. (1978), "Wake interaction in an array of windmills - theory and preliminary results", 2nd. symp. of wind energy systems. Amsterdam. BHRA.

Frandsen, S. and J.C. Christensen (1980), "On Wind Turbine Power Measurements", Third International Symposium (BHRA) on Wind Energy Systems, Copenhagen, Denmark, August.

Frandsen, S. (1992), "On the wind speed reduction in the center of large clusters of wind turbines", Journal of Wind Engineering and Industrial Aerodynamics, 39, 251-265.

Frandsen, S. and J.C. Christensen (1994), "Structural loads in large wind farm arrays", EWEC'94 Conference, Thessaloniki, Greece.

Frandsen, S. and J.C. Christensen (1994), "Vindeby Offshore Windfarm - Fatigue Measurements", EWEC'94 Conference, Thessaloniki, Greece.

Frandsen, S. (1996), "Fatigue loading on offshore wind power stations", EWEC'96, Gothenburg, Sweden, May.

Frandsen, S., C.J. Christensen, M.C. Courtney, J. Højstrup, P. sanderhoff and P. Sørensen (1996), "Nørrekær Enge II wind farm measurements, Risø-R-805(EN) report, Roskilde, Denmark; to be published.

Green, D. and A. Alexander (1985), "Measurement of velocity and turbulence profiles in flow situations relevant to wind turbine performance", Final report on ETSU contract E/5A/CON/5003/177/026, May.

Hemon, A.; S. Huberson and A. Zervos (1991), "Numerical study of wind turbine operation in complex terrain", Proceedings of the 1991- 13th BWEA Wind Energy Conference, pp 335 - 342.

Hernández J. and A. Crespo (1990), "Wind turbine wakes in the atmospheric surface layer", The PHOENICS journal of Computational Fluid Dynamics, Vol. 3, n°3, pp. 330-361).

Högstrom, U., D.N. Asimakopoulos, H. Kambezidis, C.G. Helmis and A. Smedman (1988), "A field study of the wake behind a 2 MW wind turbine", Atmospheric Environment, vol. 22, n° 4, pp. 803-820.

Højstrup, J. (1981): "A simple model for the adjustment of velocity spectra in unstabale conditions downstream of an abrupt change in roughness and heatflux". Bound. Layer Meteorol., 21, 341-356.

Højstrup, J. (1982): "Velocity spectra in the unstable planetary boundary layer", J. Atm. Sci., 39, 2239-2248.

Højstrup, J., S.E.Larsen, P.H.Madsen (1990): "Power spectra of horizontal wind components in the neutral atmospheric surface boundary layer". AMS ninth Symposium on turbulence and diffusion, Roskilde, Denmark.(American Meteorol. Soc.).

Højstrup, J. (1990), "Wake measurements on the Nibe wind-turbines in Denmark", Appendix 1, Nibe Wake 2: Data Report, Power Spectra, Final Report on CEC contract no. EN3W.0039.UK(H1).

Højstrup, J., M.S.Courtney (1993): "Turbulence in windfarms", ECWEC93, Travemünde, Germany.

Højstrup, J., R.J. Barthelmie, M.S. Courtney, and P. Sanderhof (1994), "Wind and turbulence in near coastal offshore environment", EWEC' 94.

Højstrup, J., R.J.Barthelmie, M.S.Courtney (1994): "Preliminary results of offshore meteorological monitoring at the Vindeby windfarm". Wind Engineering, 18, no.5, pp. 219-225.

Højstrup, J. (1995): "Roughness lengths in coastal terrain". In: Proceedings fro 11th Symposium on Boundary Layers and Turbulence (Am. Meteorol. Soc.), March 1995.

Højstrup, J., B.Tammelin (1996): EUWEC96, den Haag, Netherlands

IEC (1995), "Wind turbine generator systems, Part 12 - Power performance measurement techniques", IEC 88(WG6)CDV 2/8-1995.

IEC 185 (1987), "Current transformers", Second edition, Geneve.

IEC 688 (1992), "Electrical measuring transducers for converting a.c. electrical quantities to analogue or digital signals", Second edition, Geneve.

International Standard ISO 2533 (1978), "Standard Atmosphere", First Edition 1975-05-15. Corrected and reprinted 1978-12-15.

Katic, I., J. Hojstrup and N.O. Jensen (1986), "A simple model for cluster efficiency", Proceedings of the EWEC'86, Rome, pp. 407 -410.

Kambezidis, H. D., T.P. Georgakapoulos and D,N. Asimakopoulos (1990), "Calculation of velocity deficits in the wake of WECS" Proceedings of the ECWEC ' 90, Madrid, pp. 196 - 197.

Liu, M., M. Vocke and T. Myers (1983), "Mathematical model for the analysis of wind turbine wakes", Journal of Energy, Vol. 7, No. 1.

Lissaman, P.B.S. (1979), "Energy effectiveness of arbitrary arrays of wind turbines", AIAA Paper 79-0114.

Luken, E., A. Talmon and P. Vermeulen (1986), "Evaluation of two mathematical wind turbine wake models in various types of flows", TNO Report, 86-07.

Madsen, P.H. and S. Frandsen (1984), "Pitch angle regulation for power limitation", European Wind Energy Conference, Hamburg, Germany, 22-26 October.

Mann, J. (1994), "Models in Micrometeorology", Risø-R-727(EN). Risø National Laboratory, Roskilde, Denmark.

Milborrow, D. J. J. (1986), "The performance of arrays of wind turbines", Journal of Wind Engineering and Industrial Aerodynamics, 5.

Milborrow, D.J. and J.N. Ross (1983), "The influence of turbulence and rotor thrust on wind turbine wake characteristics", CERL memorandum TPRD/L/AP/0098/M83.

Moore, D. J. (1979), "Depletion of available wind power by a large network of wind generators", Proc. of the 2nd International Conference on Future Energy Concepts. I.E.E. London.

Musgrove, P. J. (1980), "Cluster efficiency and the effect of rotor drag", Proceedings of the 2nd BWEA workshop, Cranfield.

Newman, B. G. (1977), "The spacing of wind turbines in large arrays", Energy Conversion 16, 169-171.

Olesen, H.R., S.E.Larsen, J.Højstrup (1986): Modelling velocity spectra in the lower part of the planetary boundary layer", Bound. Layer Meteorol., 29, 285-312.

Panofsky, H. A. and J.A. Dutton (1984), "Atmospheric Turbulence", Willey Interscience.

Papaconstantinau, A. and G. Bergeles (1988), "Hot-wire measurements of the flow field in the vicinity of a HAWG rotor", Journal of Wind Engineering and Industrial Aerodynamics, 31.

Patankar, S.V. and D.B. Spalding (1972), "A calculation procedure for heat, mass and momentum transfer in three-dimensional parabolic flows", Int. Journal of Heat and Mass Transfer, Vol. 15.

Poppen, M. and J-Å. Dahlberg (1992), "Fatigue loads on wind turbine blades in a wind farm", FFA TN 1992-21. The aeronautical research institute of Sweden. 30p.

Quarton, D. (1989), "Wake Turbulence Characterization", Final Report from Garrad Hassan and Partners to the Energy Technology Support Unit of the Department of Energy of the UK, contract ETSU WN 5096.

Ross, J.N. and J.F. Ainslie (1981), "Wake measurements in clusters of model wind turbines", 3rd BWEA Conference, Cranfield.

Ross, J.N. and J. F. Ainslie (1982), "Measurements of the wake structure behind model wind turbines", CERL Memo LM/PHYS/283.

Scheppers, G. (1996), "Analysis of Alsvik data", contribution to the DLWFII final report, ECN. To be published.

Schlichting, H. (1968), "Boundary layer theory", Mc Graw Hill.

Schmidt, W. L. (1977), "Wind power studies", M. A. thesis, Dept. of Mechanical Engineering, University of Waterloo.

Sforza, P. M., M. Stasi, M. Smorto and P. Sheering (1979), "Wind turbine generator wakes", AIAA paper 79-0113.

Sforza, P. M., P. Sheering and M. Smorto (1981), "Three dimensional wakes of simulated wind turbines", AIAA Journal, 19(9).

Smith, D. and G.J. Taylor (1991), "Further analysis of turbine wake development and interaction data", Proceedings of the 1991- 13th BWEA Wind Energy Conference. pp 325 - 331.

Talmon, A.M. (1985), "The wake of a HAWT model", MT- TNO report 85-010121, August.

Templin, R. J. (1974) "An estimation of the interaction of windmills in widespread arrays", National Aeronautical Establishment, Laboratory Report LTR-LA-171. Otawa, Canada.

Taylor, P.A. (1969), "On wind shear stress profiles above a change in surface roughness", Royal Meteor. Soc. Quart. Jour. 95, 77-91.

Taylor, P.A. (1980), "On Wake Decay and Row Spacing for WECS Farms", 3rd Int. Symposium on Wind Energy Systems, Lyngby, Denmark.

Taylor, G.J. et al. (1985), "Wake measurements on the Nibe windmills", 7th BWEA Conference.

Taylor, G. J. (1990), "Wake measurements on the Nibe wind-turbines in Denmark. Part 2: Data collection and analysis", Final report CEC Contract No. EN3W.0039.UK(H1), National Power U.K.

Taylor, G.J. (1993), "Development of an improved eddy viscosity model - Wake and wind farm modelling", Contribution to the Final report contract CEC JOUR-0087-NL (CEC). TNO-report 93-374.

Taylor, G. J. and D. Smith (1991), "Wake measurements over complex terrain", Proceedings of the 1991- 13th BWEA Wind Energy Conference, pp 335 - 342.

Thirstrup Petersen, J. (1990), "Kinematically nonlinear finite element model of a horizontal axis wind turbine", Part 1 and 2, Risø National Laboratory.

Thomsen, K. and S.M. Petersen (1992), "Experimental investigation of gear box duration loadings on stall and pitch controlled wind turbines", Risø-R-653(EN), Risø National Laboratory, Roskilde, Denmark, 117p.

Thomsen, K., S.M. Petersen, O. Sangill and P. Lading (1993), "Analysis of loads for wind turbines in inhomogeneous terrain", Risø-R-657(EN), Risø National Laboratory, Roskilde, Denmark, 87p.

Thomsen, K., H. Binder and T.F. Pedersen (1994), "Fatigue loads on a pitch regulated wind turbine operating in a coastal wind turbine array", Risø-R-743(EN), Risø National Laboratory, Roskilde, Denmark, 34p.

Thomsen, K., S.M. Petersen, J.T. Petersen, S. Øye and M. Friedrich (1996), "Terrain induced loads on pitch regulated wind turbines", Risø-R-846(EN), Risø National Laboratory, Roskilde, Denmark, 82p.

Troen, I. and Petersen, E.L. (1989): "European Wind Atlas". ISBN 87-550-1482-2, Risø National Laboratory, Roskilde, Denmark, 656 pp.

Van Leuven, J. (1992), "The energetic effectiveness of a cluster of wind turbines", Thesis presented at the Universite Catholique de Louvain, Institut des Sciences Naturelles Appliquees, September.

H. van Oort, P.H. van Gemert and A. Crespo (1989), "Wind farms in complex terrain", Final Report of CEC contract EN3W / 0030 /NL. MT-TNO report 89 - 233.

Vermeulen, P. (1978), "A wind turbine study of the wake of a horizontal axis wind turbine", TNO report No.78-09674, September.

Vermeulen, P.E.J. (1980), "An Experimental Analysis of Wind Turbine Wakes," 3rd Int. Symposium on Wind Energy Systems, Lyngby, Denmark.

Vermeulen, P. E. J., P.J.H. Builtjes and J.B.A. Vijge (1981), "Mathematical modelling of wake interaction in wind turbine arrays", part I & II, MT-TNO Reports 81-01473, 81-02834.

Vermeulen, P. E. J. and P.J.H. Builtjes (1982), "Practical applications of mathematical wake interaction model", Proceedings of the 4th International Wind Energy Conference, Stockholm.

Vermeulen, P. E. J. and P.J.H. Builtjes (1982a), "Turbulence measurements in simulated wind turbine clusters", Proceedings of the 4th International Wind Energy Conference, MT-TNO report 82-03003.

S. G. Voutsinas, K. G. Rados and A. Zervos (1990), "The effect of the non-uniformity of the wind velocity field in the optimal design of wind parks", Proceedings of the ECWEC'90, Madrid, pp. 181 - 185.

Voutsinas, S. G., K.G. Rados and A. Zervos (1990b), "On the analysis of wake effects in wind parks", Wind Engineering, 14, pp 204 - 219.

Voutsinas, S. G., K.G. Rados and A. Zervos (1992), "On the effect of the rotor geometry on the formation and the development of its wake", Journal of Wind Engineering and Industrial Aerodynamics, 39, pp. 283-291.

Voutsinas, S. G., J.P. Glekas and A. Zervos (1992), "Investigation of the effect of the initial velocity profile on the wake development of a wind turbine", Journal of Wind Engineering and Industrial Aerodynamics, 39, pp. 291-301.

Voutsinas, S. G. and S. Huberson (1993), "Simulation of wake effects in wind parks", contribution to the Final Report of contract CEC JOUR-0087-NL (CEC). TNO-report 93-374.

Voutsinas, S. G., K.G. Rados and A. Zervos (1993a), "Wake effects in wind parks. A new modelling approach", Proceedings of ECWEC'93, pp 444-447. Travemünde, Germany.

Voutsinas, S.G., K.G. Rados and M.A. Belessis (1994), "Concluding a design tool for wind parks", EWEC' 94 pp. 342-347.

Vølund, P. (1991), "Loads on a horizontal axis wind turbine Operating in wake", Risø-M-2916. Risø National Laboratory, Roskilde, Denmark, 68p.

Wilson, R. E., P.B.S. Lissaman and S.N. Walker (1976), "Aerodynamic performance of wind turbines", ERDA /NSF/04014-76/1.

Wu, Jin (1994), "The sea surface is aerodynamically rough even under light winds", Boundary Layer Meteor.,

69, 149-158.

Zervos, A., S. Huberson and A. Hemon (1988), "Three Dimensional Free Wake Calculation of Wind Turbine Wakes", Journal of Wind Engineering and Industrial Aerodynamics, 27.

Øye, S. (1991), "Dynamic stall - simulated as time lag of separation", Proc. of the 4th IEA Symposium on the Aerodynamics of Wind Turbines, K.F. McAnulty (Ed.), Rome, Italy.

APPENDICES

APPENDIX A

Non-central moments of Normal distribution.

The integral is reformulated by substitution:

$$s_e^m = \alpha^m \int_{-\infty}^{\infty} (x+\beta)^m \frac{1}{\sigma\sqrt{2\pi}} \exp[-\tfrac{1}{2}(\frac{x-\mu}{\sigma})^2] \; dx = \alpha^m \int_{-\infty}^{\infty} x^m \frac{1}{\sigma\sqrt{2\pi}} \exp[-\tfrac{1}{2}(\frac{x-\mu_o}{\sigma})^2] \; dx$$

where $\mu_o = \mu + \beta$. The correction factor to the power m (corresponding to m'th power of the SN-curve) due to non-linearity of equivalent stress is

$$r_m^m = \frac{s^m}{\alpha^m(\mu+\beta)^m} = \frac{1}{\mu_o^m} \int_{-\infty}^{\infty} x^m \frac{1}{\sigma\sqrt{2\pi}} \exp(-\tfrac{1}{2}(\frac{x-\mu_o}{\sigma})^2) \; dx$$

$$= \int_{-\infty}^{\infty} y^m \frac{1}{\sigma\sqrt{2\pi}} \exp(-\tfrac{1}{2}(\frac{y-1}{\sigma_*})^2) \; dy$$

where $\sigma_* = \sigma/\mu_o$. The first three values are $r_0=1$, $r_1=1$ and $r_2^2=1+\sigma_*^2$. We find by partial integration of the above integral that

$$r_e = r_m = \left[r_{m-1}^{m-1} + (m-1)\sigma_*^2 r_{m-2}^{m-2} \right]^{\frac{1}{m}}$$

For small values of σ_* the correction factor may be approximated by

$$r_e \simeq 1 + \tfrac{1}{2}(m-1)\sigma_*^2$$

Integral of $(1/(\alpha\beta))(c[1+s_N(x)])^m$

The "bell-integral" is re-written:

$$s_e^m = \int_{-\alpha\beta}^{\alpha\beta} \frac{1}{2\alpha\beta} [c^m(1+\alpha \; \exp(-(\frac{x}{\beta})^2))]^m \; dx = (\frac{c^m}{2\alpha\beta}) \left[2\alpha\beta + \sum_{i=1}^{m} \begin{bmatrix} m \\ i \end{bmatrix} \int_{-\alpha\beta}^{\alpha\beta} (\exp[-(\frac{x}{\beta})^2])^i \; dx \right]$$

since

$$(1 + s_N(x))^m = 1 + \begin{bmatrix} m \\ 1 \end{bmatrix} s_N + \begin{bmatrix} m \\ 2 \end{bmatrix} s_N^2 + \ldots\ldots + \begin{bmatrix} m \\ m \end{bmatrix} s_N^m = \sum_{i=0}^{m} \begin{bmatrix} m \\ i \end{bmatrix} s_N^i$$

where the binomial coefficients are

$$\begin{bmatrix} m \\ i \end{bmatrix} = \frac{m!}{i!(m-i)!}$$

For large values of a (>3) the definite integral approaches indefinite:

$$s_e^m = (\frac{c^m}{2a\beta}) \left[2a\beta + \sum_{i=1}^{m} \begin{bmatrix} m \\ i \end{bmatrix} \int_{-\infty}^{\infty} (\exp[-(\frac{x}{\beta})^2])^i \; dx \right] = c^m \left[1 + \sum_{i=1}^{m} \begin{bmatrix} m \\ i \end{bmatrix} \frac{\sqrt{\pi}}{2a} \frac{\alpha^i}{\sqrt{i}} \right]$$

With an equivalent, rectangular width of $[-b\beta, b\beta]$ and amplitude $c[1+\alpha]$ and elsewise amplitude c in the interval $[-2a\beta, 2a\beta]$ we get the equivalent width

94

$$s_e^m = c^m \left[(1-\frac{b}{a}) + (1+\alpha)^m \frac{b}{a} \right] = c^m \left[1 + (\frac{b}{a}) \sum_{i=1}^{m} \begin{bmatrix} m \\ i \end{bmatrix} \alpha^i \right]$$

since $p=2b\beta/2a\beta=b/a$ is the probability of being in the equivalent wake. The equivalent wake width factor is found by equalizing the two expressions for s_e^m:

$$b = \frac{\sqrt{\pi}}{2} \frac{\sum_{i=1}^{m} \begin{bmatrix} m \\ i \end{bmatrix} \frac{\alpha^i}{\sqrt{i}}}{\sum_{i=1}^{m} \begin{bmatrix} m \\ i \end{bmatrix} \alpha^i} \simeq \frac{3 + \sqrt{m}\ \alpha^{1.25}}{3 + m\ \alpha^{1.25}}$$

Weibull Distribution and $s(x)=\alpha x^h$

The following is not being applied in the report (numerical integration is used); however, it is included for completeness. Considering e.g. mean wind speed alone there is evidence that equivalent stress follows

$$s(x) = \alpha\ x^h$$

Usually, wind speed is assumed Weibull distributed with scale and shape parameters A and k:

$$p(x) = \frac{k}{A} (\frac{x}{A})^{k-1} \exp[-(\frac{x}{A})^k]$$

The mean of x, μ, is tied to the Weibull parameters by

$$\mu = A\ \Gamma(1+\frac{1}{k})$$

where $\Gamma(\ )$ is the gamma function. From (7.7) the integrated equivalent stress is then determined as

$$s_e^m = \int_0^\infty p(x)(\alpha x^h)^m dx = A^{hm} \alpha^m \Gamma(1+\frac{mh}{k}) = \alpha^m \left[\frac{\mu}{\Gamma(1+\frac{1}{k})} \right]^{mh} \Gamma(1+\frac{mh}{k}) \Rightarrow$$

$$s_e = \alpha\ \mu^h \frac{\Gamma(1+(mh)/k)^{\frac{1}{m}}}{\Gamma(1+1/k)^h} = \alpha\ \mu^h\ r_e$$

If the parameter were constant at x_o, the integrated es would be αx_o^h. Therefore - by means of the factor $r_e = r_e(k,h,m)$ - an "equivalent mean of the parameter" could be defined as the constant x_e that would cause the same damage as the distributed parameter:

$$x_e = \mu\ r_e^{\frac{1}{h}}$$

Values of $r_e^{1/h}$ are tabulated in Table A.1 for $h=1$ and $k=2$ for different slopes, m, of the S-N curve. The significance of the factor is that if e.g. the ew is linear in wind speed ($h=1$), the Weibull shape parameter is $k=2$, and the annual mean wind speed is 6 m/s, then calculation of the s_e with a constant wind speed of $u_y \cdot R_e = 6 \cdot 1.68 = 10.1$ m/s results in the same s_e as when employing (23).

m	2	4	6	8	10	12
$r_e^{1/h}$	1.12	1.34	1.52	1.68	1.83	1.95

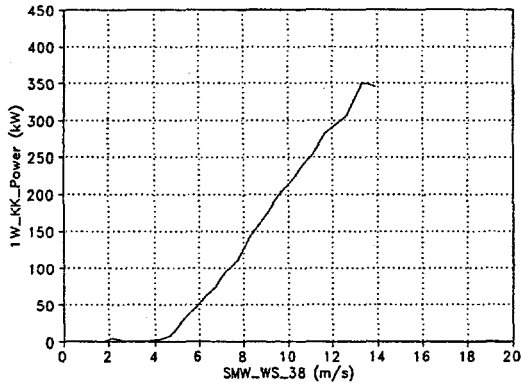*Table A.1 The equivalent stress distribution factor, for fixed values of $h=1$ and $k=2$.*

Figure B.1. *1W power curve based on SMW wind speed and control system power measurements with wind directions from 240 to 300 deg.*
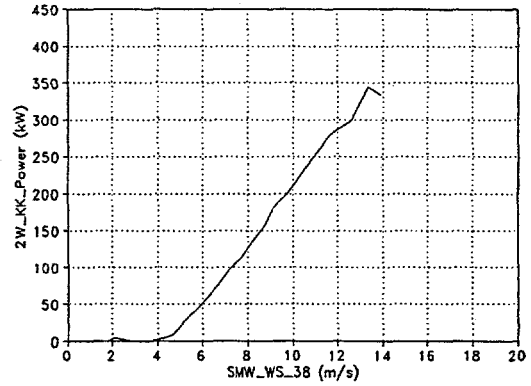
figure B.2. *2W power curve based on SMW wind speed and control system power measurements with wind directions from 240 to 300 deg.*
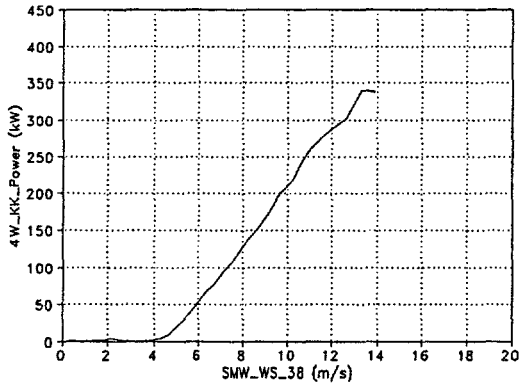

Figure B.3. *4W power curve based on SMW wind speed and control system power measurements with wind directions from 240 to 300 deg.*
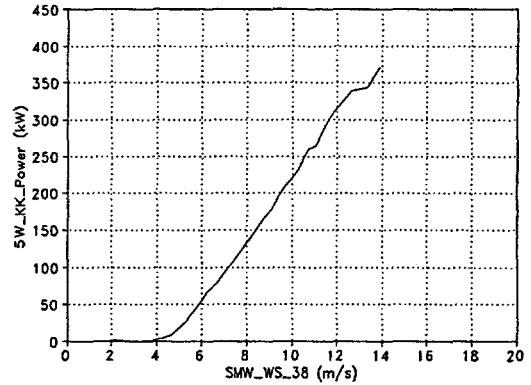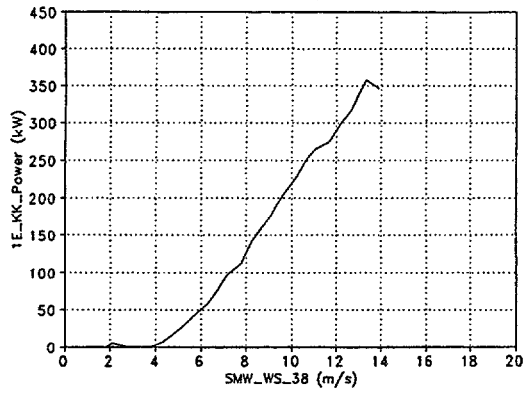
Figure B.4. *5W power curve based on SMW wind speed and control system power measurements with wind directions from 240 to 300 deg.*

Figure B.5. *1E power curve based on SMW wind speed and control system power measurements with wind directions from 240 to 300 deg.*

File name and wake distance	Wind dir.	EW (kN) - 4W		EW (kN) - 5E	
		4<U<10m/s	U>12m/s	4<U<10m/s	U>12m/s
NY_77 (4W:9.6D)	77±2°	4.61·U+3.6	3.95·U-7.1	3.01·U-0.5	4.20·U-22.2
NY_105 (4W:15.5D)	105±2°	2.57·U+12.2	4.85·U-19.2	2.76·U+6.6	3.53·U-3.7
NY_140(4W+5E:8.6D)	140±2°	3.85·U+13.6	˙2.68·U+17.4	4.00·U+12.9	˙1.96·U+26.5
NY_201 (5E:9.6D)	201±2°	2.85·U+8.3	5.85·U-33.7	4.49·U+6.8	3.22·U+10.3
NY_254 (4W:9.6D)	254±2°	1.88·U+7.2	5.31·U-35.6	4.72·U+3.5	2.82·U+12.7
NY_284 (5E:15.5D)	284±2°	1.90·U+7.8	5.48·U-34.6	3.59·U+1.5	4.29·U-15.5
5E_298 (5E:21.3D)	298±2°	1.85·U+8.1	4.72·U-24.7	2.36·U+7.8	4.28·U-16.4
NY_314 (Multiwake)	314±2°	4.34·U+5.5	˙3.07·U+14.5	4.78·U+4.3	˙3.09·U+14.2
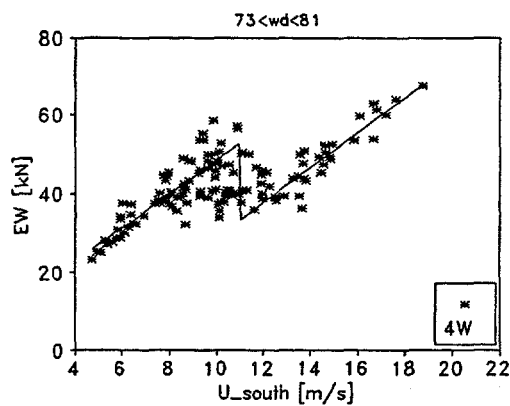
Figure C.1. *Equivalent width, single-wake,4W distance to 5E is 8.8D; free SMS tower used.*
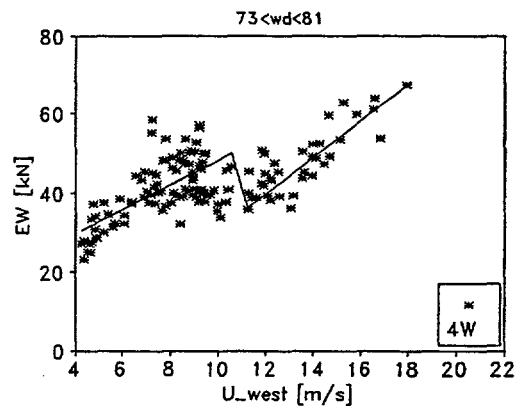
Figure C.2. *Same as last figure, but using SMW tower.*
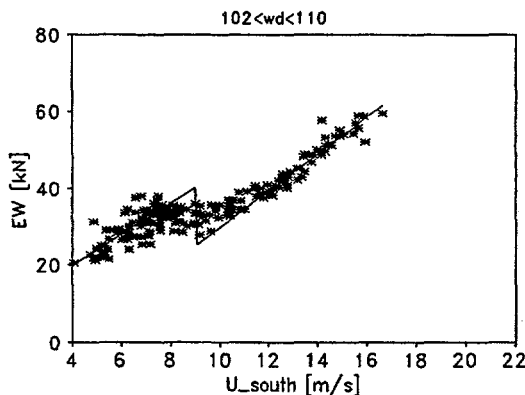
Figure C.3. *Equivalent width 4W; distance to 6E unit 14.2 D.*
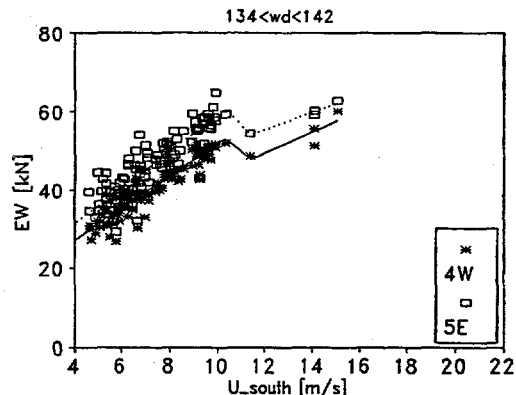
Figure C.4. *Equivalent width 4W and 5E; distance to 5W and 6E: 8 D.*
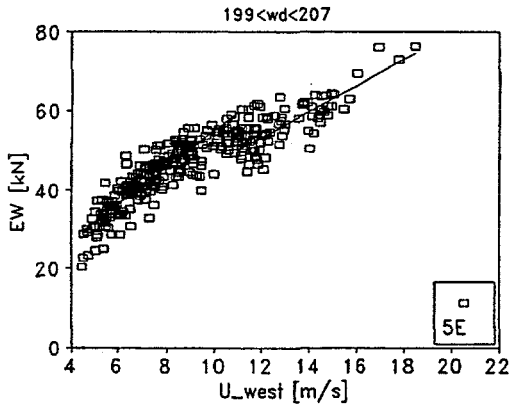
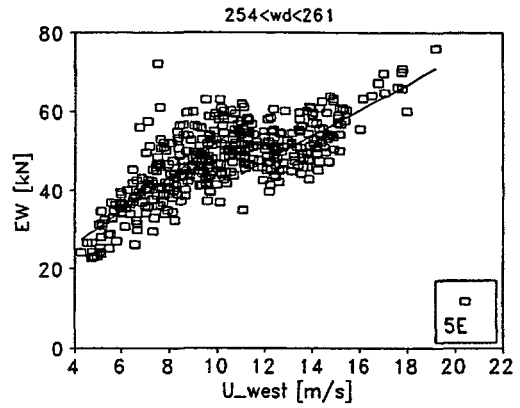**Figure C.5.** *Equivalent width of 5E; distence to 5W is 8.8 D.*

Figure C.6. *Equivalent width of 5E; distance to 4W is 8.8 D.*
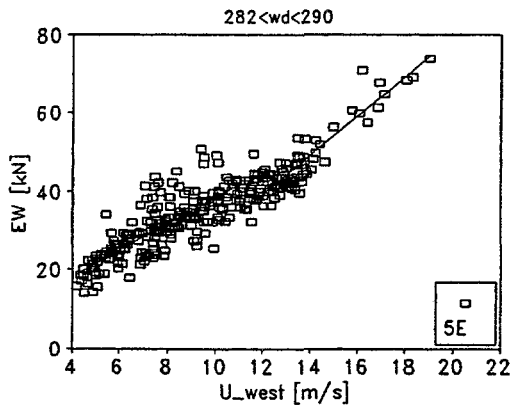

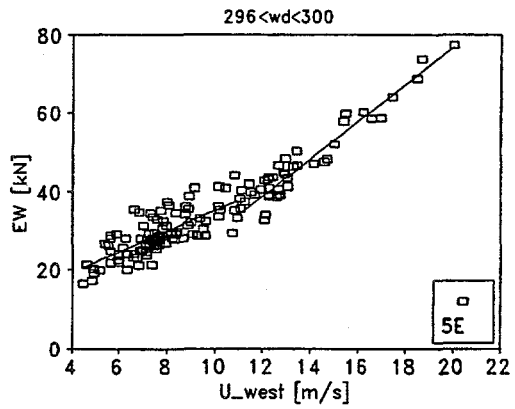**Figure C.7.** *Equivalent width of 5E; distance to 3W is 14.2 D.*

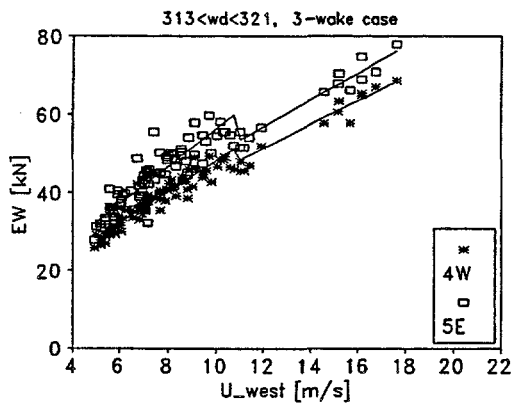**Figure C.8.** *Equivalent width of 5E; distance to 2W is 21.3 D.*

Figure C.9. *Equivalent width of 4W and 5E, multible wakes; distance to nearest turbines: 8 D.*

Bibliographic Data Sheet

Risø-R-903(EN)

Title and author(s)

Measurements on and Modelling of Offshore Wind Farms

S. Frandsen (editor), L. Chacon, A. Crespo, P. Enevoldsen, R. Gomez-Elvira, J. Hernandez, J. Højstrup, F. Manuel, K. Thomsen and P. Sørensen

Abstract (Max. 2000 characters)

The primary project component was measurement on the Vindeby Offshore Wind Farm. Also included are analyses of fatigue loading on the turbines, sea climate, performance of the wind farm and modelling of flow characteristics inside the wind farm. These individual analyses were made to meet the overall objective, which was to devise an adequate design tool to take into account the increased dynamic loading in wind farms. Measurements have been conducted for several years on the wind farm at Vindeby 2-3km off the coast of the island of Lolland in the South Baltic Sea. The Vindeby Wind Farm consists of 11 Bonus machines with installed capacities of 450kW, hub height 38m and rotor diameter 35m. The separations of the machines in the rows are 300m (8.6D), and the distance between the rows is equally 300m. Two machines, 4W and 5E are instrumented for structural measurements; tower base bending, yaw and tilt and edge and flapwise blade root bending moments are measured and statistics for ½hourly consecutive time periods are stored. The statistics include minimum, maximum, mean, standard deviation and the so-called equivalent load widths. The equivalent load width is popularly speaking the amplitude of a sinusoidal load with frequency equal - in this case - to rotational frequency of the wind turbine rotor that would consume the same fatigue life as the actual load sequence.

Modelling of fatigue loading in offshore wind farms and the offshore wind climate was carried out with good results. Also, computional flow modelling was perform.